

Intrakinetochore localization and essential functional domains of *Drosophila* Spc105

Ralf B Schittenhelm¹, Romanas Chaleckis^{1,2} and Christian F Lehner^{1,*}

1) Institute of Zoology, University of Zurich, Zurich, Switzerland

2) Present address: UAB Biotechpharma, Akademijos g. 2, LT-08412 Vilnius, Lithuania

*) Corresponding author:

Christian F. Lehner, Institute of Zoology, University of Zurich, Winterthurerstrasse 190, CH-8057 Zurich, Switzerland

e-mail: christian.lehner@zool.uzh.ch

phone: ++41 (0)44 635 48 71

fax: ++41 (0)44 635 68 20

Character count: 58516 (without references)

Running title: *Drosophila* kinetochore protein Spc105

Subject categories: Cell Cycle, Genome Stability & Dynamics

Keywords: centromere/kinetochore/mitosis/chromosome segregation/spindle assembly checkpoint

Abstract

The kinetochore is assembled during mitotic and meiotic divisions within the centromeric region of chromosomes. It is composed of more than eighty different proteins. Spc105 (also designated as Spc7, KNL-1 or Blinkin in different eukaryotes) is a comparatively large kinetochore protein which can bind to the Mis12/MIND and Ndc80 complexes and to the spindle assembly checkpoint components Bub1 and BubR1. Our genetic characterization of *Drosophila Spc105* demonstrates that a truncated version lacking the rapidly evolving, repetitive central third still provides all essential functions. Moreover, in comparison to Cenp-C, which has previously been observed to extend from the inner to the outer kinetochore region, full length Spc105 is positioned further out and is not similarly extended along the spindle axis. Thus, our results indicate that Spc105 forms neither an extended link connecting inner Cenp-A chromatin with outer kinetochore regions nor a scaffold constraining kinetochore subcomplexes and spindle assembly checkpoint components together into a geometrically rigid supercomplex. Spc105 appears to provide a platform within the outer kinetochore allowing independent assembly of various kinetochore components.

Introduction

Kinetochores are assembled within the centromeric region of eukaryotic chromosomes. They are crucial for an accurate transmission of the genetic information during mitotic and meiotic divisions (for reviews see Cheeseman & Desai, 2008; Welburn & Cheeseman, 2008; Westermann et al, 2007). Kinetochores serve as attachment sites for spindle microtubules. In addition, they host a number of proteins functioning in surveillance mechanisms that ensure a correct orientation of chromosomes within the spindle before the start of anaphase. Among these are the proteins of the spindle assembly checkpoint (SAC) which delays anaphase onset and exit from mitosis in the presence of unattached kinetochores (Musacchio & Salmon, 2007).

Surprisingly, despite the fundamental biological significance of kinetochores, its underlying centromeric DNA sequence organization has not been conserved during evolution (Allshire & Karpen, 2008). Contrasting with the point centromeres of budding yeast, higher eukaryotes including *Drosophila melanogaster* and humans have regional centromeres with megabase pairs of repetitive centromeric DNA embedded in pericentromeric heterochromatin. Nevertheless, eukaryotic kinetochores have recently been shown to be assembled from a shared set of homologous protein components (Meraldi et al, 2006; Welburn & Cheeseman, 2008; Westermann et al, 2007). More than 80 proteins contribute to functional kinetochores. The precise molecular functions and binding partners of individual kinetochore proteins remain to be defined in many cases.

Findings from different organisms have emphasized the crucial role of a centromere-specific histone H3 variant (CenH3) at the top of the kinetochore assembly pathway. CenH3 (designated as Cenp-A in humans and Cid in *Drosophila*) is present at centromeres throughout the cell cycle and is thought to make an important contribution to the epigenetic specification of centromere identity in higher eukaryotes (Allshire & Karpen, 2008). Cenp-C

is another conserved constitutive centromere component which might provide a foundation for the assembly of the S/KMN network during mitosis. This protein network contains Spc105/KNL-1 as well as the Mis12/MIND and Ndc80 complexes (Welburn & Cheeseman, 2008). In yeast and humans, the Ndc80 complex is a heterotetramer with a central rod of about 50 nm coiled coil connecting globular end domains (Ciferri et al, 2005; Ciferri et al, 2008; Wang et al, 2008; Wei et al, 2005). The globular N-terminal domains of the Ndc80/Hec1 and Nuf2 subunits on one end bind directly to microtubules (Cheeseman et al, 2006; Wei et al, 2005; Wilson-Kubalek et al, 2008). The unstructured N-terminal extension in Ndc80 is also important for microtubule binding (Guimaraes et al, 2008; Miller et al, 2008). The globular C-terminal domains of Spc24 and Spc25 on the other end of the complex are anchored within the kinetochore (Ciferri et al, 2005; Wei et al, 2006; Wei et al, 2005). This anchoring involves the Mis12/MIND complex and Spc105/KNL-1 (Cheeseman et al, 2006). High resolution light microscopic analyses have clearly demonstrated a polar orientation of the Ndc80 complex within the kinetochore with Spc24/Spc25 directed towards the inner centromere and Ndc80/Nuf2 towards the outer kinetochore microtubules (kMTs) (DeLuca et al, 2006; Schittenhelm et al, 2007). However, the molecular details of how the Mis12/MIND complex and Spc105/KNL-1 connect the Ndc80 complex with inner centromere components remain to be clarified. Co-purification behavior and localization dependencies have suggested that the Mis12 complex associates with the Cenp-C homolog in yeast and *Caenorhabditis elegans* (Cheeseman et al, 2004; Westermann et al, 2003). *Drosophila* Cenp-C has been shown to have an intrakinetochore localization that is entirely consistent with the suggestion that it might form a bridge between the inner Cenp-A chromatin and the outer S/KMN network (Schittenhelm et al, 2007). While the C-terminal domain of Cenp-C is next to Cenp-A chromatin, its N-terminal domain is further out close to Mis12. However, direct molecular

interactions between Cenp-C and Mis12 complex subunits or other S/KMN subunits have not yet been reported.

Spc105/KNL-1/Blinkin homologs are clearly crucial for kinetochore assembly in budding (Nekrasov et al, 2003) and fission yeast (Kerres et al, 2004), *C. elegans* (Desai et al, 2003), *D. melanogaster* (Przewloka et al, 2007) and humans (Cheeseman et al, 2008; Kiyomitsu et al, 2007). In principle, this comparatively large kinetochore protein might function as a linker connecting inner and outer kinetochore components. Initial analyses have revealed co-immunoprecipitation with Cenp-C and the Mis12 and Ndc80 complexes (Cheeseman et al, 2004; Desai et al, 2003; Kerres et al, 2004; Nekrasov et al, 2003; Obuse et al, 2004). The human Spc105/KNL-1 homolog Blinkin has recently been shown to interact with the SAC components Zwint-1, Bub1 and BubR1 (Kiyomitsu et al, 2007). Moreover, the fission yeast microtubule plus end-binding protein Mal3/EB1 has been detected in Spc7/Spc105 immunoprecipitates (Kerres et al, 2004). Direct microtubule binding has been observed with *C. elegans* KNL-1 in vitro (Cheeseman et al, 2006). Therefore it is also conceivable that Spc105/KNL-1 forms the kinetochore fibers that connect the outer kinetochore with kMT ends according to recent ultrastructural analyses (McIntosh et al, 2008).

The characterization of the *Drosophila* homolog described here constrains the models for Spc105 function. We show that drastically truncated versions can still provide all of the essential functions. These genetic analyses in combination with intrakinetochore mapping suggest that Spc105 does not function as an extended axial intrakinetochore linker and is unlikely to act as a scaffold forcing all its interaction partners into a geometrically rigid supercomplex.

Results

Drosophila Spc105 is an essential kinetochore protein

In general, the sequences of known *Drosophila* centromere and kinetochore protein homologs are more strongly diverged than those of other eukaryotic lineages (Heeger et al, 2005; Meraldi et al, 2006; Przewloka et al, 2007; Schittenhelm et al, 2007; Talbert et al, 2004). Moreover, several genes for kinetochore components, which in a wide range of eukaryotes are clearly detectable by sequence-based searches, cannot be found in the *Drosophila* genome (Meraldi et al, 2006; C.F.L., unpublished observations). Cenp-C was therefore proposed to be absent initially, before it was revealed by a genetic modifier screen (Heeger et al, 2005). This genetic approach also led us to the highly diverged *Drosophila Spc105* gene. We identified a deficiency which comparable to Cenp-C deficiencies (Heeger et al, 2005) resulted in a strong dominant enhancement of a phenotype caused by Separase inhibition during eye development. Subsequent analyses revealed that the enhanced phenotype (Figure 1A) was caused by a second site mutation present on the chromosome carrying this particular deficiency. Mapping placed the enhancer locus in a chromosomal region which also contained the gene *CG11451*, a known E2F1 target (Dimova et al, 2003) important for normal proliferation and metaphase morphology in Schneider S2 cells (Bjorklund et al, 2006; Goshima et al, 2007). Therefore, it appeared conceivable that a mutation in *CG11451* further exacerbates progression through an already compromised mitosis. Indeed, sequence analysis revealed a DOC transposable element insertion in the *CG11451* gene isolated from the chromosome with the enhancer mutation (Figure 1B). This incomplete DOC retroposon disrupts the third exon. A transgene containing wild-type *CG11451* reverted the dominant enhancement of eye imaginal disk-specific Separase inhibition (Figure 1A and B) and prevented the recessive lethality associated with the DOC insertion in *CG11451*. Moreover, another chromosome with a P element insertion in *CG11451* (Figure 1B; Quinones-Coello et

al, 2007) behaved like the DOC insertion. It also resulted in dominant enhancement of eye-specific Separase inhibition and recessive lethality which were both suppressed by the wild-type *CG11451* transgene (data not shown). Therefore, we conclude that *CG11451* is essential and interacts genetically with Separase function, as previously reported for *Drosophila Cenp-C*.

To analyze the intracellular localization of the *CG11451* protein product, we expressed versions with N- or C-terminal EGFP extensions in S2R+ cells. EGFP fluorescence was observed at the kinetochore of mitotic chromosomes, as indicated by double labeling with an antibody against the centromere-specific Cenp-A/Cid protein (data not shown). In interphase, weak EGFP signals were detected mainly in the cytoplasm but not at centromeres. Mitosis-specific kinetochore localization was also observed in transgenic embryos expressing the CG11451-EGFP fusion (Figure 1C). Finally, we also obtained mitosis-specific kinetochore signals when staining S2R+ cells with specific antibodies raised against CG11451 (Supplementary Figure 1).

Careful comparison of the CG11451 sequence with that of kinetochore proteins described in other eukaryotes revealed very limited similarity to the Spc105/Spc7/KNL-1/Blinkin protein family (Supplementary Figure 2), as also described recently (Przewloka et al, 2007). Spc105 homologs participate in the conserved S/KMN network of kinetochore complexes (Cheeseman et al, 2004; Desai et al, 2003; Kerres et al, 2004; Nekrasov et al, 2003; Obuse et al, 2004). Recent proteomic analyses have demonstrated that the CG11451 protein is part of the *Drosophila* S/KMN network (Przewloka et al, 2007). Our independent proteomic analyses of EGFP-Nuf2 and EGFP-Mis12 immunoprecipitates from transgenic embryos confirmed this finding (Schittenhelm et al, 2007; data not shown). In addition, we performed reciprocal Y2H experiments with *Drosophila* outer kinetochore components (Figure 1D and Supplementary Figure 3). The CG11451 protein was found to interact with *Drosophila* Nsl1/Kmn1 (CG1558)

and the N-terminal regions of Bub1 (CG14030, amino acids 1-182). Similar Y2H interactions have been observed with the human homolog Blinkin (Kiyomitsu et al, 2007). Our localization and interaction data therefore confirm and extend the evidence that *CG11451* encodes the *Drosophila* Spc105 homolog.

As an interaction between Spc105 and Bub1 is observed in both humans and *Drosophila*, we analyzed whether the short conserved RR[I/V]SF motif, which occurs in the N-terminal region of all Spc105 family members, might be required for Bub1 binding. However, by exchanging the RRISF sequence to AAGAA, we found this motif to be dispensable for Bub1 binding in Y2H assays. Moreover, an Spc105^{AAGAA}-EGFP version was observed to localize to the kinetochore and rescues the mitotic defects during mitosis 16 when expressed in *Spc105¹* mutant embryos (see below, data not shown).

Drosophila Spc105 is required for normal kinetochore assembly and function

For an analysis of the Spc105 expression pattern during embryogenesis, we used a transgenic line expressing a Spc105-EGFP fusion under control of the *Spc105* cis-regulatory region (*gSpc105-EGFP*). This transgene rescued the lethality of *Spc105¹* and *Spc105²* hemizyosity. Moreover, the rescued flies were fertile. Therefore, we conclude that the *gSpc105-EGFP* transgene provides all essential *Spc105* functions.

Immunoblotting indicated that Spc105-EGFP (data not shown) and Spc105 (Supplementary Figure 4) is present during embryonic stages associated with mitotic divisions. The high Spc105 levels, which were observed during the initial syncytial stages when nuclei divide rapidly, presumably represent a maternal contribution. Cell cycle progression after cellularization was accompanied by zygotic expression. Spc105 levels were found to be minimal during the final stages of embryogenesis, when only very few cells continue with mitotic cell cycle progression. Unfortunately, the antibodies against Spc105 resulted in

relatively high background signals in embryos, precluding reliable immunofluorescent detection of Spc105. However, analysis of EGFP fluorescence in *gSpc105-EGFP* embryos confirmed the correlation of Spc105 expression and mitotic proliferation. After germband retraction, EGFP signals were no longer observed in the epidermis and other postmitotic tissues while they were still detected in mitotic cells of the nervous system (Supplementary Figure 4).

The maternal *Spc105* contribution is expected to support normal development in *Spc105* mutant embryos initially. Indeed, phenotypic abnormalities in *Spc105* mutant embryos were not detected before cells progress through the fifteenth round of mitosis. During mitosis 16, strong abnormalities were observed. In particular, abnormal anaphase and telophase figures were apparent (Figure 2A). While centromeres are tightly clustered into two groups in over 90% of the anaphase/telophase figures observed in sibling control embryos, we detected lagging centromeres or far more severe perturbations in over 90% of the anaphase/telophase figures of *Spc105* mutant embryos ($n > 100$ from > 10 embryos). *Spc105¹* and *Spc105²* hemizygous and transheterozygous embryos displayed comparable phenotypes as *Spc105¹* homozygotes, suggesting that both alleles result in a complete loss-of-gene function (Figure 2A). Immunoblotting experiments confirmed that Spc105 was severely reduced in *Spc105* mutant embryos at the stage of mitosis 16 to less than 5% of the normal levels (Supplementary Figure 1)

In vivo imaging was used for a further characterization of the apparent mitotic defects in *Spc105¹* embryos. We analyzed embryos expressing histone H2Av-mRFP and Cenp-A/Cid-EGFP. Time-lapse analysis of the fourteenth round of mitosis did not reveal obvious defects in chromosome congression and segregation, confirming that maternally contributed Spc105 is likely to be still sufficient at this early stage (data not shown). However, as also observed with fixed embryos, the following fifteenth round of mitosis was found to be slightly

abnormal in *Spc105^l* mutants (Figure 2B). Lagging centromeres were frequently observed during anaphase (27 lagging centromeres in seven mutant anaphases compared to no lagging centromeres in nine control anaphases), but the duration of mitosis 15 did not appear to be increased. During the subsequent mitosis 16, time-lapse analysis revealed more striking abnormalities in *Spc105^l* mutants. Two classes of mitotic abnormalities were evident (Figure 2B). Mitotic cells in the first class displayed similar but more severe defects as those apparent in the previous mitosis. These cells were still able to align chromosomes in a metaphase plate. Moreover, after a prolonged metaphase (more than 10 min compared to 2.3 ± 0.3 min in sibling controls, $n = 10$), they entered an abnormal anaphase. Many chromatids were not moved efficiently towards the poles. Cells in the second class remained in prometaphase during the analyzed time period, i.e. for more than 14 minutes (Figure 2B, $n = 5$). They were unable to align their chromosomes into a metaphase plate and did not enter anaphase. In contrast, the duration of prometaphase 16 in control embryos was only 4.5 ± 0.3 min ($n = 10$). These observations confirm that Spc105 is required for normal kinetochore function. In the mutants, Spc105 levels remaining at the stage of mitosis 16 are evidently no longer sufficient for efficient chromosome congression during prometaphase and chromosome segregation during anaphase.

The reduced Spc105 levels in the mutant embryos do not appear to abolish SAC function during mitosis 16. Unaligned kinetochores apparently still activate this checkpoint and thereby delay anaphase onset and exit from mitosis. To confirm SAC function in *Spc105^l* mutants, we analysed their response to colchicine treatment. Colchicine depolymerises microtubules and therefore prevents mitotic spindle formation. The resulting unattached kinetochores activate the SAC in wild-type embryos and thereby arrest cells in mitosis with phospho-histone H3 (PH3)-positive, condensed chromosomes. After a 20 minute incubation in colchicine, we observed a similar increase in the number of PH3-positive cells in sibling

control and *Spc105^l* mutant embryos at the stage of mitosis 15 and 16 (Supplementary Figure 5 and data not shown). In the absence of colchicine, the number of PH3-positive cells was not detectably elevated in *Spc105^l* compared to sibling control embryos in both mitosis 15 and 16. These latter observations were not entirely consistent with the delayed mitoses observed in mutant embryos by time-lapse analyses at the stage of mitosis 16. However, class II behaviour was observed in a minority of cells (~20%). We assume therefore that more extensive quantitative analyses of fixed embryos would have revealed the expected enrichment of PH3-positive cells in untreated *Spc105^l* compared to sibling control embryos. However, the results with colchicine-treated embryos clearly demonstrate that *Spc105^l* embryos still have SAC function at the stage of mitosis 16. The fact that at this stage residual amounts of EGFP-BubR1 (kinetochore signal intensity during prometaphase 68% of that in sibling control embryos; Figure 3A and Supplementary Figure 6) are detectable on kinetochores in *Spc105^l* mutant embryos corroborates this conclusion.

In principle, the chromosome congression and segregation defects observed in *Spc105^l* mutants could reflect a direct Spc105 involvement in microtubule binding (Cheeseman et al, 2006) or an indirect effect on other kinetochore components. Therefore, we analyzed the role of Spc105 in kinetochore assembly. Our findings with mutant embryos confirmed and extended previous observations obtained using RNA interference (RNAi) in cultured *Drosophila* cells (Przewloka et al, 2007). The mitotic localization of EGFP-tagged versions of the kinetochore components Mis12, Nsl1, Spc25, Nuf2 and Ndc80 was found to depend on Spc105. In contrast, EGFP-tagged Cenp-C could still be recruited to kinetochores in the absence of Spc105. Our results (Figure 3A and Supplementary Figure 6), which were observed in a highly reproducible manner in all embryos of a given genotype in multiple independently fixed embryo collections, agree with those of the RNAi analysis (Przewloka et al, 2007) in case of Cenp-C and the Ndc80 complex components (Spc25, Nuf2, Ndc80). They

are at variance in case of Mis12 complex components, as both Mis12-EGFP and EGFP-Nsl1 failed to localize normally to the kinetochore during mitosis 16 in *Spc105¹* mutant embryos (Figure 3A and Supplementary Figure 6). We also analyzed the dependence of Spc105 kinetochore localization on various centromere and kinetochore components. Spc105 localization was clearly affected in *Cenp-A/cid*, *Cenp-C* and *mis12* mutants (Figure 3B and data not shown). In summary, our findings in *Drosophila* largely agree with earlier analyses in *C. elegans* (Cheeseman et al, 2004) and human cells (Cheeseman et al, 2008; Kiyomitsu et al, 2007), although the relationship between Spc105 and the Ndc80 and Mis12 complexes might be somewhat different in human cells. In *Drosophila* embryos, Spc105 is clearly required for normal recruitment of the Mis12 and Ndc80 complexes and therefore crucial for kinetochore assembly.

Spatial organization of Spc105 within the kinetochore

The importance of Spc105 for kinetochore organization, as well as its size and overall organization are comparable to Cenp-C. Both proteins are comparatively large kinetochore components (> 150 kDa) with more strongly conserved N- and C-terminal domains connected with a rapidly evolving linker region (Supplementary Figure 2; Heeger et al, 2005). Cenp-C was recently shown to have an extended and polar orientation within the kinetochore with its N-terminal domain oriented towards the spindle pole and its C-terminal domain towards the inner centromere (Figure 4B; Schittenhelm et al, 2007). Cenp-C might therefore function as a linker protein connecting the inner centromere chromatin with microtubule binding complexes in the outer region of the kinetochore. To evaluate the possibility that Spc105 might also act as a linker protein, potentially in close association with Cenp-C, we analyzed its spatial organization within the kinetochore using our previously described approach (Schittenhelm et al, 2007).

By imaging native chromosomes released from mitotic syncytial embryos expressing EGFP-Spc105 and red fluorescent Cenp-A/Cid, we obtained an average separation of about 41.5 nm between the fluorescent tags (Figure 4A). This places the N-terminus of Spc105 within the region where Mis12 and Spc25 are located according to our earlier measurements (Schittenhelm et al, 2007; Figure 4B). Measurements using Spc105-EGFP in combination with mRFP-Cenp-C revealed a separation by 5 nm and placed the C-terminus of Spc105 close to its N-terminus (Figure 4B). Evaluation of EGFP-Spc105-mRFP indicated a somewhat wider separation of the N- and C-termini by 9 nm (Figure 4B). In summary, our analyses revealed a smaller distance between the N- and C-termini of Spc105 than in the previously analyzed Cenp-C (Schittenhelm et al, 2007), indicating that Spc105 does not have a similarly extended orientation within the kinetochore as Cenp-C.

Since our Y2H data suggested a direct interaction between Spc105 and Nsl1, we also integrated the position of Nsl1 into our kinetochore map by measuring the average separation from the C-terminus of Cenp-C (Figure 4B). Consistent with a direct interaction, this placed Nsl1 at the same place as the C-terminus of Spc105, and close to Mis12 and Spc25. As an additional control for the accuracy of our intrakinetochore mapping method, we measured the average separation between the N-terminal ends of the microtubule binding proteins Ndc80 and Nuf2, which reside on the spindle proximal end of the Ndc80 complex. As expected from the known X-ray structure of the Ndc80 complex (Ciferri et al, 2008; Wilson-Kubalek et al, 2008), these N-termini were found to be close neighbours (Figure 4B).

The repetitive linker region of Spc105 is dispensable for protein function

To characterize the functional significance of the comparatively large size of Spc105 in further detail, we shortened its middle linker region. As in other Spc105 homologs, this central region is also repetitive in *D. melanogaster*. However, the motif which is repeated 16

times in *DmSpc105* forms a consensus that is different from the M[E/D][L/I][S/T] consensus observed in yeast, *C. elegans* and human homologs (Figure 5A and Supplementary Figure 2). The recent sequencing of 12 Drosophilid genomes (Clark et al, 2007) allowed evolutionary comparisons of *D. melanogaster* Spc105 with homologs in more closely related species. Interestingly, these comparisons demonstrated that the repeats in the linker region of *D. willistoni* Spc105 are far less diverged than those in *D. melanogaster* and other Drosophilids at the amino acid (Figure 5A) and DNA (data not shown) sequence levels. Most of the 31 *D. willistoni* repeats are present in a tandem array with 5.5 copies of a higher order period each composed of four repeats (Figure 5A). Thus the *D. willistoni* repeats appear to have resulted from an evolutionary recent repeat expansion possibly at the expense of older repeats. Apart from this recent repeat homogenization in the *D. willistoni* lineage, we detected a *Spc105* gene duplication in the lineage leading to the *obscura* group. The most extensive differences between the Spc105 duplicates in both *D. pseudoobscura* and *D. persimilis* represent repeat number changes in the linker region (Supplementary Figure 2). These observations demonstrate that the repetitive Spc105 linker region can evolve very rapidly.

To address the functional significance of the repetitive Spc105 linker region, we generated transgenes expressing *DmSpc105* with an altered central domain (Figure 5B). In a first transgene (*gSpc105^{wr30}*), the *D. willistoni* repeat region was used to replace the *D. melanogaster* repeat region. Therefore, the product of this transgene has more (30 instead of 16) and somewhat different repeats than *DmSpc105*. In a second transgene (*gSpc105^{wr18}*), the repeat region encompassed only 18 of the *D. willistoni* repeats. Finally, we deleted all but one of the *D. melanogaster* repeats in a third transgene (*gSpc105^{wr1}*). Strikingly, complementation tests demonstrated that all three transgenes promoted development of *Spc105¹* and *Spc105²* hemizygotes to fertile adults. Moreover, the *gSpc105^{wr1}* transgene almost completely prevented the abnormal anaphase/telophase figures at the stage of mitosis 16 in

Spc105¹/Spc105² embryos (12% abnormal anaphases/telophases in *gSpc105^{wr1}*; *Spc105¹/Spc105²* embryos, n = 310, versus 5% abnormal anaphases/telophases in *gSpc105*; *Spc105¹/Spc105²* embryos, n = 118; compare with Figure 2A). Moreover, all the analyzed kinetochore components (EGFP-Ndc80, EGFP-Nuf2, Spc25-EGFP, Mis12-EGFP and EGFP-BubR1) were found to have a normal localization in *Spc105* mutant embryos rescued by *gSpc105^{wr1}* (Supplementary Figure 6). We also failed to detect defects during progression through the syncytial cell cycles in embryos collected from *Spc105* mutant females rescued by *gSpc105^{wr1}* or *gSpc105^{wr30}*, and the SAC was observed to be fully functional in these embryos (Supplementary Figure 7). We therefore conclude that the repeat region does not provide essential Spc105 functions.

The C-terminal region of Spc105 partially rescues the Spc105 mutant phenotype

As neither length nor exact sequence of the repeat region was found to be of functional importance, we analyzed whether the N- or C-terminal regions of Spc105 can provide function when expressed individually. Therefore, we generated transgenic lines allowing expression of either the N- or C-terminal or the middle repetitive linker region fused to EGFP (Figure 6A). Expression of these constructs in embryos (Figure 6A) and S2R+ cells (data not shown) indicated that the C-terminal region is sufficient for kinetochore localization as also described for human and fission yeast Spc105/Spc7/Blinkin (Kerres et al, 2004; Kiyomitsu et al, 2007). In contrast, the N-terminal and the linker domain were not detected on mitotic kinetochores (Figure 6A), while weak nuclear signals during interphase clearly confirmed their expression (data not shown).

To address whether isolated Spc105 subdomains can rescue the mitotic defects observed in *Spc105¹* mutants, we fixed embryos expressing different *UAS* transgenes at the stage of mitosis 16 and analyzed the appearance of mitotic figures (Figure 6B and C). While full

length Spc105-EGFP completely rescued the mitotic defects in *Spc105^l* mutants as expected, neither the N-terminal domain nor the linker region of Spc105 was able to prevent the mitotic defects (Figure 6B and C). Interestingly, however, mitotic defects were almost completely eliminated by expression of the C-terminal region of Spc105 (Figure 6B and C). Moreover, all the analyzed kinetochore proteins (EGFP-Ndc80, EGFP-Nuf2, Spc25-EGFP and Mis12-EGFP) were observed to be present at the kinetochore although slightly diminished in *Spc105^l* mutant embryos carrying *gSpc105(C)*, a transgene driving expression of the C-terminal region of Spc105 under control of the normal *Spc105* cis-regulatory region (Supplementary Figure 6).

The N-terminal region of human Blinkin/Spc105 is required for kinetochore localization of Bub1 and BubR1, as well as for SAC function (Kiyomitsu et al, 2007). However, after incubation with the spindle inhibitor colchicine, *gSpc105(C); Spc105^l* embryos displayed an increase in mitotic cells comparable to that of control embryos and in contrast to *mad2* mutant embryos which lack SAC function (Figure 6D). Moreover, EGFP-BubR1 was observed to be present at prometaphase kinetochores in *gSpc105(C); Spc105^l* embryos at almost normal levels (85% of level in *Spc105⁺* sibling control embryos; Supplementary Figure 6).

As the extent of rescue observed in *Spc105^l* mutants expressing Spc105(C) was extensive, we determined whether *gSpc105(C)* is able to rescue all of the essential *Spc105* functions. However, *gSpc105(C)* transgenes were not able to rescue the recessive lethality associated with the *Spc105^l* mutations, in contrast to *gSpc105* or *gSpc105^{wr1}*. Moreover, after prolonged strong overexpression of *UAS* transgenes during wing or eye development, the C-terminal but not full length Spc105 or the other domains (N-terminal and linker region) interfered with normal development (Supplementary Figure 8). These observations indicate that the C-terminal region is not functionally equivalent to wild-type Spc105.

Discussion

Spc105 homologs have been shown to be important kinetochore components in budding and fission yeast, *C. elegans* and human cells. They are considerably larger than most other kinetochore proteins. An increasing number of interaction partners have been reported to associate with Spc105 homologs. Spc105 is therefore an attractive candidate scaffold or linker protein, promoting assembly of additional kinetochore components and/or connecting between inner and outer kinetochore proteins or between outer kinetochore and kMTs. Our high resolution mapping of Spc105 within the *Drosophila* kinetochore, in combination with our genetic data provides novel insights into the actual function of this kinetochore component.

In general, most kinetochore protein sequences evolve very rapidly, in particular in the *Drosophila* lineage (Meraldi et al, 2006). Sequence-based searches have therefore failed to identify the *Drosophila* Spc105 homolog. However, both proteomics (Przewloka et al, 2007) as well as our genetic screen for potential regulators of Separase function have led to the identification of a Spc105 candidate protein which we have shown here to be localized at the kinetochore. Sequence comparisons including the recently published 12 Drosophilid genomes reveal a particularly fast sequence evolution within the central repetitive part of Spc105, thereby dividing the protein into three parts, the N -, M - and C regions.

The N-terminal region of the human Spc105 homolog Blinkin/AF15q14 has recently been shown to bind the protein kinases Bub1 and BubR1 (Kiyomitsu et al, 2007) which are important for the SAC and for kinetochore attachment to kMTs. Moreover, Blinkin has been shown to be required for the recruitment of Bub1 and BubR1 to the kinetochore and for the SAC (Kiyomitsu et al, 2007). In *Drosophila*, we also detect an interaction between the N-terminal regions of Spc105 and Bub1 with Y2H assays. However, we have not observed an

interaction with BubR1. Moreover, EGFP-BubR1 signals at kinetochores in *Spc105* mutants at a stage where Spc105 levels are clearly below 5% of the normal wild-type level are only reduced by about 30%. Thus, *Drosophila* Spc105 might not be the only binding partner of *Drosophila* BubR1 at the kinetochore. That *Drosophila* Bub1 also interacts with the Mis12 complex component Nsl1 according to our Y2H data might hint at alternative pathways for Bub1 and BubR1 recruitment to the kinetochore. Consistent with the significant levels of EGFP-BubR1 remaining at kinetochores in *Spc105* mutants with or without expression of the C-terminal Spc105 region, we find that the SAC appears to be functional at the stage of mitosis 16.

The repetitive middle region of Spc105 evolves most rapidly. The significant size difference among eukaryote Spc105 homologs (from 917 aa in *S. cerevisiae* to 2342 aa in humans) largely reflects variability within the repetitive middle region. Our sequence comparisons have revealed a concerted evolution of the repeat region of Drosophilid *Spc105* genes in a minisatellite like manner. Repeat expansion and contractions appear to have caused rapid changes in repeat numbers. Moreover, occasional repeat homogenizations might explain why a repeat consensus different from that of other eukaryotes has been maintained in the Drosophilid lineage even though this repeat region does not appear to be functionally important. Our work clearly demonstrates that the repeat region, which amounts to 44% of the full length *D. melanogaster* protein, does not provide essential functions. The *gSpc105^{wr1}* transgene, which lacks all but one of the repeats, complements the recessive embryonic lethality of *Spc105* null mutations.

We point out, however, that a slightly elevated number of abnormal mitotic figures was apparent in embryos that depend on the *gSpc105^{wr1}* transgene. In addition, the repeat consensus in *Drosophila* contains several acidic as well as basic residues followed by a threonine which appears to be phosphorylated in vivo (Bodenmiller et al, 2007), possibly by

Aurora B, as it is within a corresponding kinase consensus site (Ohashi et al, 2006). Thus, it is tempting to speculate that the middle region could contribute to regulated electrostatic interactions with spindle microtubules, similar as the N-terminal tails of Ndc80 (Cheeseman et al, 2006; DeLuca et al, 2006; Guimaraes et al, 2008; Miller et al, 2008). As the *Drosophila* Spc105 repeat consensus appears to be different from that of other eukaryotes, the possibility of a distinct functional significance of the repeat region in *Drosophila* should be kept in mind.

The C-terminal region of Spc105 interacts with Mis12 complex components according to Y2H data from both human (Kiyomitsu et al, 2007) and *Drosophila* proteins (this study). While heterodimerization of the Mis12 complex components Nsl1/hMis14 and Dsn1/hMis13 appears to be required for an association with Spc105-C in humans, *Drosophila* Nsl1 alone is already capable to interact with Spc105-C. This apparent discrepancy might reflect the possibility that *Dsn1* might have been lost during evolution of *Drosophila* where extensive proteomic analyses have failed to reveal the corresponding homolog so far (Przewloka et al, 2007; Schittenhelm et al, 2007). The suggestion that Nsl1 might have taken over the Dsn1 functions is also consistent with our additional Y2H data concerning interactions between Mis12 complex components. *Drosophila* Nsl1 can readily interact with the other components Mis12 and Nnf1a, while an association of human Nsl1 with Mis12 and Nnf1 depends on Dsn1 (Kiyomitsu et al, 2007). Thus, although the S/KMN network, which includes Spc105/KNL-1, Mis12 - and Ndc80 complexes, appears to be present in all eukaryotes, some of the molecular details of the interaction network appear to have evolved divergently in different eukaryote lineages. Differences in Ndc80 complex organization further support this conclusion. While the Ndc80 complexes of both humans and budding yeast are anchored at the kinetochore by an intimate Spc24/Spc25 heterodimer (Ciferri et al, 2008; DeLuca et al, 2006; Wei et al, 2006), *C. elegans* and *D. melanogaster* do not appear to express a canonical Spc24 homolog (Cheeseman et al, 2006; Przewloka et al, 2007; Schittenhelm et al, 2007).

The variant S/KMN network details might also contribute to a striking difference in kinetochore localization dependencies. While *Drosophila* Spc105 is clearly required for Ndc80 complex localization at the kinetochore (Przewloka et al, 2007; this work), the human and fission yeast Spc105 homologs are not (Cheeseman et al, 2008; Kerres et al, 2007; Kiyomitsu et al, 2007). The relationship between Spc105 and the Ndc80 complex in *Drosophila* is therefore the same as in *C. elegans* (Cheeseman et al, 2004). Interestingly, both these organisms appear to have lost the constitutive centromere-associated network (CCAN), which is present in fission yeast and humans. The CCAN has recently been shown to contribute to the Spc105-independent kinetochore localization of the human Ndc80 complex (Cheeseman et al, 2008). Apart from the variable interaction with the Ndc80 complex and BubR1, all other kinetochore localization dependencies observed for *Drosophila* Spc105 (Przewloka et al, 2007; this work) appear to correspond to those reported from yeast, *C. elegans* and humans. Localization of *Drosophila* Spc105 depends on Cenp-A/Cid and Cenp-C, but not vice versa. In contrast, the localization of Spc105 and the Mis12 complex appears to be interdependent, at least in embryos. Finally, Spc105 localization does not depend on the Ndc80 complex.

The C-terminal region of Spc105, which anchors this protein in the S/KMN complex, appears to provide the most important Spc105 functions in *Drosophila*. Expression of Spc105-C largely restores progression through mitosis 16 in *Spc105* mutant embryos. This observation might suggest that not only the Spc105-M but also the Spc105-N region might not be crucial. However, we emphasize that Spc105-C cannot support development of *Spc105* mutants to the adult stage. Moreover, Spc105-C fails to restore kinetochore levels of EGFP-BubR1, Mis12 and Ndc80 complex components fully during mitosis 16, when low residual levels of maternally provided Spc105 might contribute to the extent of mitosis 16 rescue in *Spc105* mutants. In addition, prolonged Spc105-C expression during wing or eye

development in a *Spc105*⁺ background results in defects that might reflect a dominant-negative effect. The N-terminal region therefore clearly provides important Spc105 functions.

Our finding that the Spc105-M region is not essential demonstrates that the comparatively large size of *Drosophila* wild-type Spc105 is not required for instance to link kinetochore layers or kinetochore and kMTs. Our high resolution mapping of Spc105 within the kinetochore argues into the same direction. In contrast to Cenp-C, a protein of comparable size with an extended polar orientation bridging between inner and outer kinetochore regions (Schittenhelm et al, 2007), Spc105 does not display a similarly extended layout along the inter sister kinetochore axis. However, consistent with the known molecular interactions, it is close to the Mis12 complex components. Moreover, it is also close to the N-terminal region of Cenp-C and the Spc25 end of the Ndc80 complex, consistent with co-immunoprecipitation data (Cheeseman et al, 2004; Przewloka et al, 2007; Schittenhelm et al, 2007; Westermann et al, 2003). We emphasize that our kinetochore mapping data has been obtained with released native chromosomes that are not attached to the spindle. Our data thus leaves open the possibility that the orientation of Spc105 might change upon attachment of the kinetochore to kMTs. During revision of our work, high resolution data concerning the intrakinetochore localization of Spc105 in yeast and human cells has been reported (Joglekar et al, 2009; Wan et al, 2009). These studies have analyzed kinetochore organization along the spindle axis in kinetochores that are attached to the spindle. A comparison with these studies suggests that the N-terminal region of Spc105 is localized somewhat further out towards the kMTs after attachment, while the C-terminal region remains close to the Mis12 complex and the Spc25 end of the Ndc80 complex.

In summary, rather than serving as an extended connecting linker or rigid scaffold protein, Spc105 is more likely to function as a platform which contributes to the recruitment of

various kinetochore components including SAC proteins without enforcing exact and rigid geometries between all the recruited entities.

Materials and methods

Fly genetics

The *Spc105*¹ allele was identified with the genetic modifier screen strategy described previously (Heeger et al, 2005) and the Exelixis deficiency set (Parks et al, 2004) (see Supplementary Information for a detailed description of the screen). The *Df(3R)Exel9014* chromosome resulted in the strongest dominant enhancement of the adult rough eye phenotype caused by eye-specific Separase inhibition. Meiotic recombination resulted in a separation of the enhancer locus from the deficiency. The enhancer locus was mapped by meiotic recombination and complementation tests with deficiencies (see Supplementary Information). The allele *Spc105*² (kindly provided by L. Cooley, Yale University School of Medicine, New Haven, CT) was isolated in a GFP trap screen as line *P01511LE* (Quinones-Coello et al, 2007). It contains a recombinant P element with a GFP exon (PTT; Morin et al, 2001) in the first *Spc105* intron. The expressed GFP fluorescence is not localized to the kinetochore, indicating that the encoded product is not a functional Spc105 variant.

The mutations *mad2*^P, *Mis12*^{f03756}, *Cenp-C*^{pr141}, *cid*^{T12-1} and *cid*^{T22-4} have been described before (Blower et al, 2006; Buffin et al, 2007; Heeger et al, 2005; Schittenhelm et al, 2007) as well as the *GAL4* driver lines *ey-GAL4* (Hazelett et al, 1998), *MS1096* (Capdevila & Guerrero, 1994), *prd-GAL4* (Brand & Perrimon, 1993) and *α4tub-GAL4-VP16* (Hacker & Perrimon, 1998). In our experiments with *α4tub-GAL4-VP16*, maternally derived GAL4-VP16 was used to drive zygotic expression from paternally inherited *UAS* transgenes which starts during cellularization. The following transgenic lines have previously been described: *gHis2AvD-mRFP1* and *gcid-EGFP-cid* (Schuh et al, 2007), *gcid-mRFP1-cid*, *gCenp-C-EGFP*, *gEGFP-Ndc80*, *gEGFP-Nuf2*, *gSpc25-EGFP* and *gMis12-EGFP* (Schittenhelm et al, 2007), *gEYFP-Cenp-C* (Heeger et al, 2005), *GFP-BubR1* (Buffin et al, 2005). Lines with the transgenes *gSpc105*, *gSpc105(C)*, *gEGFP-Spc105*, *gSpc105-EGFP*, *gEGFP-Spc105-mRFP1*,

gSpc105^{wr1}, *gSpc105^{wr15}*, *gSpc105^{wr30}*, *UAS-Spc105-EGFP*, *UAS-Spc105(N)-EGFP*, *UAS-EGFP-Spc105(M)*, *UAS-EGFP-Spc105(C)*, *giEGFP-Cenp-C* and *gEGFP-NsII* were generated using standard P element-mediated germ line transformation. In contrast to *gSpc105* and *gSpc105-EGFP*, the *gEGFP-Spc105* and *gEGFP-Spc105-mRFP* transgenes were not capable of rescuing *Spc105* mutants, although the products localized to kinetochores just like *Spc105-EGFP*. Lines expressing transgene combinations or transgenes in mutant backgrounds were established by standard crosses and/or meiotic recombination.

Plasmids, transfections and yeast two hybrid assays

Genomic DNA of *D. willistoni* was obtained from the *Drosophila* species stock center (University of Arizona, Tucson, USA). *pP{CaSpeR-4}* (Thummel & Pirrotta, 1991) was used for transgene constructs allowing expression of fluorescently tagged or untagged kinetochore proteins under control of their normal genomic regulatory region. *pPUAST* (Brand & Perrimon, 1993) was used for transgene constructs for *GAL4*-regulated expression. Moreover, these constructs were also used for transfection of S2R+ cells after which basal expression was analyzed. Transfection of S2R+ cells was conducted with the FuGeneHD Transfection Reagent (Roche) essentially as described previously (Schittenhelm et al, 2007). Protein-protein interactions were analyzed using the Matchmaker Two-Hybrid system and the yeast strain AH109 (Clontech) after transformation with *pGADT7* and *pGBKT7* constructs essentially as described before (Jäger et al, 2004). A detailed description of all plasmids is provided in the Supplementary Information.

In vivo imaging and immunofluorescence

Embryos collected from *gHis2AvD-mRFP1 II.2*, *gcid-EGFP-cid II.1*; *Spc105¹/TM3*, *Sb*, *twi-GAL4*, *UAS-GFP* parents were analyzed by in vivo imaging essentially as described

previously (Pandey et al, 2005). *Spc105* mutant embryos were identified due to the absence of *twi-GAL4*-directed *UAS-GFP* expression. As controls, we analyzed *gHis2AvD-mRFP1 II.2*, *gcid-EGFP-cid II.1* embryos analogously.

Immunofluorescence and DNA labeling of fixed embryos and S2R+ cells was conducted as described before (Pandey et al, 2005; Schittenhelm et al, 2007). For SAC assays, embryo collections were split into two aliquots after dechorionization and incubated for either 20 min (during pre-cellularization stages) or 45 min (during post-cellularization stages) in a 1:1 mixture of octane and Schneider's tissue culture medium with or without demecolcine (10 μ M, Sigma) before fixation. We used rabbit anti-Cenp-A/Cid (Jäger et al, 2005) at 1:1000, rabbit anti-Cenp-C (Heeger et al, 2005) at 1:5000, rabbit anti-phospho-histone H3 (Upstate) at 1:800 and mouse anti- β -galactosidase (Promega) at 1:1000. Two affinity-purified rabbit antibodies against the bacterially expressed and His-tagged N-terminus (amino acids 1-471) of *Drosophila* *Spc105* were generated and used at 1:3000 with S2R+ cells. Details concerning quantification and presentation of light microscopic data are given in the Supplementary Information.

Embryo extracts, immunoblotting and immunoprecipitation

For the analysis of *Spc105* levels during embryogenesis, extracts from *w* mutant embryos of defined stages were obtained as described (Edgar et al, 1994). For the preparation of *Spc105^l* embryo extracts, we collected embryos from *Spc105^l/TM3*, *Sb*, *Ubx-lacZ* flies. After fixation with methanol and immunofluorescent staining with mouse anti- β -galactosidase (Promega; 1:300) and Hoechst 33258, we sorted embryos with from those without *lacZ* expression using an inverted fluorescence microscope. The pooled embryos were solubilized in SDS-PAGE sample buffer. Hybond-ECL membranes and ECL-detection (Amersham Biosciences) were

used for immunoblotting. The affinity-purified rabbit antibodies against Spc105 were used at 1:9000 and mouse anti- α -tubulin (Neomarkers) at 1:50000.

Preparation and analysis of native chromosomes

We prepared and analyzed native mitotic chromosomes from syncytial embryos expressing fluorescently tagged kinetochore proteins essentially as described previously (Schittenhelm et al, 2007). For the embryo collections, we used the following *Drosophila* strains: (1) *gEGFP-Spc105 II.1*, *gcid-mRFP1-cid II.1*, (2) *gSpc105-EGFP II.1*, *gmRFP-Cenp-C II.2*, (3) *gEGFP-Spc105-mRFP1 II.1*, (4) *gEGFP-Nsl1 II.1*, *gCenp-C-mRFP1 II.1* and (5) *gEGFP-Nuf2 II.1*, *gmRFP1-Ndc80 II.1*. The distribution of the obtained d_{RGintra} values (see Supplementary Figure 9) was found to be similar to those described previously (Schittenhelm et al, 2007).

Supplementary data

Supplementary information (Supplementary Materials and methods, 11 Supplementary Figures, 2 Supplementary Tables) are available at The EMBO Journal Online (<http://www.embojournal.org>).

Acknowledgements

We thank Anne Walter for assistance during the co-purification experiments, Christian Böhm, Stefan Heidmann and Hendrik Pauli for their contributions to the deficiency screening, as well as Brigitte Jaunich and Sina Niebur for technical help. We also gratefully acknowledge diverse additional support by Stefan Heidmann. This work was supported by a grant of the Swiss National Science Foundation (SNF 3100A0-120276/1).

References

- Allshire RC, Karpen GH (2008) Epigenetic regulation of centromeric chromatin: old dogs, new tricks? *Nat Rev Genet* **9**: 923-937
- Bjorklund M, Taipale M, Varjosalo M, Saharinen J, Lahdenpera J, Taipale J (2006) Identification of pathways regulating cell size and cell-cycle progression by RNAi. *Nature* **439**: 1009-1013
- Blower MD, Daigle T, Kaufman T, Karpen GH (2006) Drosophila CENP-A mutations cause a BubR1-dependent early mitotic delay without normal localization of kinetochore components. *PLoS Genet* **2**: e110
- Bodenmiller B, Malmstrom J, Gerrits B, Campbell D, Lam H, Schmidt A, Rinner O, Mueller LN, Shannon PT, Pedrioli PG, Panse C, Lee HK, Schlapbach R, Aebersold R (2007) PhosphoPep--a phosphoproteome resource for systems biology research in Drosophila Kc167 cells. *Mol Syst Biol* **3**: 139
- Brand AH, Perrimon N (1993) Targeted gene expression as a means of altering cell fates and generating dominant phenotypes. *Development* **118**: 401-415
- Buffin E, Lefebvre C, Huang J, Gagou ME, Karess RE (2005) Recruitment of Mad2 to the kinetochore requires the Rod/Zw10 complex. *Curr Biol* **15**: 856-861
- Buffin E, Emre D, Karess RE (2007) Flies without a spindle checkpoint. *Nat Cell Biol* **9**: 565-572
- Capdevila J, Guerrero I (1994) Targeted expression of the signaling molecule decapentaplegic induces pattern duplications and growth alterations in Drosophila wings. *EMBO J* **13**: 4459-4468
- Cheeseman IM, Chappie JS, Wilson-Kubalek EM, Desai A (2006) The Conserved KMN Network Constitutes the Core Microtubule-Binding Site of the Kinetochore. *Cell* **127**: 983-997
- Cheeseman IM, Desai A (2008) Molecular architecture of the kinetochore-microtubule interface. *Nat Rev Mol Cell Biol* **9**: 33-46
- Cheeseman IM, Hori T, Fukagawa T, Desai A (2008) KNL1 and the CENP-H/I/K complex coordinately direct kinetochore assembly in vertebrates. *Mol Biol Cell* **19**: 587-594

Cheeseman IM, Niessen S, Anderson S, Hyndman F, Yates JR, 3rd, Oegema K, Desai A (2004) A conserved protein network controls assembly of the outer kinetochore and its ability to sustain tension. *Genes Dev* **18**: 2255-2268

Ciferri C, De Luca J, Monzani S, Ferrari KJ, Ristic D, Wyman C, Stark H, Kilmartin J, Salmon ED, Musacchio A (2005) Architecture of the human ndc80-hec1 complex, a critical constituent of the outer kinetochore. *J Biol Chem* **280**: 29088-29095

Ciferri C, Pasqualato S, Screpanti E, Varetto G, Santaguida S, Dos Reis G, Maiolica A, Polka J, De Luca JG, De Wulf P, Salek M, Rappsilber J, Moores CA, Salmon ED, Musacchio A (2008) Implications for kinetochore-microtubule attachment from the structure of an engineered Ndc80 complex. *Cell* **133**: 427-439

Clark AG, Eisen MB, Smith DR, Bergman CM, Oliver B, Markow TA, Kaufman TC, Kellis M, Gelbart W, Iyer VN, Pollard DA, Sackton TB, Larracuenta AM, Singh ND, Abad JP, Abt DN, Adryan B, Aguade M, Akashi H, Anderson WW et al (2007) Evolution of genes and genomes on the Drosophila phylogeny. *Nature* **450**: 203-218

Crooks GE, Hon G, Chandonia JM, Brenner SE (2004) WebLogo: a sequence logo generator. *Genome research* **14**: 1188-1190

DeLuca JG, Gall WE, Ciferri C, Cimini D, Musacchio A, Salmon ED (2006) Kinetochore microtubule dynamics and attachment stability are regulated by hec1. *Cell* **127**: 969-982

Desai A, Rybina S, Muller-Reichert T, Shevchenko A, Shevchenko A, Hyman A, Oegema K (2003) KNL-1 directs assembly of the microtubule-binding interface of the kinetochore in *C. elegans*. *Genes Dev* **17**: 2421-2435

Dimova DK, Stevaux O, Frolov MV, Dyson NJ (2003) Cell cycle-dependent and cell cycle-independent control of transcription by the Drosophila E2F/RB pathway. *Genes Dev* **17**: 2308-2320.

Edgar BA, Sprenger F, Duronio RJ, Leopold P, O'Farrell PH (1994) Distinct molecular mechanisms regulate cell cycle timing at successive stages of Drosophila embryogenesis. *Genes Dev* **8**: 440-452

Goshima G, Wollman R, Goodwin SS, Zhang N, Scholey JM, Vale RD, Stuurman N (2007) Genes required for mitotic spindle assembly in Drosophila S2 cells. *Science* **316**: 417-421

Guimaraes GJ, Dong Y, McEwen BF, DeLuca JG (2008) Kinetochore-microtubule attachment relies on the disordered N-terminal tail domain of hec1. *Curr Biol* **18**: 1778-1784

Hacker U, Perrimon N (1998) DRhoGEF2 encodes a member of the Dbl family of oncogenes and controls cell shape changes during gastrulation in *Drosophila*. *Genes Dev* **12**: 274-284

Hazelett DJ, Bourouis M, Walldorf U, Treisman JE (1998) decapentaplegic and wingless are regulated by eyes absent and eyegone and interact to direct the pattern of retinal differentiation in the eye disc. *Development* **125**: 3741-3751

Heeger S, Leismann O, Schittenhelm R, Schraidt O, Heidmann S, Lehner CF (2005) Genetic interactions of Separase regulatory subunits reveal the diverged *Drosophila* Cenp-C homolog. *Genes Dev* **19**: 2041-2053

Jäger H, Herzig B, Herzig A, Sticht H, Lehner CF, Heidmann S (2004) Structure predictions and interaction studies indicate homology of separase N-terminal regulatory domains and *Drosophila* THR. *Cell Cycle* **3**: 182-188.

Jäger H, Rauch M, Heidmann S (2005) The *Drosophila melanogaster* condensin subunit Cap-G interacts with the centromere-specific histone H3 variant CID. *Chromosoma* **113**: 350-361

Joglekar AP, Bloom K, Salmon ED (2009) In vivo protein architecture of the eukaryotic kinetochore with nanometer scale accuracy. *Curr Biol* **19**: 694-699

Kerres A, Jakopec V, Fleig U (2007) The conserved Spc7 protein is required for spindle integrity and links kinetochore complexes in fission yeast. *Mol Biol Cell* **18**: 2441-2454

Kerres A, Vietmeier-Decker C, Ortiz J, Karig I, Beuter C, Hegemann J, Lechner J, Fleig U (2004) The fission yeast kinetochore component Spc7 associates with the EBI family member Mal3 and is required for kinetochore-spindle association. *Mol Biol Cell* **15**: 5255-5267

Kiyomitsu T, Obuse C, Yanagida M (2007) Human Blinkin/AF15q14 is required for chromosome alignment and the mitotic checkpoint through direct interaction with Bub1 and BubR1. *Dev Cell* **13**: 663-676

McIntosh JR, Grishchuk EL, Mophew MK, Efremov AK, Zhudenzov K, Volkov VA, Cheeseman IM, Desai A, Mastrorade DN, Ataullakhanov FI (2008) Fibrils connect microtubule tips with kinetochores: a mechanism to couple tubulin dynamics to chromosome motion. *Cell* **135**: 322-333

Meraldi P, McAinsh AD, Rheinbay E, Sorger PK (2006) Phylogenetic and structural analysis of centromeric DNA and kinetochore proteins. *Genome Biol* **7**: R23

Miller SA, Johnson ML, Stukenberg PT (2008) Kinetochores Attachments Require an Interaction between Unstructured Tails on Microtubules and Ndc80(Hec1). *Curr Biol* **18**: 1785-1791

Morin X, Daneman R, Zavortink M, Chia W (2001) A protein trap strategy to detect GFP-tagged proteins expressed from their endogenous loci in *Drosophila*. *Proc Natl Acad Sci U S A* **98**: 15050-15055.

Musacchio A, Salmon ED (2007) The spindle-assembly checkpoint in space and time. *Nat Rev Mol Cell Biol* **8**: 379-393

Nekrasov VS, Smith MA, Peak-Chew S, Kilmartin JV (2003) Interactions between centromere complexes in *Saccharomyces cerevisiae*. *Mol Biol Cell* **14**: 4931-4946

Obuse C, Iwasaki O, Kiyomitsu T, Goshima G, Toyoda Y, Yanagida M (2004) A conserved Mis12 centromere complex is linked to heterochromatic HP1 and outer kinetochore protein Zwint-1. *Nat Cell Biol* **6**: 1135-1141

Ohashi S, Sakashita G, Ban R, Nagasawa M, Matsuzaki H, Murata Y, Taniguchi H, Shima H, Furukawa K, Urano T (2006) Phospho-regulation of human protein kinase Aurora-A: analysis using anti-phospho-Thr288 monoclonal antibodies. *Oncogene* **25**: 7691-7702

Pandey R, Heidmann S, Lehner CF (2005) Epithelial re-organization and dynamics of progression through mitosis in *Drosophila* separase complex mutants. *J Cell Sci* **118**: 733-742

Parks AL, Cook KR, Belvin M, Dompe NA, Fawcett R, Huppert K, Tan LR, Winter CG, Bogart KP, Deal JE, Deal-Herr ME, Grant D, Marcinko M, Miyazaki WY, Robertson S, Shaw KJ, Tabios M, Vysotskaia V, Zhao L, Andrade RS et al (2004) Systematic generation of high-resolution deletion coverage of the *Drosophila melanogaster* genome. *Nat Genet* **36**: 288-292

Przewlorka MR, Zhang W, Costa P, Archambault V, D'Avino PP, Lilley KS, Laue ED, McAinsh AD, Glover DM (2007) Molecular analysis of core kinetochore composition and assembly in *Drosophila melanogaster*. *PLoS ONE* **2**: e478

Quinones-Coello AT, Petrella LN, Ayers K, Melillo A, Mazzalupo S, Hudson AM, Wang S, Castiblanco C, Buszczak M, Hoskins RA, Cooley L (2007) Exploring strategies for protein trapping in *Drosophila*. *Genetics* **175**: 1089-1104

Schuh M, Lehner CF, Heidmann S (2007) Incorporation of *Drosophila* CID/CENP-A and CENP-C into centromeres during early embryonic anaphase. *Curr Biol* **17**: 237-243

Schittenhelm RB, Heeger S, Althoff F, Walter A, Heidmann S, Mechtler K, Lehner CF (2007) Spatial organization of a ubiquitous eukaryotic kinetochore protein network in *Drosophila* chromosomes. *Chromosoma* **116**: 385-402

Talbert PB, Bryson TD, Henikoff S (2004) Adaptive evolution of centromere proteins in plants and animals. *J Biol* **3**: 18

Thummel CS, Pirrotta V (1991) Technical Notes: New pCaSpeR P-element vectors. *Drosophila Information Service* **71**: 150

Wan X, O'Quinn RP, Pierce HL, Joglekar AP, Gall WE, DeLuca JG, Carroll CW, Liu ST, Yen TJ, McEwen BF, Stukenberg PT, Desai A, Salmon ED (2009) Protein architecture of the human kinetochore microtubule attachment site. *Cell* **137**: 672-684

Wang HW, Long S, Ciferri C, Westermann S, Drubin D, Barnes G, Nogales E (2008) Architecture and Flexibility of the Yeast Ndc80 Kinetochore Complex. *J Mol Biol* **383**: 894-903

Wei RR, Schnell JR, Larsen NA, Sorger PK, Chou JJ, Harrison SC (2006) Structure of a central component of the yeast kinetochore: the Spc24p/Spc25p globular domain. *Structure* **14**: 1003-1009

Wei RR, Sorger PK, Harrison SC (2005) Molecular organization of the Ndc80 complex, an essential kinetochore component. *Proc Natl Acad Sci U S A* **102**: 5363-5367

Welburn JP, Cheeseman IM (2008) Toward a molecular structure of the eukaryotic kinetochore. *Dev Cell* **15**: 645-655

Westermann S, Cheeseman IM, Anderson S, Yates JR, 3rd, Drubin DG, Barnes G (2003) Architecture of the budding yeast kinetochore reveals a conserved molecular core. *J Cell Biol* **163**: 215-222

Westermann S, Drubin DG, Barnes G (2007) Structures and functions of yeast kinetochore complexes. *Annu Rev Biochem* **76**: 563-591

Wilson-Kubalek EM, Cheeseman IM, Yoshioka C, Desai A, Milligan RA (2008) Orientation and structure of the Ndc80 complex on the microtubule lattice. *J Cell Biol* **182**: 1055-1061

Figure legends

Figure 1. Identification of *Drosophila Spc105*.

(A) The *Spc105^l* mutation was identified as a dominant enhancer of a rough eye phenotype caused by *GMR-thrΔC*, which results in eye-specific expression of a dominant-negative Separase regulatory subunit. *GMR-thrΔC* was expressed in either *Spc105^{+/+}* (*GMR-thrΔC*; +/+) or *Spc105^{-/+}* (*GMR-thrΔC*; *Spc105^l/+*) flies. The increased eye abnormalities observed in *Spc105^l* heterozygous flies were reverted by the presence of the *gSpc105* transgene driving expression of wild-type Spc105 (*GMR-thrΔC*; *Spc105^l/+*; *gSpc105*).

(B) The structure of wild-type and mutant *Spc105/CG11451* alleles, as well as the *gSpc105* transgene is illustrated schematically. Triangles indicate the insertion sites of an incomplete DOC element in *Spc105^l* and of a P element (*P01511LE*) in *Spc105²*. The genomic fragment used for the construction of the *gSpc105* transgene is indicated by the *thin black line* below the gene model. *Arrows* above the gene models indicate the direction of transcription. *Boxes* represent exons with UTR regions (*white*) and coding regions (*black*).

(C) The intracellular localization of *Drosophila Spc105* was analyzed in syncytial embryos expressing a Spc105-EGFP fusion (*Spc105-EGFP*) after double labeling with an antibody against Cenp-A/Cid (*Cenp-A*) and a DNA stain (*DNA*). EGFP signals were detected at centromeres only during mitosis (*lower row*) and not during interphase (*upper row*). Bar = 5 μm.

(D) Y2H experiments were used for an analysis of protein-protein interactions of Spc105, Mis12/MIND complex subunits (Mis12, Nsl1, Nnf1a) and the N-terminal region of Bub1. Spc105 was divided up into an N-terminal (*N*), middle (*M*) and C-terminal region (*C*). Interactions represented by *single arrows* were only observed when the protein next to the arrowhead was fused to the transcriptional activation domain and the protein at the base of the arrow to the DNA-binding domain of *GAL4*, but not with the reciprocal fusion protein

configuration. Interactions indicated by *double arrows* were observed with both configurations.

Figure 2. Abnormal chromosome segregation during mitosis in *Spc105* mutants.

(A) Embryos were collected from *Spc105¹/TM3, Ubx-lacZ* flies and fixed at the stage of the 16th round of mitosis. Embryos were labeled with a DNA stain (*DNA*), an antibody against Cenp-A/Cid (*Cenp-A*) and an antibody against β -galactosidase for genotype determination (not shown). In *Spc105⁺* sibling control embryos (*Spc105⁺*, *left panel*), centromeres form a tight cluster during anaphase/telophase on the poleward side of the chromosomes (see *arrows* for example). In *Spc105* mutants (*Spc105⁻*; *right panel*), centromeres are rarely clustered in anaphase/telophase and lagging chromosomes are frequent (see *arrows* for example). Moreover, more severe perturbations during anaphase/telophase were also apparent (*dashed circles*). The *bar diagram* indicates the percentage of abnormal anaphase/telophase figures in wild-type and *Spc105* mutant embryos. The total number of the observed anaphase/telophase figures ($n > 100$) in the analyzed epidermal regions from at least 6 different embryos per genotype was set to 100%. Genotypes are indicated below the bars. Bar = 2 μ m.

(B) Time-lapse in vivo imaging of mitoses in *Spc105⁺* or *Spc105⁻* embryos expressing Cenp-A/Cid-EGFP and histone H2AvD-mRFP1. The time (min:sec) indicated in each frame is given relative to the first anaphase frame, which was set to zero in the *top three rows*, or relative to the start of chromosome condensation in the *bottom row*. The *top two rows* illustrate progression through mitosis 15 where chromosome segregation during anaphase is already less synchronous in *Spc105* mutants (*second row*). The *bottom two rows* illustrate progression through mitosis 16 in *Spc105* mutants where chromosome congression was either no longer observed (*class I, fourth row*) or where it was followed by an abnormal delayed anaphase (*class II, third row*). Bar = 3 μ m.

Figure 3. Requirements for kinetochore localization of Spc105 and other kinetochore proteins.

(A) Localization of EGFP-fusions of Cenp-C, Mis12, Nsl1, Spc25, Ndc80, Nuf2 and BubR1 in *Spc105^l* (*Spc105⁻*) and *Spc105⁺* sibling control embryos (*Spc105⁺*) during mitosis 16. Representative anaphase figures are shown (except for prometaphases in case of BubR1) with kinetochore proteins in green and DNA staining in red. Bar = 3 μ m.

(B) Localization of Spc105-EGFP (shown in green) in *Cenp-C^{pr141}* (*Cenp-C*) and *Mis12⁰³⁷⁵⁶* (*Mis12⁻*) mutant embryos in comparison to sibling control embryos (*Cenp-C⁺* and *Mis12⁺*, respectively). Representative anaphases with DNA staining in red are shown at the stage where mitotic abnormalities start in the mutant embryos, i.e. during mitosis 16 in *Cenp-C* mutants and during the later mitotic divisions in the CNS in *Mis12* mutants. Bar = 3 μ m.

Figure 4. High resolution localization of Spc105 within the kinetochore.

(A) The localization of Spc105 was compared with that of Cenp-A/Cid. Native chromosomes released from syncytial embryos coexpressing EGFP-Spc105 (*EGFP-Spc105*) and a red fluorescent Cenp-A/Cid (*Cenp-A-mRFP*) were labeled with a DNA stain (*DNA*). The green and red signal intensities were quantified along the inter-kinetochore axis (*white line*). The spatial separation between the red and green fluorescent proteins was determined as described by Schittenhelm et al (2007) by averaging data obtained from 100 chromosomes. Bar = 100 nm.

(B) The average spatial separation observed in experiments with Spc105 and other kinetochore proteins is indicated in the context of a kinetochore map. The position of Cenp-A/Cid, N- and C-terminus of Cenp-C, Spc25, Mis12 and Nuf2 along the inner-outer kinetochore axis is given in nm as determined previously (Schittenhelm et al, 2007). *Double*

arrows and *numbers* below indicate the spacing (nm) observed in additional experiments with Spc105, Nsl1 and Ndc80.

Figure 5. The rapidly evolving repeat region of Spc105 does not provide essential functions.

(A) The repetitive middle region of Spc105 evolves rapidly by repeat loss and expansions. The repeat motifs in the middle region of *DmSpc105* (*red boxes*) and *DwSpc105* (*blue boxes*) are illustrated. Most of the *D. willistoni* repeats appear to have arisen recently from an expansion of a period composed of four repeats. These 5.5 periods are indicated on the *line* below the *blue boxes*. Reflecting their recent expansion, the *D. willistoni* (*Dw*) repeats are more similar to each other than the *D. melanogaster* (*Dm*) repeats, as illustrated by the *logo* representation (Crooks et al, 2004) of the repeat consensus sequences. The *numbers* (amino acid positions) and *dashed lines* illustrate the repeat domain swap constructs (see also panel B)

(B) For a functional characterization of the repetitive middle region, the transgenes *gSpc105^{wr30}* (*wr30*) *gSpc105^{wr18}* (*wr18*) and *gSpc105^{wr1}* (*wr1*) expressing *DmSpc105* with a variable number of *D. willistoni* repeats instead of the *D. melanogaster* repeats were generated. These transgenes provide all essential *Spc105* functions in *D. melanogaster* according to complementation tests.

Figure 6. The C-terminal domain of Spc105 partially rescues the *Spc105* mutant phenotypes.

(A) For an analysis of the different Spc105 domains, *UAS* transgenes expressing either the N-terminal (*N*), middle (*M*) or the C-terminal (*C*) region fused to EGFP (*green boxes*) were generated with the indicated fragments. *Numbers* indicate amino acid positions. The subcellular localization of these domains was analyzed after zygotic expression of paternally inherited *UAS* transgenes driven by maternal *α4tub-GAL4-VP16*. Embryos at the stage of

mitosis 16 were double labeled with an antibody against Cenp-A/Cid (*Cenp-A*) and a DNA stain (*DNA*). Representative metaphase figures illustrate that the C-terminal domain localizes to the kinetochore, as full length *Spc105* (FL), while the middle and the N-terminal domain do not display kinetochore localization. Bar = 4 μm .

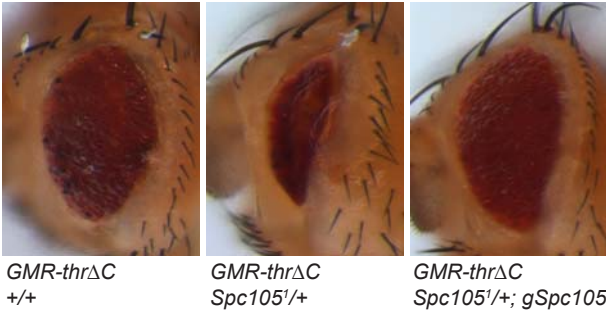
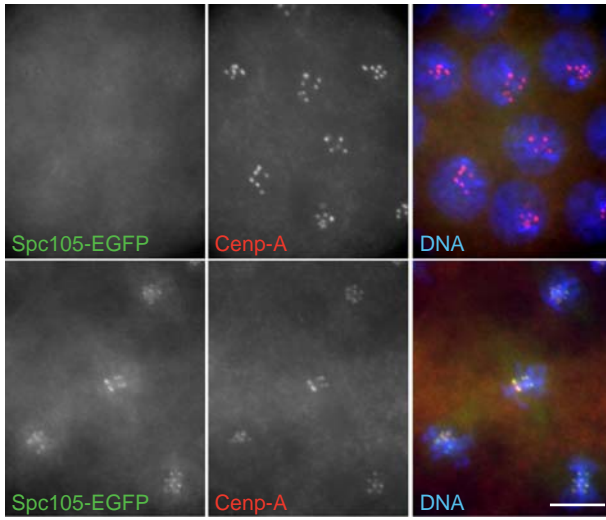
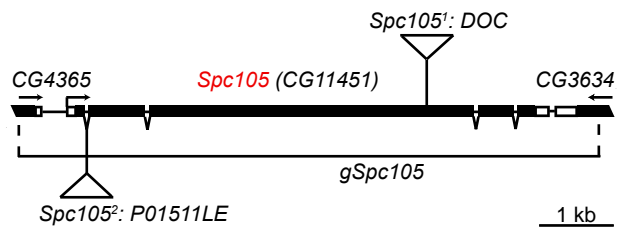
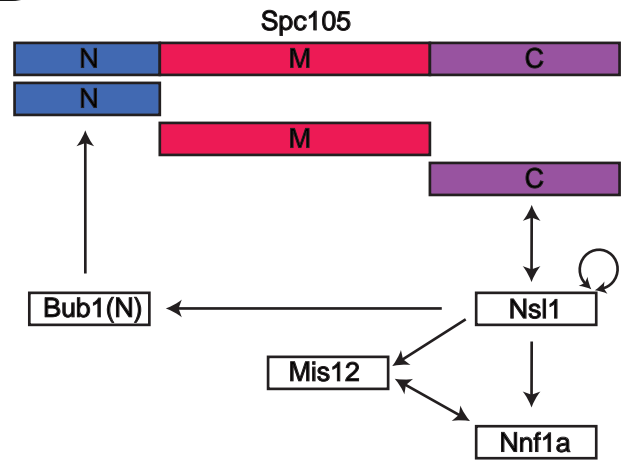
(B) *Spc105^l* embryos expressing the *UAS* transgenes (see Panel A) were fixed at the stage of mitosis 16 and double labeled with an antibody against Cenp-A/Cid (*Cenp-A*) and a DNA stain (*DNA*). *Spc105^l* embryos without a *UAS* transgene served as controls (-). Expression of *UAS-Spc105(N)-EGFP* and *UAS-EGFP-Spc105(M)* in *Spc105^l* embryos does not prevent the mitotic defects during mitosis 16. Centromeres are rarely clustered in anaphase and lagging chromosomes are frequent (*dashed circles*). In contrast, in *Spc105^l* embryos expressing *UAS-Spc105(FL)-EGFP* or *UAS-EGFP-Spc105(C)*, centromeres form a tight cluster during anaphase on the poleward side of the chromosomes (*arrows*). See also C. Bar = 6 μm .

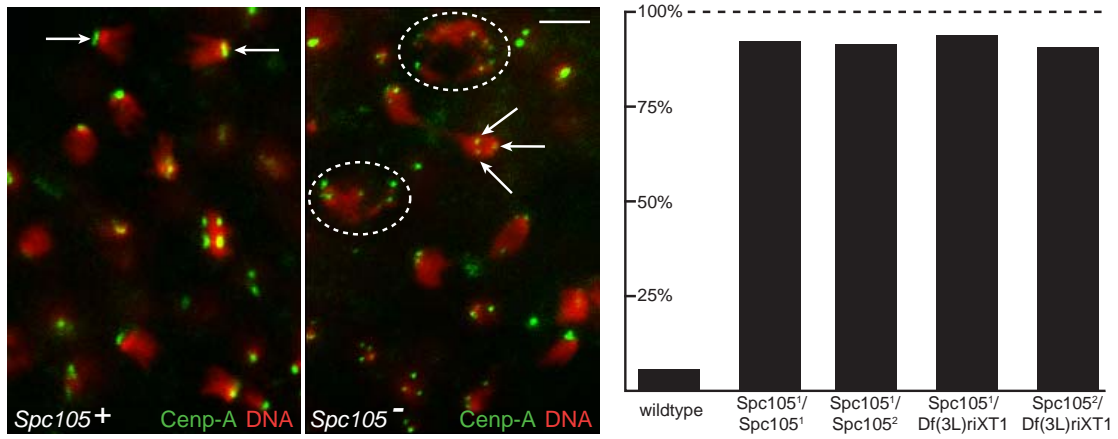
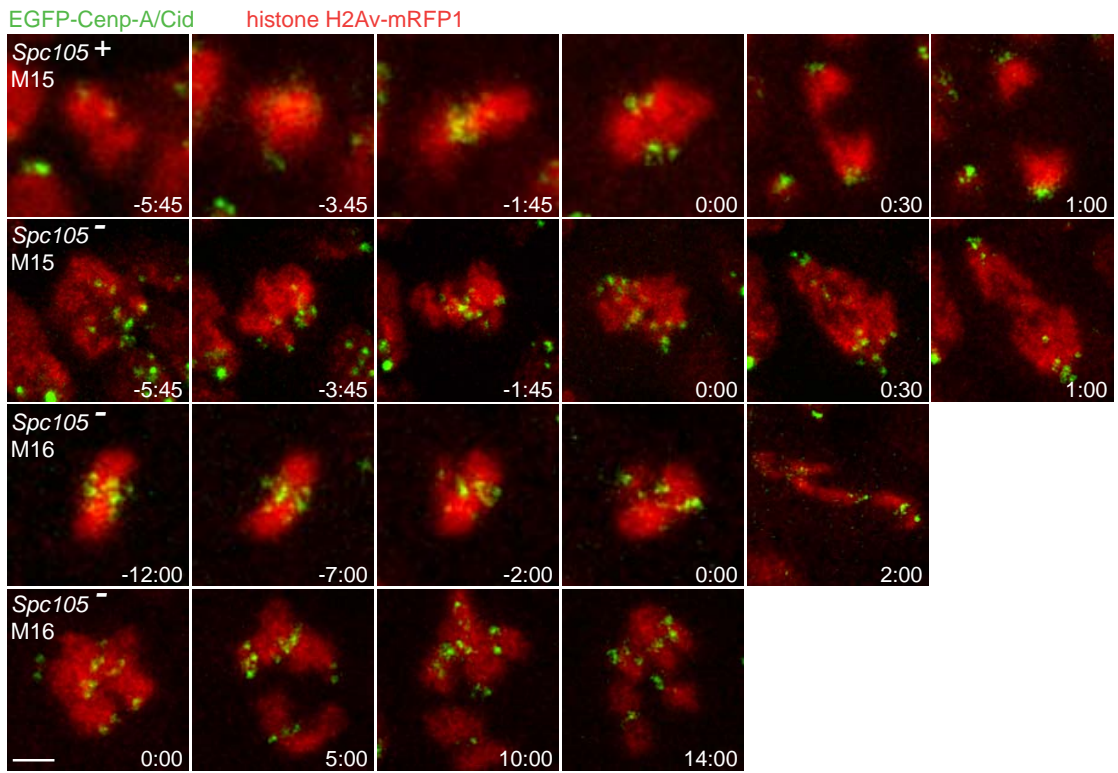
(C) The *bar diagram* indicates the percentage of abnormal anaphase/telophase figures in *Spc105^l* mutant embryos at the stage of mitosis 16 after *α 4tub-GAL4-VP16*-mediated expression of *Spc105(FL)-EGFP* (*FL*), *Spc105(N)-EGFP* (*N*), *EGFP-Spc105(M)* (*M*) or *EGFP-Spc105(C)* (*C*). *Spc105^l* embryos without a *UAS* transgene served as control (-).

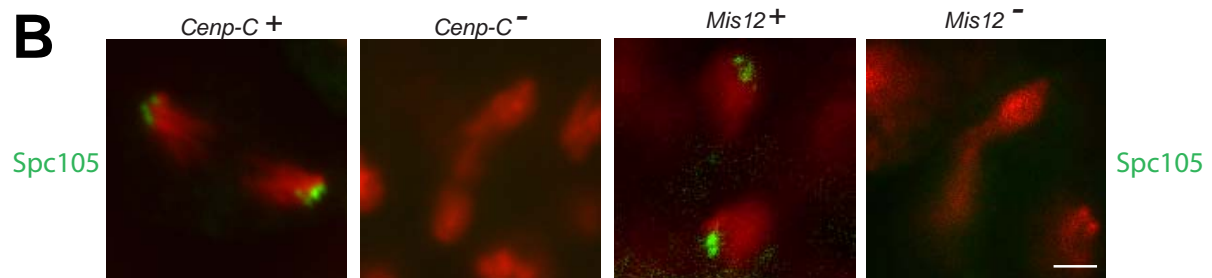
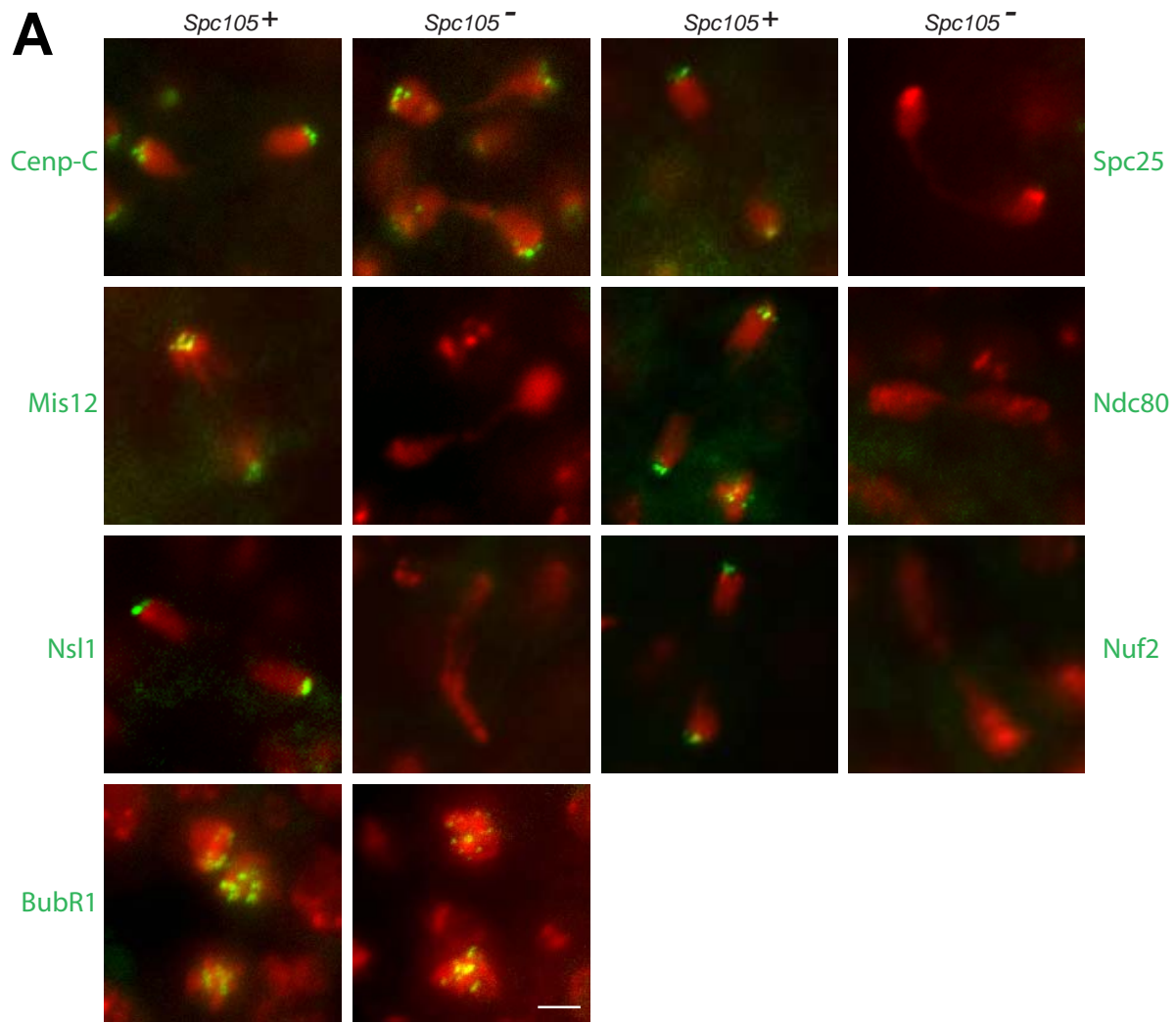
(D) To evaluate SAC function, 10-12 hour embryos were incubated for 45 min in medium without (- colchicine) or with colchicine (+ colchicine) before fixation and labeling with a DNA stain (*DNA*) and antibodies against phospho-histone H3 (*PH3*) and against β -galactosidase for genotype identification (not shown). High magnification views of CNS regions are shown from *Spc105⁺* sibling embryos (*Spc105⁺*), from *Spc105^l* mutant embryos with transgenes driving the expression of either full length (*Spc105^l + FL*) or the C-terminal region of *Spc105* (*Spc105^l + C*), as well as of *mad2* mutant embryos (*mad2^P*). Bar = 20 μm .

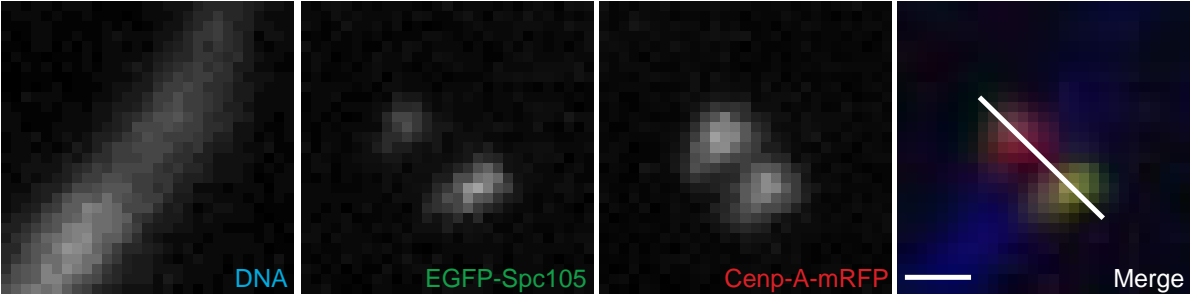
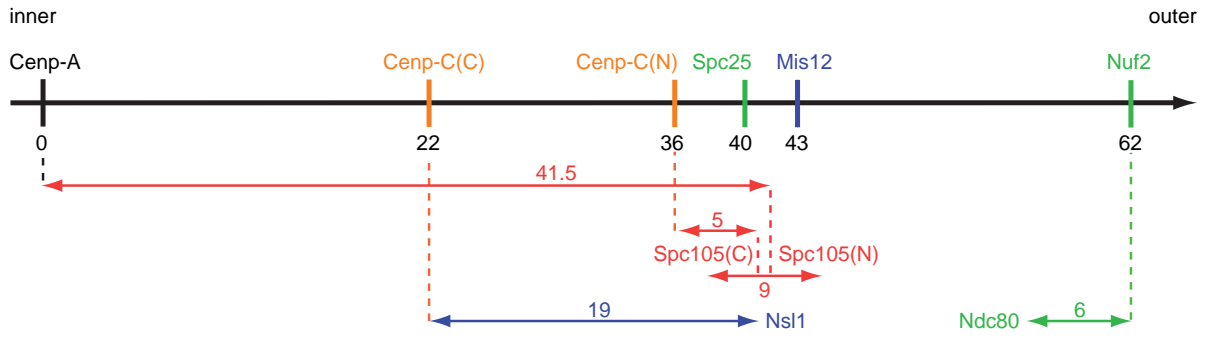
(E) The bar diagram represents quantification of the number of *PH3*-positive cells in the CNS of embryos treated as described and illustrated in panel D. The average density of *PH3* cells

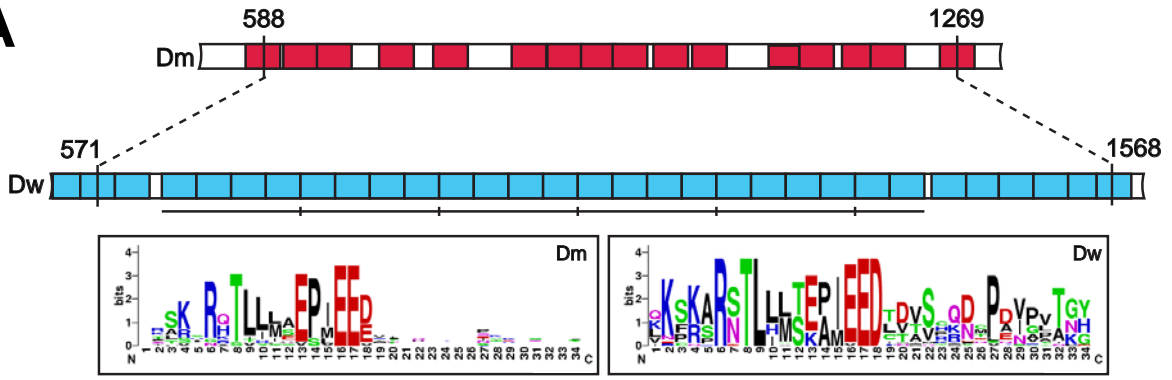
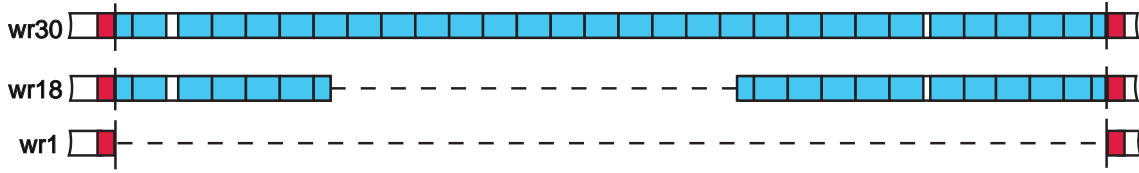
in mock-treated *Spc105*⁺ sibling embryos was set to 1. Ten embryos were analyzed for each of the genotypes indicated below the bars.

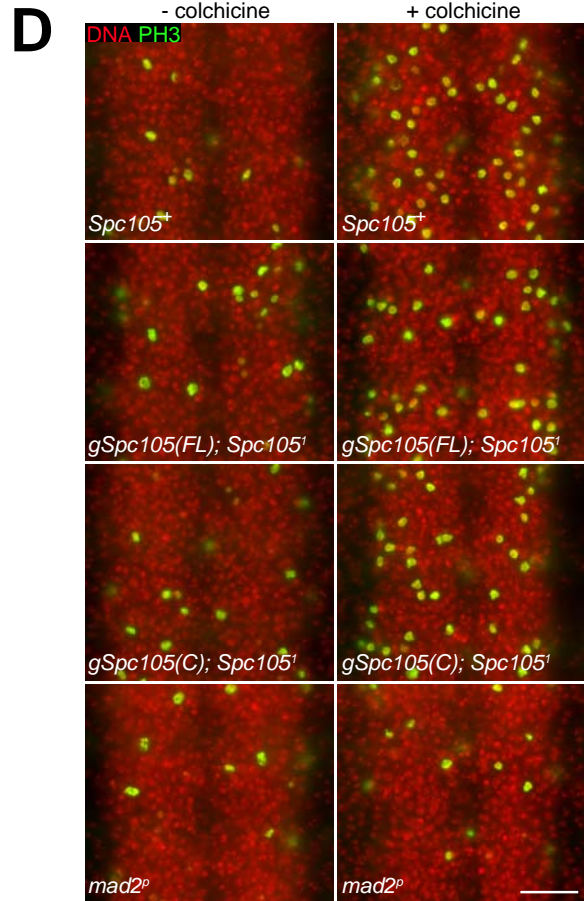
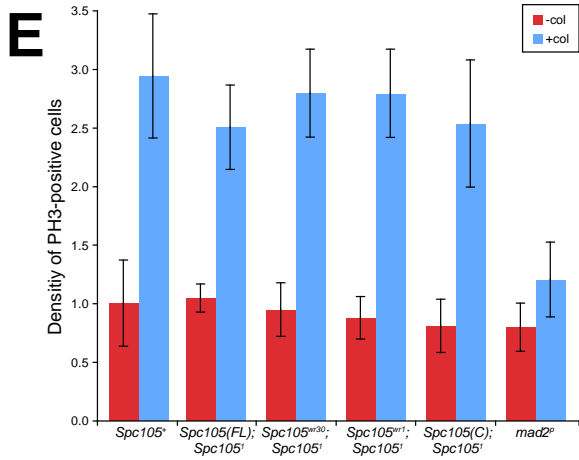
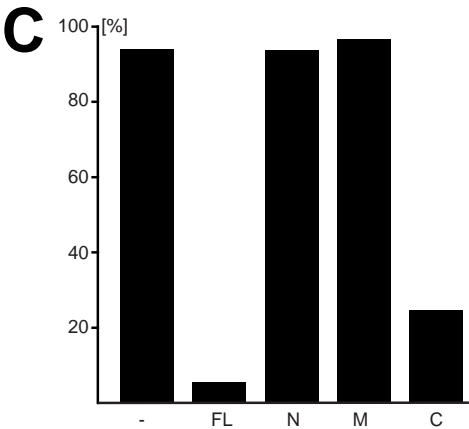
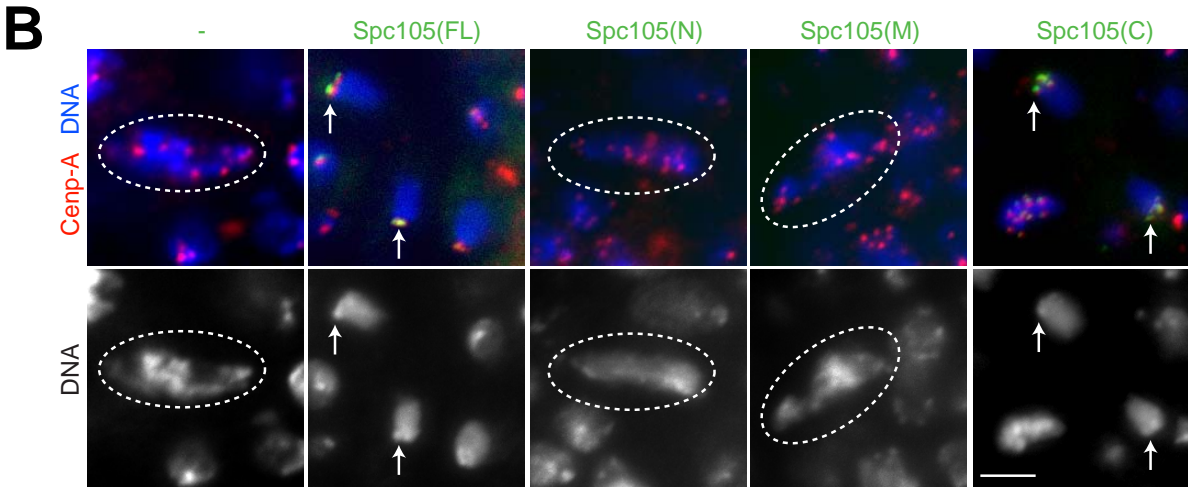
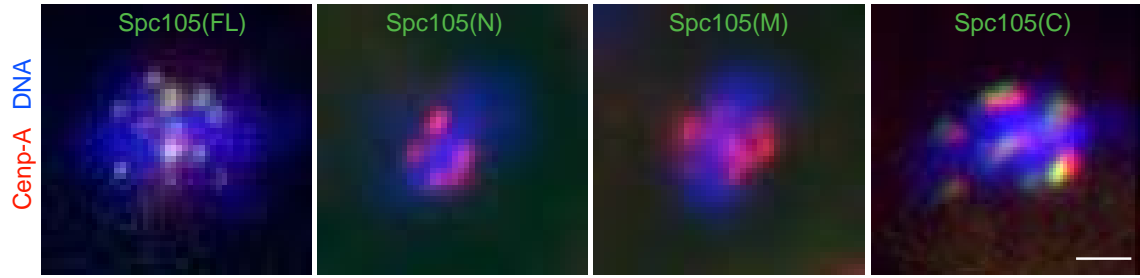
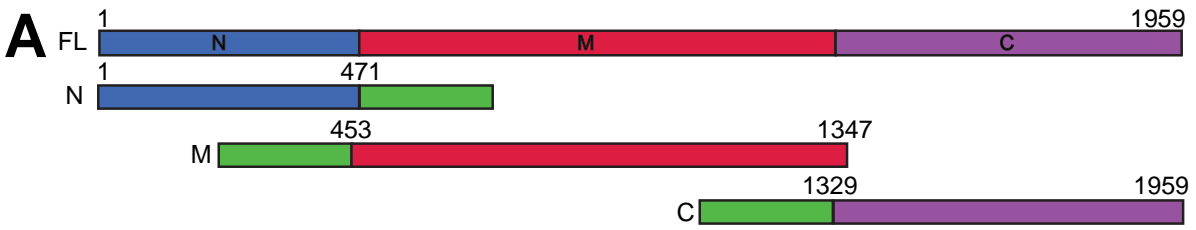
A**C****B****D**

A**B**



A**B**

A**B**



Intrakinetochore localization and essential functional domains of *Drosophila* Spc105

Ralf B Schittenhelm, Romanas Chaleckis and Christian F Lehner

Institute of Zoology, University of Zurich, Winterthurerstrasse 190, CH-8057 Zurich, Switzerland (christian.lehner@zool.uzh.ch)

Supplementary Information

Supplementary Materials and Methods

Genetic identification of *Drosophila* Spc105

The modifier screen that led to the identification of *Drosophila* Spc105 was analogous to the one which led to the identification of *Drosophila* Cenp-C (Heeger et al, 2005). We used the Exelixis set of chromosomal deficiencies which provides about 56% coverage of the euchromatin (Parks et al, 2004). The deficiencies were crossed individually into a background carrying the *GMR-thrΔC* transgene (Heeger et al, 2005). This transgene drives overexpression of a dominant negative, C-terminally truncated version of the Three rows (Thr) protein during eye development. Wild-type Thr is required for *Drosophila* Separase function and sister chromatid separation during mitosis (Jäger et al, 2001). The *GMR-thrΔC* transgene results in a rough eye phenotype visible in adult flies. Deficiencies, which behaved as dominant enhancers or suppressors of this rough eye phenotype, were further characterized. To assess the specificity of the observed genetic interactions, all deficiencies were also crossed individually in parallel into several other transgenic backgrounds. A first background contained *GMR-GAL4* and *UAS-pim-myc* (Heeger et al, 2005). *pimples* (*pim*) encodes the *Drosophila* securin and *pim* overexpression inhibits Separase function and sister chromatid separation during mitosis (Leismann & Lehner, 2003). A second background contained *GMR-GAL4* and *UAS-EGFP-Cenp-C(C)*. The overexpression of the C-terminal region of *Drosophila* Cenp-C (amino acids 1009 - 1411)

fused to EGFP leads to an aberrant eye phenotype as described before (Heeger et al, 2005). A third and fourth background contained *GMR-GAL4*, *UAS-OTD* or *GMR-OTD M.1* (Heeger et al, 2005). GMR-directed overexpression of the OTD transcription factor does also result in a rough eye phenotype for reasons that have not been characterized in detail, but are unlikely to be connected with sister chromatid separation or centromere defects. Deficiencies, which also resulted in a modification of the *GMR-OTD M.1* or *GMR-GAL4*, *UAS-OTD* phenotype, were therefore not further analyzed. The results of our Exelixis deficiency screen are summarized in Supplementary Table I.

Of all the analyzed deficiencies, the chromosome with *Df(3R)Exel9014* displayed the strongest specific interactions with *GMR-thrΔC* and *GMR-GAL4*, *UAS-pim-myc*. However, meiotic recombination with a wild-type chromosome allowed a genetic separation of the interaction locus from the deficiency. Recombinant chromosomes carrying the interaction locus, but not the deficiency, were found to be associated with recessive lethality. Meiotic recombination mapping of the recessive lethality was achieved with defined P element insertions as described (Zhai et al, 2003). As illustrated in Supplementary Figure 10, this placed the locus near the centromere of chromosome III. Available deficiencies deleting centromeric or pericentromeric regions were obtained from the Bloomington *Drosophila* Stock Center and tested for complementation of the recessive lethality associated with the interacting chromosomes. Among these *Df(3L)Exel6136*, *Df(3L)ri-79c* and *Df(3L)Pc-Mk*, but not *Df(3L)ri-XT1*, were found to complement. These observations suggested the presence of the interacting locus within the chromosomal region 77E1-78A2 which contains about 200 kb and 55 genes with *CG11451* as the most likely candidate.

For a molecular characterization of the *CG11451* gene on the interacting chromosome by PCR, we collected eggs from a line containing the interacting chromosome balanced over *TM6C*, *Sb*, *Dfd-GFP* and sorted 5 embryos without GFP expression (embryos homozygous for the interacting chromosome) from 5 embryos with strong GFP expression (embryos homozygous for the balancer chromosome) using an inverted fluorescence microscope. Genomic DNA isolated from the pooled embryos was used as a template for PCR assays with several primer pairs (RaS146/RC15, RC1/RC2, RaS175/RaS176, RC20/RaS177, RC26/RaS178, RC21/

RaS179, RC24/RaS179; see Supplementary Table II) which target various regions within the *CG11451/Spc105* gene. With genomic DNA isolated from embryos homozygous for the interacting chromosome, the primer pair RC26/RaS178 did not generate a PCR fragment except after increasing the elongation step. In this case, the PCR fragment was ~4.2 kb longer than the expected fragment observed with the control DNA (Supplementary Figure 10). Subsequent DNA sequencing revealed the presence of an incomplete DOC transposable element insertion in the 3rd exon of *CG11451/Spc105*. The resulting mutant allele *Spc105^l* codes for a fusion protein in which the first 1548 amino acids of Spc105 are fused to the last 436 amino acids of the putative DOC nucleic acid binding protein. By immunoblotting experiments (Supplementary Figure 1), expression of this fusion protein was found to be very low at most.

Plasmid constructions

pP{CaSpeR-4} (Thummel & Pirrotta, 1991) constructs were made for transgene constructs allowing expression of fluorescently tagged or untagged kinetochores proteins under control of their normal genomic regulatory region. Genomic fragments of *Nsll/Kmn1* (*CG1558*) were amplified from DNA isolated from a *w* mutant fly by PCR. ANW39 and ANW40 were used to amplify a 5' part and ANW41 and ANW42 to amplify a 3' part. The sequence of these primers as well as all other primers used in this work is given in Supplementary Table II. The PCR fragments were introduced into the *EcoRI* – *NotI* and *SpeI* – *XbaI* restriction sites of *pP{CaSpeR-4}*, respectively. The coding sequence of *EGFP* was amplified with ANW43 and HS6 and introduced into the *NotI* – *SpeI* sites between the 5' and 3' parts resulting in *pP{CaSpeR-4}-gEGFP-Nsll*. For the construction of *pP{CaSpeR-4}-giEGFP-Cenp-C*, the coding sequence of *EGFP* was amplified with CS4 and CS5 and introduced into the *BsiWI* restriction site of *pP{CaSpeR-4}-gCenp-C* (Heeger et al, 2005). This construct expresses functional Cenp-C with an internally EGFP fusion after amino acid position 872 of Cenp-C.

For the construction of *Spc105* transgenes, the bacterial artificial chromosome (BAC) clone BACR22116 (Hoskins et al, 2000) was digested with *NotI* and *StuI*. An 8.5 kb fragment containing *Spc105* was inserted into *pBluescript II KS+* (Stratagene) using the *NotI* and *SmaI* sites. The unique restriction site *AfeI* just upstream of the *Spc105* start codon was used to introduce the

EGFP coding sequence isolated by PCR with RaS135 and RaS136. In addition, an inverse PCR with RaS249 and RaS250 was used to delete the N- and M- regions. For the construction of *gSpc105*, *gEGFP-Spc105* and *gSpc105(C)*, *NotI* - *SalI* fragments isolated from the cloning intermediates were inserted into the *NotI* and *XhoI* sites of *pP{CaSpeR-4}*. Additional *Spc105* constructs were generated after introduction of a *NheI* restriction site directly upstream of the stop codon of *Spc105* in *pP{CaSpeR-4}-gSpc105* and *pP{CaSpeR-4}-gEGFP-Spc105*. To this end, two PCR fragments of the C-terminal part of *Spc105* (amplified with RaS140/RaS141 and RaS142/RaS143, respectively), which partially overlapped at their *NheI* containing ends, served as template for an additional PCR with the primers RaS140 and RaS143. The resulting fragment with the introduced *NheI* restriction site was inserted into *pP{CaSpeR-4}-gSpc105* and *pP{CaSpeR-4}-gEGFP-Spc105* by exchanging the corresponding *BglII* – *SpeI* region. The coding sequences of *EGFP*, amplified with RaS80 and RaS144, or *mRFP1*, amplified with RaS92 and RaS 145, were introduced into this *NheI* site resulting in *pP{CaSpeR-4}-gSpc105-EGFP* and *pP{CaSpeR-4}-gEGFP-Spc105-mRFP1*.

The cloning strategy used for the construction of *pP{CaSpeR-4}-gSpc105^{wr1}*, *pP{CaSpeR-4}-gSpc105^{wr18}* and *pP{CaSpeR-4}-gSpc105^{wr30}* is illustrated in Supplementary Figure 11. We first created the construct *pBS-Spc105^{wr1}* (steps 1 – 5). An *NcoI* and an *NheI* restriction site was introduced into the multiple cloning site region of *pBS* by inserting a double stranded oligonucleotide (RaS195/RaS196) into the *SpeI* and *SalI* sites (step 1). Thereafter, four different PCR fragments (*Spc105-1*, *Spc105-2*, *Spc105-3*, *Spc105-4*) were amplified from the *DmSpc105* cDNA clone *LP22061^{FL}* (see below) using the primer pairs RC1/RaS199, RaS200/RaS201, RaS202/RaS203, and RaS204/RaS205, respectively, and consecutively inserted into the *NotI*, *SpeI*, *NcoI*, *NheI* or *SalI* sites of the modified *pBS* vector (steps 2 – 5). The resulting construct *pBS-Spc105^{wr1}* lacked the repetitive middle region of *DmSpc105*. Moreover, it no longer contained the two *NcoI* restriction sites within *DmSpc105* which were exchanged by *SpeI* and *NheI*, respectively. However, it included a novel *NcoI* site between *Spc105-2* and *Spc105-3* which was used to insert *D. willistoni* *Spc105* repeat sequences.

The *DwSpc105* repeat region was first introduced into a cloning intermediate (*pSL-Dw_{wr30}*) constructed with the vector *pSLfa1101fa* (Horn & Wimmer, 2000). First, we removed the

EcoRI restriction site from this vector (step 6) and introduced a PCR fragment containing the *DwSpc105* repeat region into the *NcoI* and *HindIII* restriction sites (step 7). This repeat region was amplified with RaS207 and RaS208 from genomic *D. willistoni* DNA (Tucson *Drosophila* Stock Center). The *NcoI* site at the 5' end was removed from the resulting intermediate (step 8) and additional *NcoI* sites were introduced at the beginning and at the end of the repeat region (steps 9 and 10). These additional *NcoI* sites were introduced by inverse PCR using the primer pairs RaS189/RaS190 and RaS191/RaS192, respectively, after subcloning the *NdeI/MunI* and *EcoRI/HindIII* fragments of *DwSpc105* separately into *pSLfa1101fa*. The mutated *NdeI/MunI* and *EcoRI/HindIII* fragments containing *NcoI* sites were used to replace the non-mutated fragments without *NcoI* sites. The resulting *pSL-Dw_wr30* was subjected to a partial digest with *BglII* (step 11) to create repeat deletions since the *D. willistoni* repeat motif includes a *BglII* site. Several deletions were identified by DNA sequencing and the deletion *pSL-Dw_wr18* was selected for transgene construction. The additional cloning intermediates *pBS-Spc105^{wr30}* and *pBS-Spc105^{wr18}* were obtained by transposing the *NcoI* fragments from *pSL-Dw_wr30* or *pSL-Dw_wr18* into the *NcoI* site of *pBS-Spc105^{wr1}* (step 12). Moreover, the *NotI* and *SalI* fragments of the three *pBS* constructs (*Spc105^{wr1}*, *Spc105^{wr18}* and *Spc105^{wr30}*) were transferred into *pPUAST* (Brand & Perrimon, 1993; *pPUAST-Spc105^{wr1}*, *pPUAST-Spc105^{wr18}* and *pPUAST-Spc105^{wr30}*). Finally, the *BstEII* and *XhoI* fragments of the three *pPUAST* constructs were used to replace the corresponding fragments in *pP{CaSpeR-4}-gSpc105* resulting in *pP{CaSpeR-4}-gSpc105^{wr1}*, *pP{CaSpeR-4}-gSpc105^{wr18}* and *pP{CaSpeR-4}-gSpc105^{wr30}*.

pPUAST constructs containing fragments of *Spc105* cDNA fused to *EGFP* were used for transfection of *Drosophila* S2R+ cells and for generation of transgenic lines allowing *GAL4*-dependent expression during embryogenesis and during eye or wing development. For these constructions, we used the *pPUAST-EGFP(N)* and *pPUAST-EGFP(C)* variants (Schittenhelm et al, 2007) and the plasmid *LP22061* (Rubin et al, 2000). Since this EST clone did not contain the complete *Spc105* cDNA, we added the missing 5' sequences by amplification of a genomic fragment followed by removal of the first intron by inverse PCR. In addition, based on DNA sequencing, *LP22061* also contained a single base pair frame shift mutation near the C-terminal end. We therefore exchanged the mutated region of *LP22061* with the corresponding region of

the incomplete EST clone *LD41231* (Stapleton et al, 2002). The modified plasmid *LP22061^{FL}* was used for PCR isolation of *Spc105* fragments which were subsequently inserted into the *pPUAST-EGFP* variants. Primer pairs used for amplification of the *Spc105* cDNA fragments were RC1/RaS194, RC1/RC2, RC3/RC4 and RC5/RC6 for *pPUAST-Spc105-EGFP*, *pPUAST-Spc105(N)-EGFP*, *pPUAST-EGFP-Spc105(M)* and *pPUAST-EGFP-Spc105(C)*, respectively.

pGBKT7 and *pGADT7* (Clontech) constructs expressing fragments of kinetochore proteins fused to either the DNA-binding or the transcriptional activation domain of *GAL4* were made for yeast two hybrid (Y2H) assays. For these constructions, cDNA fragments were amplified by PCR and inserted into the polylinker site of the vectors. The following EST plasmids were used: *LD22855* (*Bub1*), *RE19545* (*Mis12*), *RE03006* (*Nsl1*), *RE42502* (*Nnf1a*), *LP22061^{FL}* (*Spc105*; see above). Primer pairs used for amplification were: RC55/RC56 for *pGBKT7-Bub1(N)/pGADT7-Bub1(N)*, RC11/RC12 for *pGBKT7-Mis12/pGADT7-Mis12*, RC50/RC51 for *pGBKT7-Nsl1/pGADT7-Nsl1*, RC52/RC53 for *pGBKT7-Nnf1a/pGADT7-Nnf1a*, RC17/RC18 for *pGBKT7-Spc105(N)/pGADT7-Spc105(N)*, RC7/RC8 for *pGBKT7-Spc105(M)/pGADT7-Spc105(M)*, RC9/RC10 for *pGBKT7-Spc105(C)/pGADT7-Spc105(C)*.

Sequence comparisons

The Flybase BLAST Browser was used to identify orthologous Spc105 proteins in different *Drosophila* species (Clark et al, 2007). Quick2D (Biegert et al, 2006) was used for secondary structure predictions and ClustalW (Larkin et al, 2007; Thompson et al, 1994) for multiple sequence alignments. Moreover, repeated protein sequences were identified with RADAR (Heger & Holm, 2000) in combination with visual inspections. Consensus sequences of multiple protein alignments were generated with WebLogo 3 (Crooks et al, 2004). The percentage of identical amino acids between two protein sequences were obtained using BLAST 2 SEQUENCES (Tatusova & Madden, 1999); <http://blast.ncbi.nlm.nih.gov/bl2seq/wblast2.cgi>.

Presentation and quantification of light microscopic data

The immunofluorescent images of fixed samples represent either single focal planes (Figures 1C, 3A, 3B, 4A, 6A, 6B and S5) or multi-focal stacks (Figures 2A, 6D, S1B, S4B, S6A and S7A

with 3, 3, 6, 10, 10 and 10 sections and 250, 700, 250, 500, 250 and 250 nm spacing, respectively). The acquired images were further processed with ImageJ and/or Adobe Photoshop CS3. Stacks were converted into maximum projections in the z direction. Brightness and contrast levels were adjusted in parallel in case of genotype comparisons.

For the quantification of kinetochore signal intensities (Supplementary Figure 6B), *Spc105¹/TM3,Sb,P{w[+m*]=Ubx-lacZ.w[+]}* female flies carrying one of the following transgenes (*gEGFP-Ndc80 II.1*, *gEGFP-Nuf2 II.1*, *gSpc25-EGFP II.1*, *gMis12-EGFP II.1* or *gEGFP-BubR1 X.1*) were crossed to *Spc105¹/TM3,Sb,P{w[+m*]=Ubx-lacZ.w[+]}* males carrying either *gSpc105^{wr1} II.1* or *gSpc105(C) II.4* transgenes, or a wild-type chromosome. 6-8 hour old embryos were collected at 25°C and stained with a mouse monoclonal antibody against β -galactosidase for genotype determination, with a DNA stain (Hoechst 33258) and with a rabbit antibody against Cenp-A/Cid. Multi-focal stacks (250 nm spacing) were acquired from epidermal cells undergoing the 16th round of mitosis using a 100x/1.4 oil immersion objective. The stacks were deconvolved (Huygens Remote Manager v1.0 beta 2; Montpellier RIO imaging) and subsequently converted into maximum projections in the z direction using ImageJ. Kinetochore signal intensity in a mitotic cell was determined essentially as described (Joglekar et al, 2006). Two concentric squares (60 px x 60 px and 80 px x 80 px, respectively) which both completely enclosed all of the kinetochore signals were selected. The mean signal intensity per pixel within the smaller square was corrected by the background value which was defined as the average pixel intensity present in the region enclosed by the larger but not by the smaller square in each Z section. Background corrected signal intensities were integrated over the complete stack. More than 20 mitotic cells from at least five different embryos were analyzed for each genotype.

For the quantification of phospho-histone H3 (PH3)-positive cells (Figure 6E), stacks including the CNS were acquired from 10-12 hour embryos. After maximum projection, the number of PH3-positive cells in the CNS region was counted. The analyzed CNS regions in case of *Spc105⁺* sibling embryos incubated without colchicine contained 21 +/- 7 PH3-positive cells.

Time-lapse analyses of *Spc105* mutant and sibling control embryos were performed with a

Leica TCS SP1 confocal microscope acquiring stacks of 5 sections with 240 nm spacing every 15 seconds using a 63x objective. After maximum projection of the stacks, Gaussian filtering was applied followed by adjustment of brightness and contrast.

Supplementary References

Biegert A, Mayer C, Remmert M, Soding J, Lupas AN (2006) The MPI Bioinformatics Toolkit for protein sequence analysis. *Nucleic Acids Res* **34**: W335-339

Brand AH, Perrimon N (1993) Targeted gene expression as a means of altering cell fates and generating dominant phenotypes. *Development* **118**: 401-415

Buffin E, Emre D, Karess RE (2007) Flies without a spindle checkpoint. *Nat Cell Biol* **9**: 565-572

Clark AG, Eisen MB, Smith DR, Bergman CM, Oliver B, Markow TA, Kaufman TC, Kellis M, Gelbart W, Iyer VN, Pollard DA, Sackton TB, Larracunte AM, Singh ND, Abad JP, Abt DN, Adryan B, Aguade M, Akashi H, Anderson WW et al (2007) Evolution of genes and genomes on the *Drosophila* phylogeny. *Nature* **450**: 203-218

Crooks GE, Hon G, Chandonia JM, Brenner SE (2004) WebLogo: a sequence logo generator. *Genome Res* **14**: 1188-1190

Heeger S, Leismann O, Schittenhelm R, Schraidt O, Heidmann S, Lehner CF (2005) Genetic interactions of Separase regulatory subunits reveal the diverged *Drosophila* Cenp-C homolog. *Genes Dev* **19**: 2041-2053

Heger A, Holm L (2000) Rapid automatic detection and alignment of repeats in protein sequences. *Proteins* **41**: 224-237

Horn C, Wimmer EA (2000) A versatile vector set for animal transgenesis. *Dev Genes Evol* **210**: 630-637

Hoskins RA, Nelson CR, Berman BP, Lavery TR, George RA, Ciesiolka L, Naemuddin M, Arenson AD, Durbin J, David RG, Tabor PE, Bailey MR, DeShazo DR, Catanese J, Mammoser A, Osoegawa K, de Jong PJ, Celniker SE, Gibbs RA, Rubin GM et al (2000) A BAC-based physical map of the major autosomes of *Drosophila melanogaster*. *Science* **287**: 2271-2274

Jäger H, Herzig A, Lehner CF, Heidmann S (2001) *Drosophila* separase is required for sister chromatid separation and binds to PIM and THR. *Genes Dev* **15**: 2572-2584.

Joglekar AP, Bouck DC, Molk JN, Bloom KS, Salmon ED (2006) Molecular architecture of a kinetochores-microtubule attachment site. *Nat Cell Biol* **8**:581-5

Larkin MA, Blackshields G, Brown NP, Chenna R, McGettigan PA, McWilliam H, Valentin F, Wallace IM, Wilm A, Lopez R, Thompson JD, Gibson TJ, Higgins DG (2007) Clustal W and Clustal X version 2.0. *Bioinformatics* **23**: 2947-2948

Leismann O, Lehner CF (2003) *Drosophila* securin destruction involves a D-box and a KEN-box and promotes anaphase in parallel with Cyclin A degradation. *J Cell Sci* **116**: 2453-2460

Parks AL, Cook KR, Belvin M, Dompe NA, Fawcett R, Huppert K, Tan LR, Winter CG, Bogart KP, Deal JE, Deal-Herr ME, Grant D, Marcinko M, Miyazaki WY, Robertson S, Shaw KJ, Tabios M, Vysotskaia V, Zhao L, Andrade RS et al (2004) Systematic generation of high-resolution deletion coverage of the *Drosophila melanogaster* genome. *Nat Genet* **36**: 288-292

Rubin GM, Yandell MD, Wortman JR, Gabor Miklos GL, Nelson CR, Hariharan IK, Fortini ME, Li PW, Apweiler R, Fleischmann W, Cherry JM, Henikoff S, Skupski MP, Misra S, Ashburner M, Birney E, Boguski MS, Brody T, Brokstein P, Celniker SE et al (2000) Comparative genomics of the eukaryotes. *Science* **287**: 2204-2215.

Schittenhelm RB, Heeger S, Althoff F, Walter A, Heidmann S, Mechtler K, Lehner CF (2007) Spatial organization of a ubiquitous eukaryotic kinetochore protein network in *Drosophila* chromosomes. *Chromosoma* **116**: 385-402

Stapleton M, Carlson J, Brokstein P, Yu C, Champe M, George R, Guarin H, Kronmiller B, Pacleb J, Park S, Wan K, Rubin GM, Celniker SE (2002) A *Drosophila* full-length cDNA resource. *Genome Biol* **3**: RESEARCH0080.0081-0080.0088

Tatusova TA, Madden TL (1999) BLAST 2 Sequences, a new tool for comparing protein and nucleotide sequences. *FEMS Microbiol Lett* **174**: 247-250

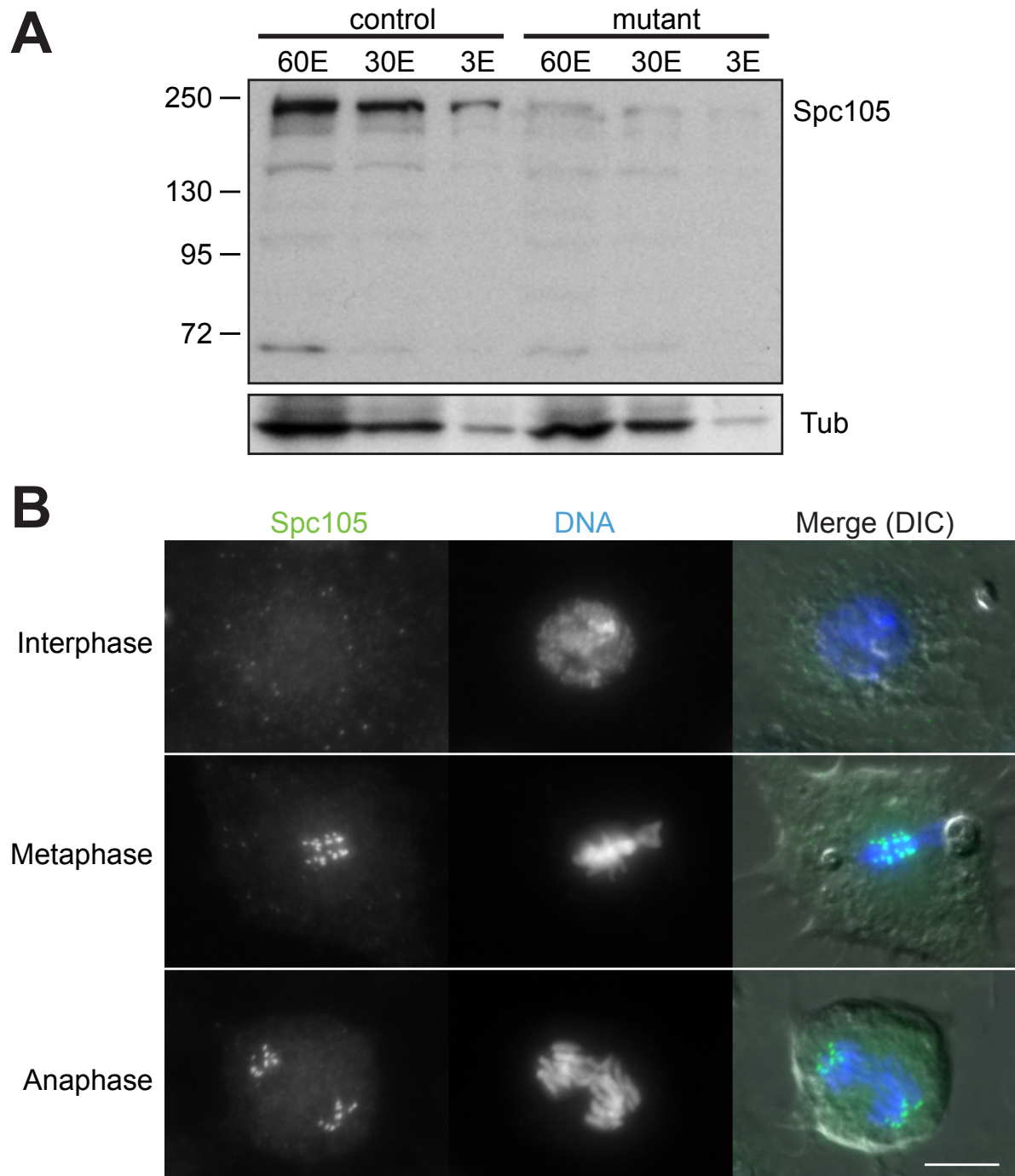
Thompson JD, Higgins DG, Gibson TJ (1994) CLUSTAL W: improving the sensitivity of progressive multiple sequence alignment through sequence weighting, position-specific gap penalties and weight matrix choice. *Nucleic Acids Res* **22**: 4673-4680

Thummel CS, Pirrotta V (1991) Technical Notes: New pCaSpeR P-element vectors. *Drosophila Information Newsletter* **2**

Zhai RG, Hiesinger PR, Koh TW, Verstreken P, Schulze KL, Cao Y, Jafar-Nejad H, Norga KK, Pan H, Bayat V, Greenbaum MP, Bellen HJ (2003) Mapping *Drosophila* mutations with molecularly defined P element insertions. *Proc Natl Acad Sci U S A* **100**: 10860-10865

Supplementary Figures

Supplementary Figure 1

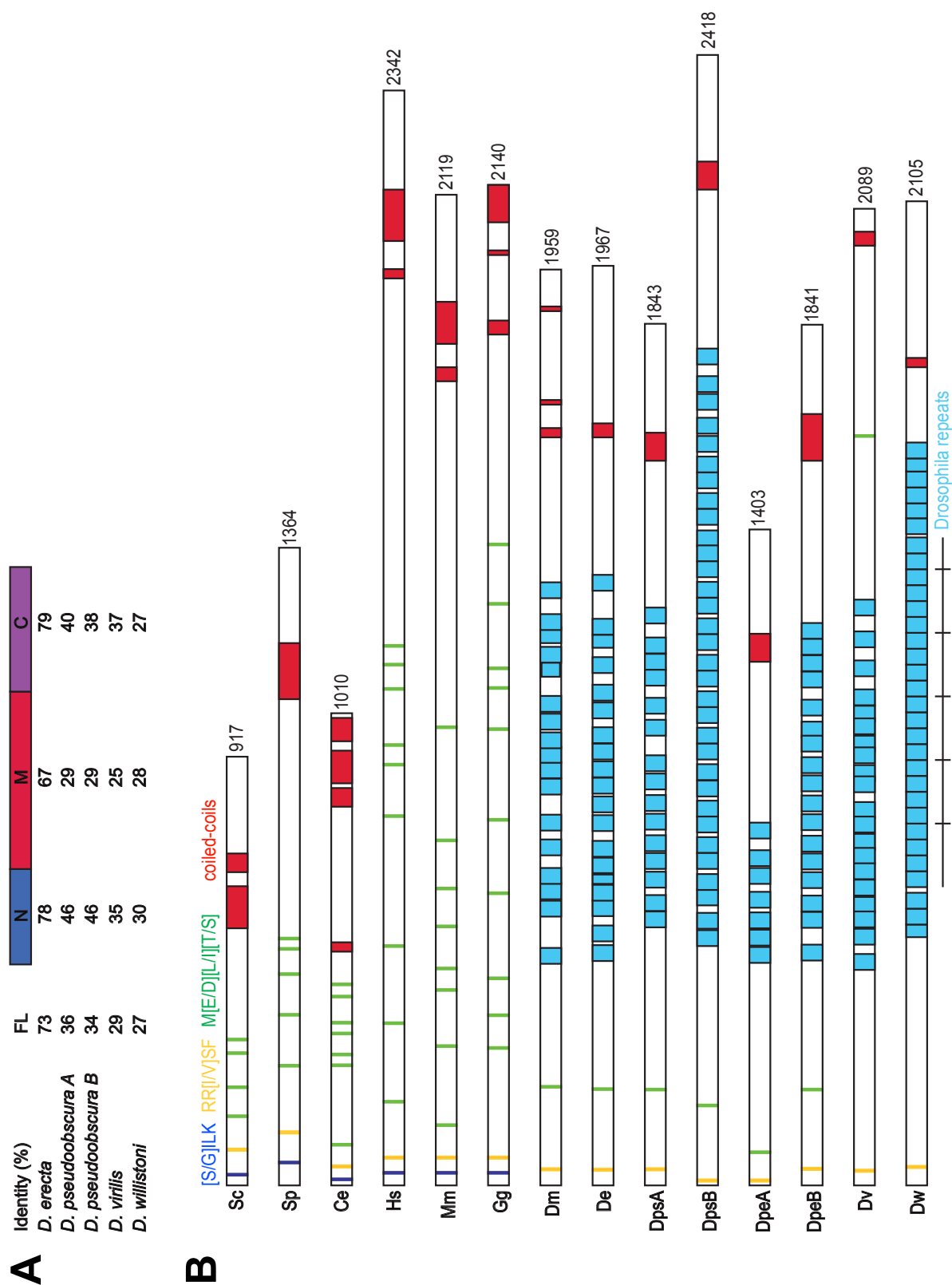


Supplementary Figure 1. Detection of Spc105 by immunoblotting and immunofluorescence with affinity-purified antibodies.

(A) Extracts prepared from sorted homozygous *Spc105^l* (*mutant*) and sibling control embryos (*control*) at the stage of mitosis 16 were analyzed by immunoblotting with affinity-purified antibodies (1O1) against *Drosophila* Spc105 (Spc105). The equivalent of 60, 30 or 3 embryos was loaded as indicated (*60E*, *30E*, *3E*). Our molecular analysis suggests that a protein product with the first 1548 amino acids of Spc105 fused to the last 436 amino acids of the putative DOC nucleic acid binding protein might be expressed from the *Spc105^l* allele. As the size of this fusion protein is nearly identical to wild-type Spc105, we do not know to what extent the weak band observed in *Spc105^l* mutant extracts represents this predicted *Spc105^l* fusion protein or residual maternally contributed wild-type Spc105. It is clear, however, that the levels of wild-type Spc105 present in *Spc105^l* mutant embryos at the stage of mitosis 16 must be less than 10% of the Spc105 levels present in wild type. Probing with an antibody against α -tubulin (*Tub*) served as a loading control. The *numbers* on the left side mark the position of molecular weight markers (kDa).

(B) Affinity-purified antibodies against Spc105 (2D7) were used for immunofluorescent labeling of *Drosophila* S2R⁺ cells. Similar results were obtained with another affinity-purified antibody (1O1) against Spc105 (not shown). Cells were also labeled with a DNA stain. While weak diffuse anti-Spc105 signals as well as some dots were observed in interphase cells (*upper row*), prominent signals at kinetochores were apparent during metaphase (*middle row*), anaphase (*bottom row*) and other mitotic stages (data not shown). Bar = 5.5 μ m.

Supplementary Figure 2



Supplementary Figure 2. Comparison of eukaryotic Spc105 homologs.

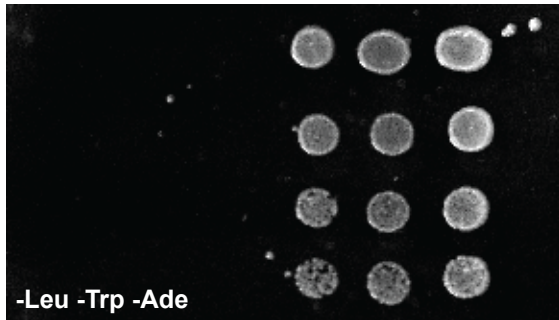
(A) Amino acid sequence comparisons between Drosophilid Spc105 homologs indicate that the N- and C-terminal regions display a higher conservation than the repetitive middle region. Amino acid identities observed between *D. melanogaster* Spc105 and other Drosophilid homologs (*D. erecta*, *D. pseudoobscura*, *D. virilis* and *D. willistoni*) are given in %. Duplicated genes (*Spc105A* and *Spc105B*) were identified in *D. pseudoobscura*. Values obtained with either the predicted full length proteins (*FL*), the N-terminal (*N*), middle (*M*) or C-terminal (*C*) domains are listed.

(B) The structure of the Spc105 homologs of *Saccharomyces cerevisiae* (*Sc*), *Schizosaccharomyces pombe* (*Sp*), *Caenorhabditis elegans* (*Ce*), *Homo sapiens* (*Hs*), *Mus musculus* (*Mm*), *Gallus gallus* (*Gg*), *Drosophila melanogaster* (*Dm*), *Drosophila erecta* (*De*), *Drosophila pseudoobscura* (*DpsA* and *DpsB*), *Drosophila persimilis* (*DpeA* and *DpeB*), *Drosophila virilis* (*Dv*) and *Drosophila willistoni* (*Dw*) is illustrated schematically. The *obscura* group species *Drosophila pseudoobscura* and *Drosophila persimilis* are characterized by duplicated *Spc105* genes. The *numbers* indicate the length of the Spc105 homologs in amino acids. The *red boxes* indicate putative coiled-coiled regions. The positions of the [S/G]ILK, RR[I/V]SF and the repeated M[E/D][L/I][T/S] motifs are depicted by the *dark blue*, *yellow* and *green lines*, respectively. The repeats in Drosophilid species, which are indicated by the *light blue boxes*, do not correspond to the M[E/D][L/I][T/S] consensus which is observed in the repeats of other eukaryotes. The *solid line* below *DwSpc105* depicts the clustering of its core repeats into 5.5 periods. Each period consists of four repeats.

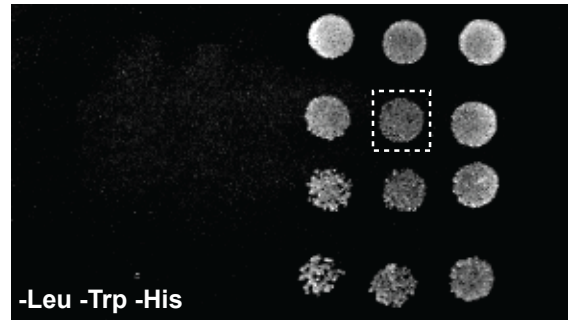
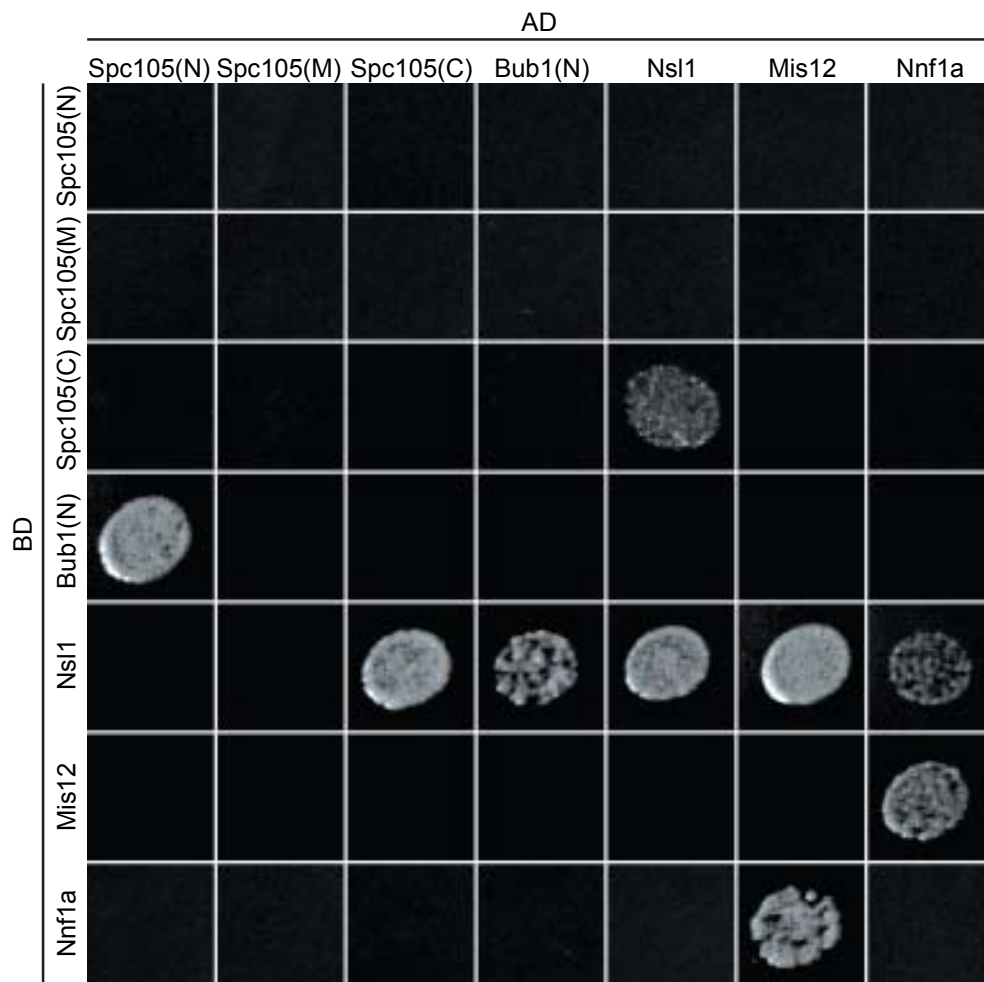
Supplementary Figure 3

A

AD: Nsl1
 BD: Spc105
 N N M M C C + -



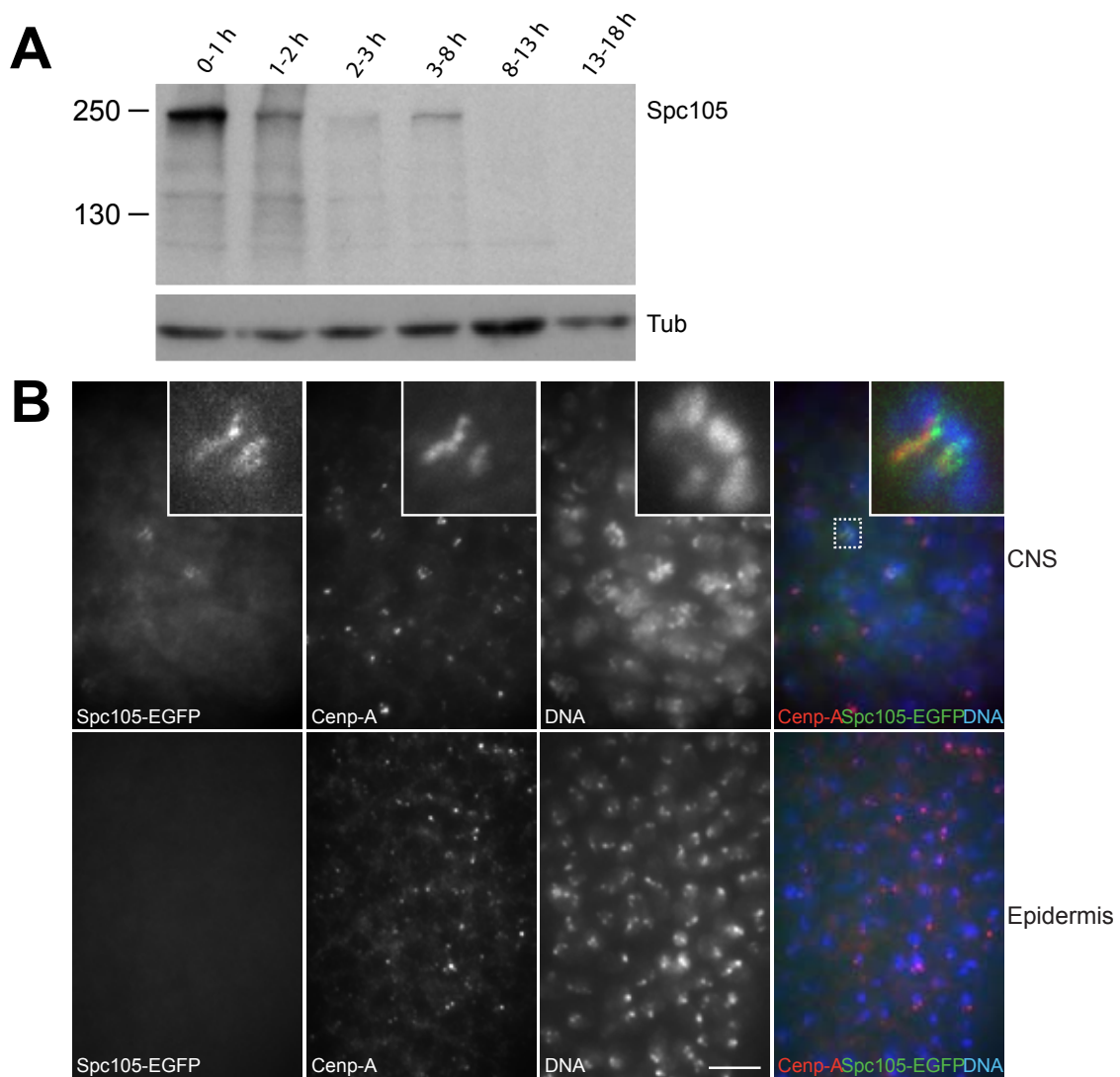
AD: Nsl1
 BD: Spc105
 N N M M C C + -

**B**

Supplementary Figure 3. Yeast two-hybrid analysis of protein-protein interactions of Spc105.

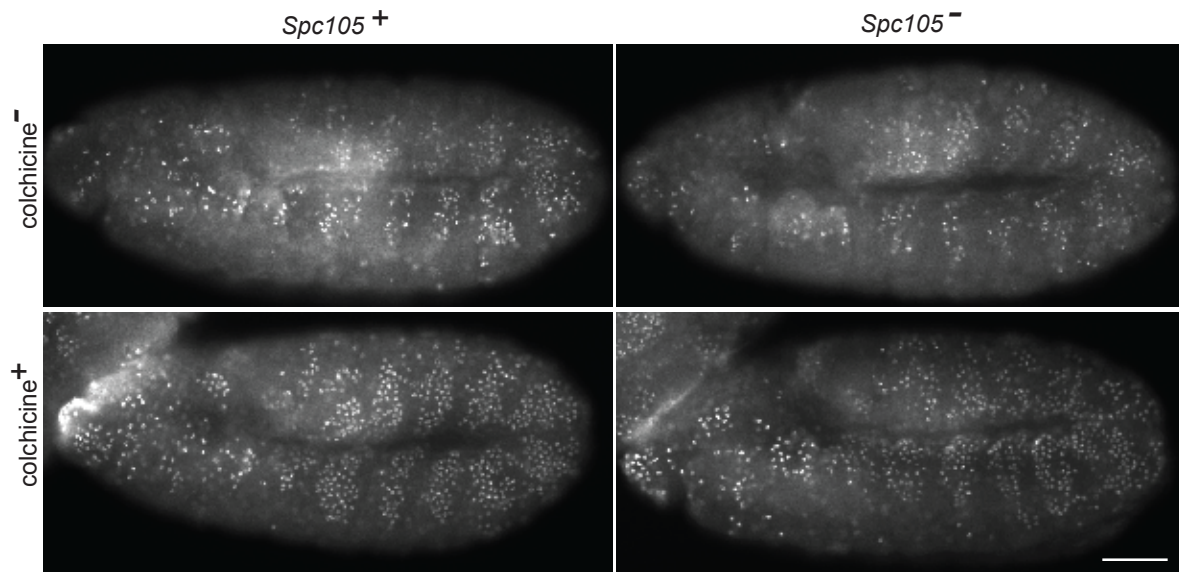
(A) Yeast two-hybrid experiments were performed as illustrated for our analysis of the interaction of *Drosophila Nsl1* with the N-terminal (N), repetitive middle (M) and C-terminal (C) domain of Spc105. *Nsl1* was expressed as a fusion with the transcriptional activation domain of *GAL4* (AD) from a first construct. The *Spc105* domains were expressed as fusions with the DNA binding domain of *GAL4* (BD) from a second one. After selection of cotransformants, serial dilutions were spotted on appropriate selective plates (-Leu, -Trp, -Ade in the left panel, -Leu, -Trp, -His in the right panel) to assay for interaction-mediated growth. Cotransformation of the two constructs *pGADT7-SV40T* and *pGBKT7-p53* was used for positive control (+). Cotransformation of the *pGADT7* and *pGBKT7* vectors served as negative control (-).

(B) A summary of our analysis is presented with the same selected regions from selective medium plates lacking leucine, tryptophan and histidine (as illustrated with the hatched white square in panel A).

Supplementary Figure 4**Supplementary Figure 4. Expression pattern of Spc105 during embryogenesis.**

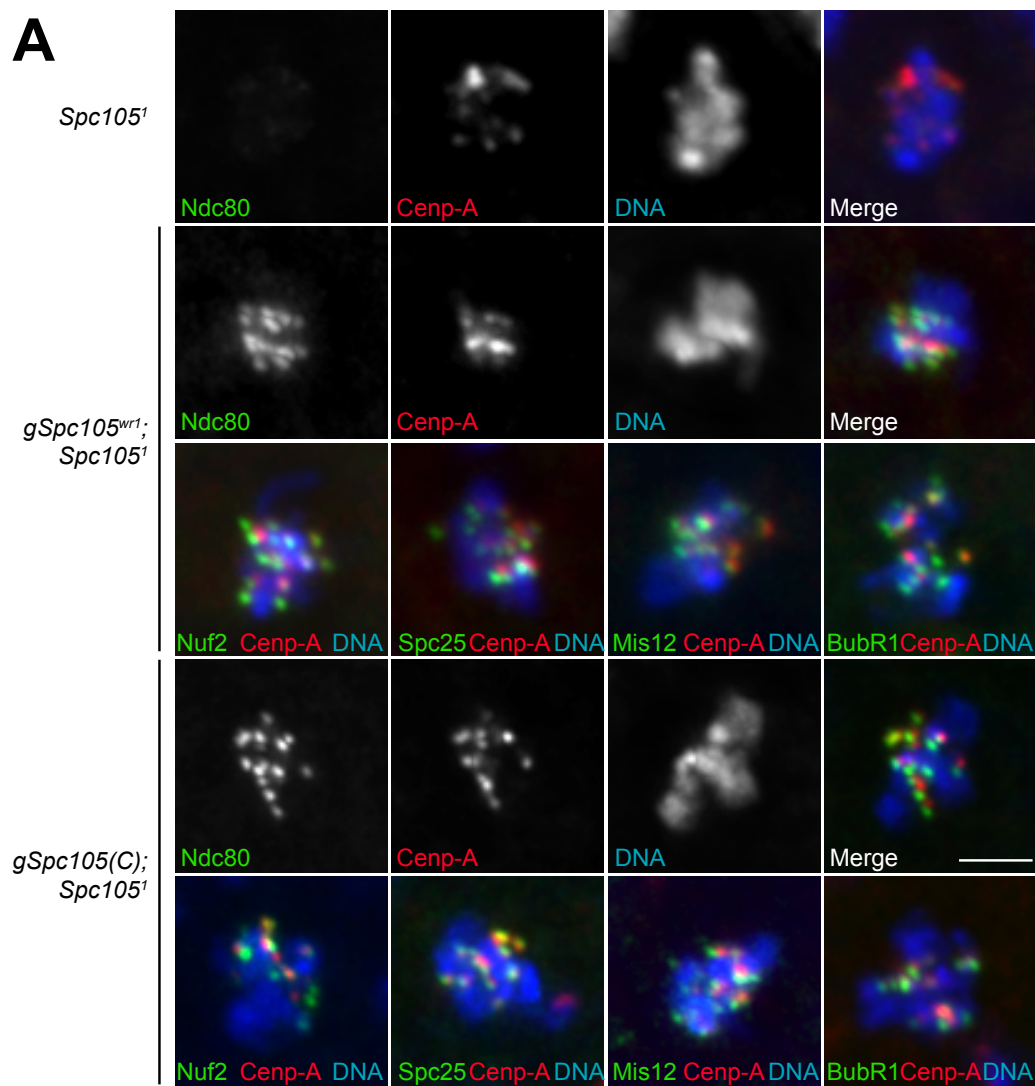
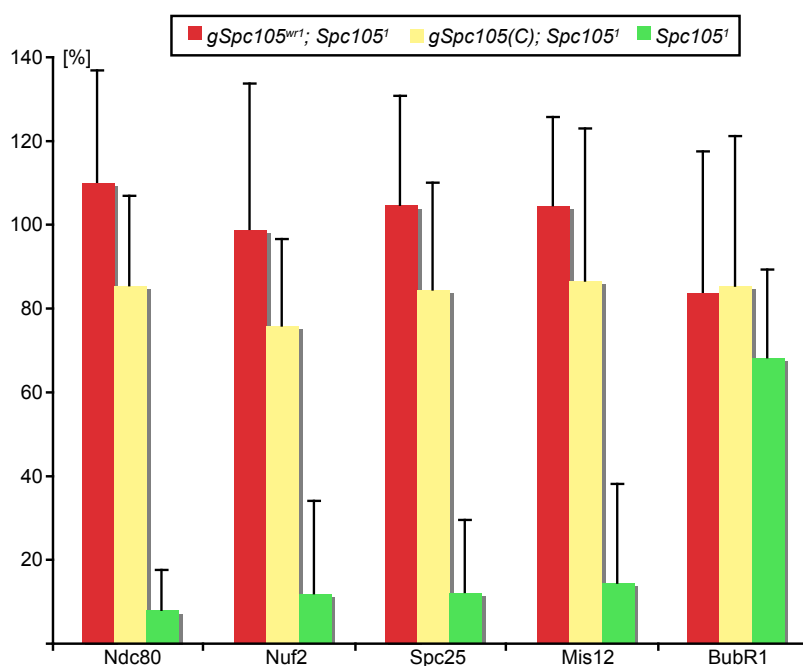
(A) Control embryos were collected and aged as indicated above the lanes before extract preparation and immunoblotting with rabbit antibody 101 against Spc105 (*Spc105*) and anti- α -tubulin (*Tub*) to control for loading. Analogous results were obtained with *gSpc105-EGFP* embryos and anti-EGFP (not shown). The *numbers* on the left side mark the position of molecular weight markers (kDa).

(B) Analysis of Spc105-EGFP levels in *gSpc105-EGFP* embryos after germband retraction (about 11 hours after egg deposition) revealed signals in mitotic CNS cells. In contrast, Spc105-EGFP was not detected in the postmitotic epidermal cells. Centromeres and chromosomes were revealed by double labeling with anti-Cenp-A/Cid (*Cenp-A*) and a DNA stain (*DNA*). The *insets* in the *upper row* show a prometaphase cell at higher magnification. Bar = 10 μ m.

Supplementary Figure 5**Supplementary Figure 5. Analysis of spindle assembly checkpoint function in *Spc105* mutants at the stage of mitosis 16.**

Spc105⁺ (left column) and *Spc105*⁻ (right column) embryos were fixed and labeled with an antibody against phospho-histone H3 (PH3) after a 20 minute incubation with (lower row) or without colchicine (upper row). A similar increase in the number of PH3-positive cells was observed in *Spc105*⁺ sibling control and in *Spc105*⁻ mutant embryos after incubation in colchicine. Moreover, in the absence of colchicine, the number of Ph3-positive cells was not detectably elevated in *Spc105*⁻ compared to *Spc105*⁺ embryos. Bar = 60 μ m.

Supplementary Figure 6

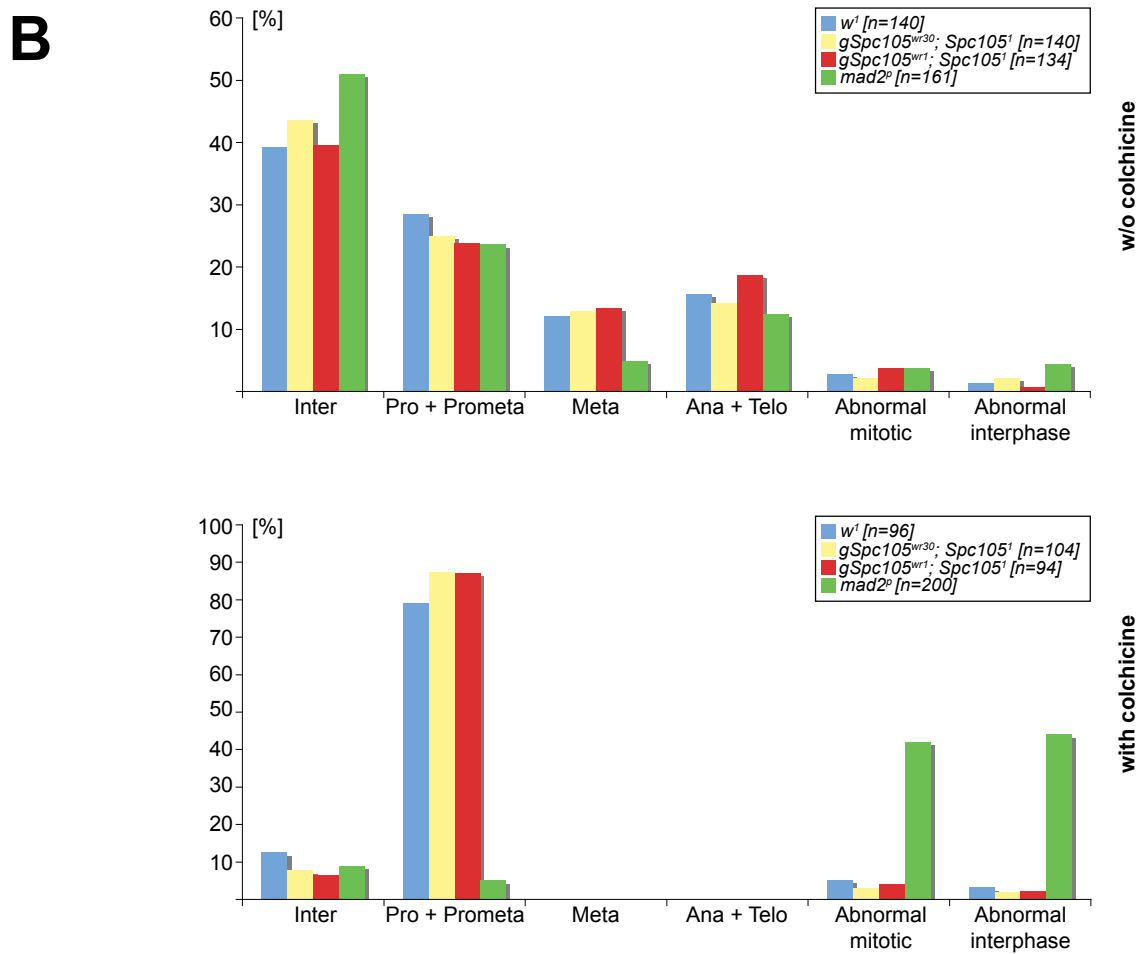
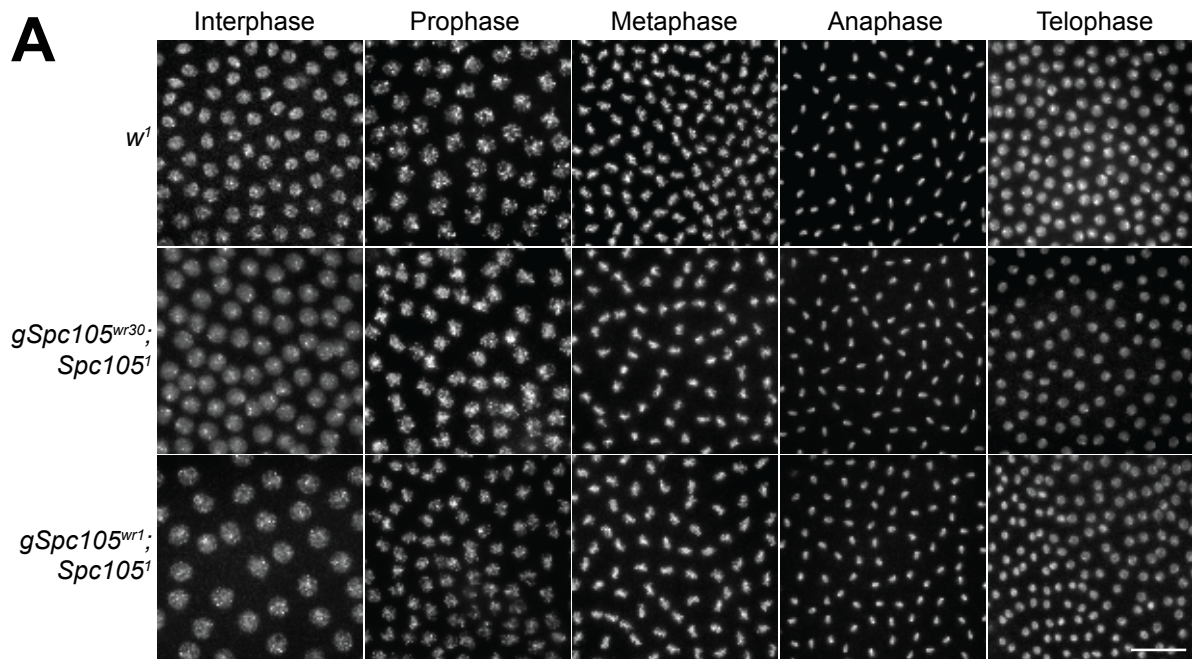
**B**

Supplementary Figure 6. Localization of kinetochore proteins in *Spc105* mutants.

(A) EGFP fusions of Ndc80, Nuf2, Spc25, Mis12 and BubR1 were expressed in *Spc105^l* embryos without (1st row) or with the transgene *gSpc105^{wr1}* (2nd and 3rd row) or *gSpc105(C)* (4th and 5th row). Embryos at the stage of mitosis 16 were double labeled with an antibody against Cenp-A/Cid (*Cenp-A*) and a DNA stain (*DNA*). Bar = 5 μ m.

(B) EGFP signal intensities in prometaphase of mitosis 16 from embryos as illustrated in panel A were quantified. For every EGFP fusion and genotype, *Spc105⁺* sibling embryos present in the same collection were analyzed in parallel and the average EGFP signal intensity in these embryos was set to 100%. Relative intensities in *Spc105^l* (green), *gSpc105^{wr1}*; *Spc105^l* (red) and *gSpc105(C)*; *Spc105^l* (yellow) are indicated by bars (with s.d.)

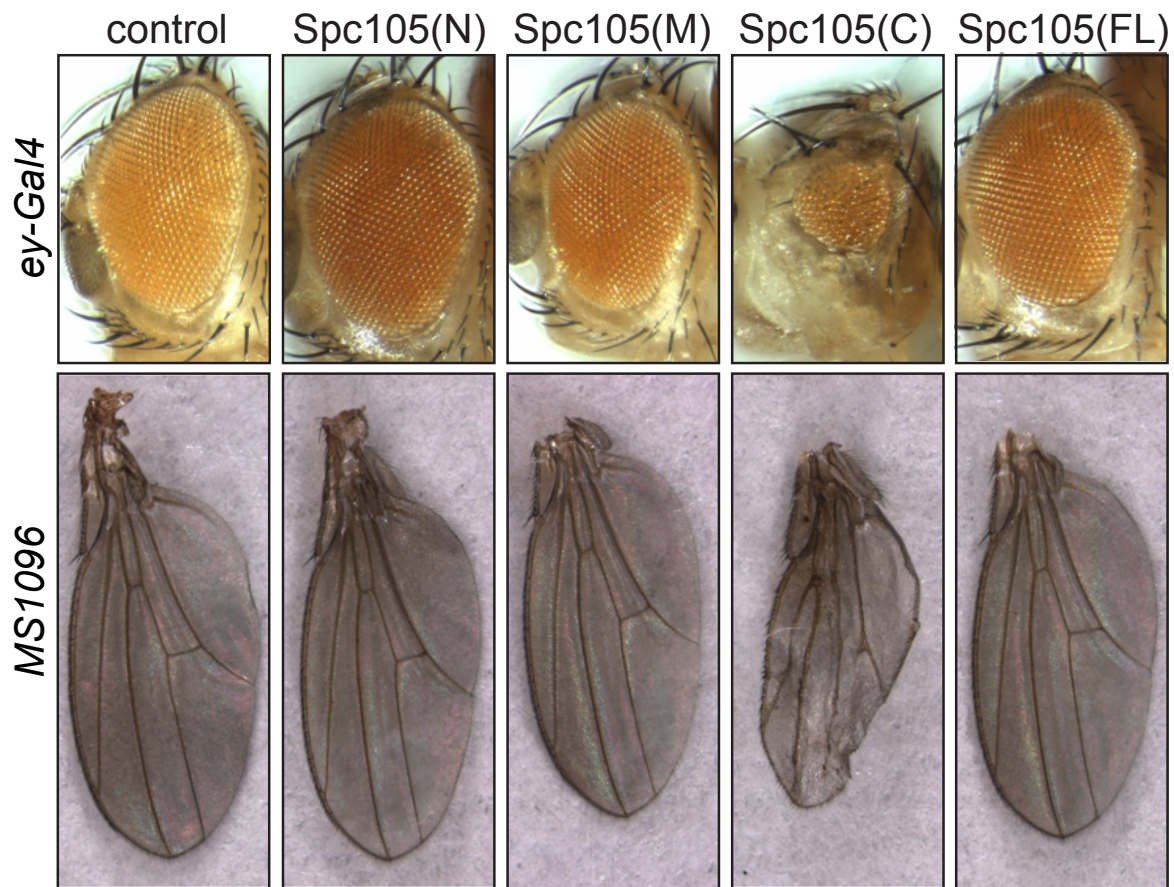
Supplementary Figure 7



Supplementary Figure 7. Cell cycle progression and SAC function in *Spc105* mutants.

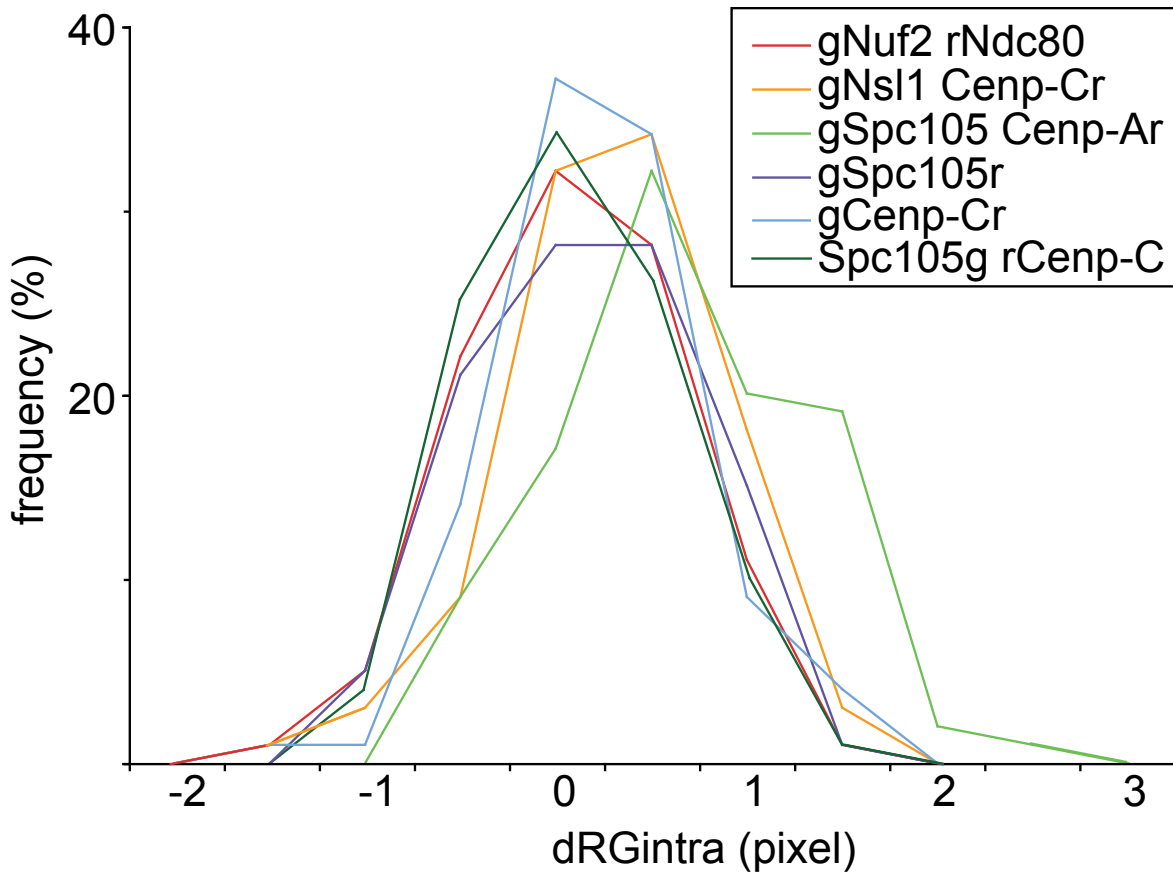
(A) Embryos (1-2 hours after egg deposition) were collected, fixed and labeled with a DNA stain. The genotype of the females was either w^l (top row), $gSpc105^{wr30}$; $Spc105^l$ (middle row) or $gSpc105^{wr1}$; $Spc105^l$ (bottom row). Selected regions from embryos in interphase, prophase, metaphase, anaphase and telophase illustrate that *D. melanogaster* Spc105 containing either 30 *D. willistonii* repeats, or only one repeat instead of the normal repetitive middle domain, allows a normal progression through the syncytial blastoderm cycles. Bar = 20 μ m.

(B) Embryos (1-2 hours after egg deposition) were incubated for 20 min either without (upper row) or with colchicine (lower row) before fixation and DNA staining. The frequency of embryos in different cell cycle stages was determined and is indicated in the bar diagrams. A normal progression through the syncytial blastoderm cycles is observed with all the different genotypes in mock treated embryos (w^l and $gSpc105^{wr30}$; $Spc105^l$ and $gSpc105^{wr1}$; $Spc105^l$ and $mad2^P$). However, $mad2^P$ mutant embryos do not have a functional SAC (Buffin et al, 2007) and therefore fail to arrest in mitosis after incubation with the microtubule inhibitor. In contrast, normal SAC function is observed in the presence of *D. melanogaster* Spc105 containing either 30 *D. willistonii* repeats or only 1 repeat instead of the normal repetitive middle domain.

Supplementary Figure 8

Supplementary Figure 8. The C-terminal domain of Spc105 causes defects after overexpression during eye or wing development.

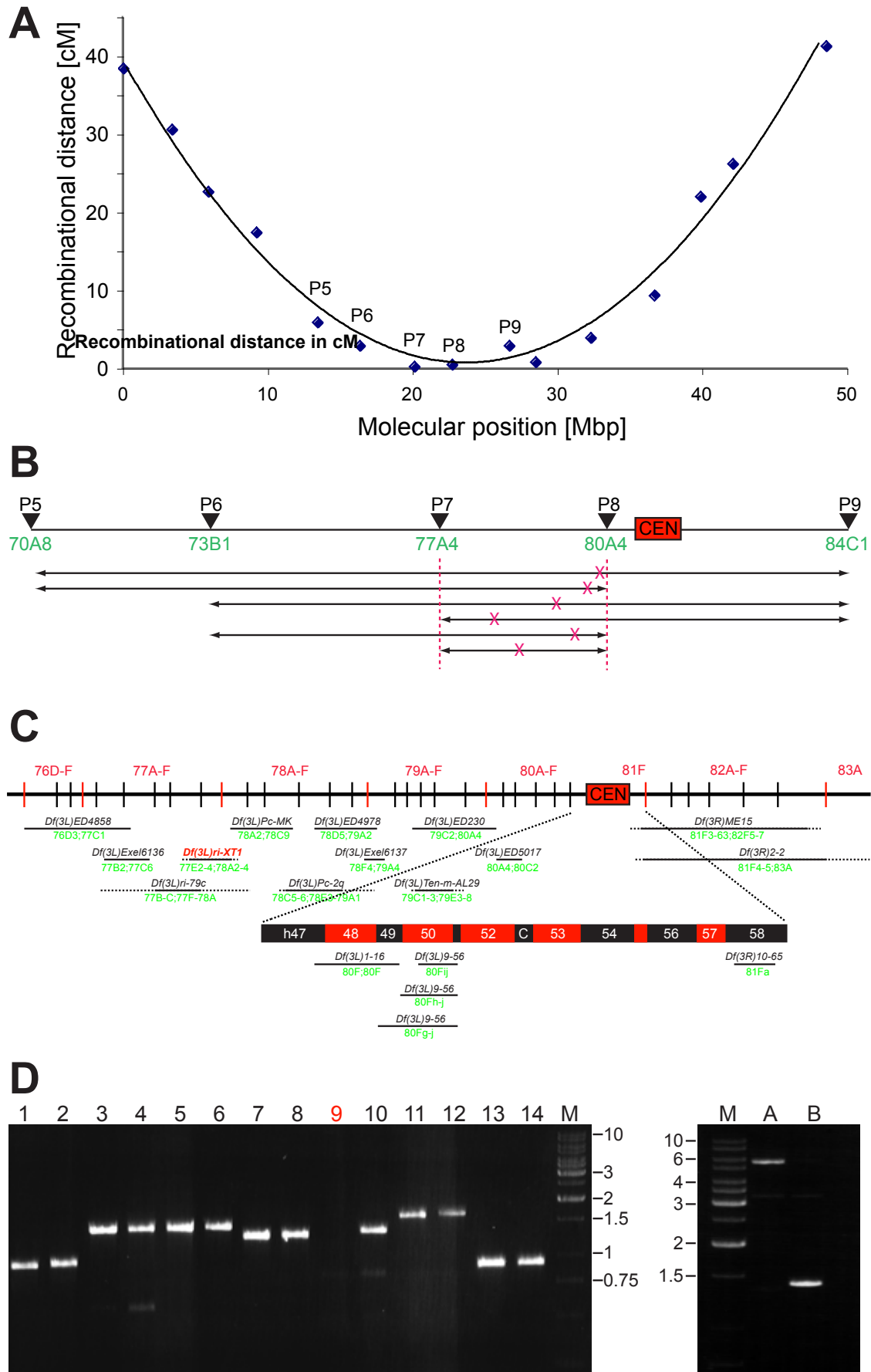
ey-GAL4 and *MS1096* were used to express various *UAS* transgenes encoding different Spc105 domains during wing (*bottom row*) and eye (*top row*) development, respectively. Wild-type wings and eyes were present in control flies (*control*) which carried only the *GAL4* transgenes. Aberrant wing and eye phenotypes were observed after overexpression of the C-terminal domain (*Spc105(C)*). Overexpression of the N-terminal domain (*Spc105(N)*), the middle region (*Spc105(M)*) or full length Spc105 (*Spc105(FL)*) had no effect.

Supplementary Figure 9

Supplementary Figure 9. Analyses of native chromosomes released from mitotic syncytial embryos coexpressing a red and a green fluorescent kinetochore component.

The histogram curves illustrate the distribution of the d_{RGintra} values (in pixel) obtained in pairwise analyses of 100 chromosomes from embryos expressing a red (“r”) and a green (“g”) fluorescent kinetochore component. 1 pixel = 62.4 nm.

Supplementary Figure 10



Supplementary Figure 10. Positional cloning of *Spc105*.

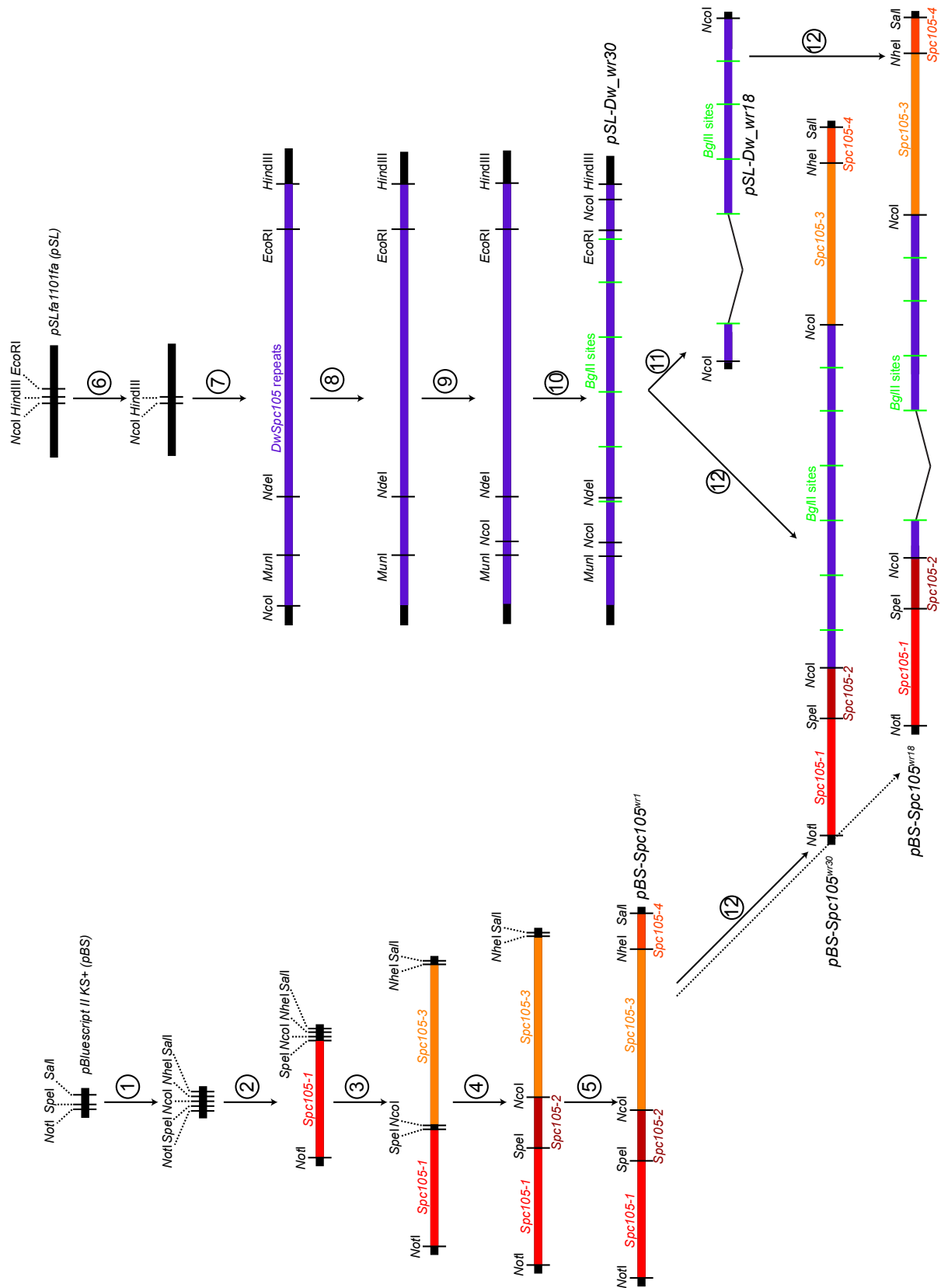
(A) The recombinational distance [cM] between the recessive lethal mutation (*Spc105^l*) and molecularly mapped P element insertions is plotted against the molecular positions [Mbp] of the P elements along the third chromosome (for details, see Zhai et al, 2003). Each dot represents one of the following P elements: *KG02776* (0.085 Mbp; P1), *KG09489* (3.461 Mbp; P2), *KG00023* (5.936 Mbp; P3), *KG02042* (9.260 Mbp; P4), *BG00690* (13.486 Mbp; P5), *BG01582* (16.401 Mbp; P6), *BG02493* (20.149 Mbp; P7), *BG01780* (22.755 Mbp; P8), *BG02270* (26.712 Mbp; P9), *BG02748* (28.534 Mbp; P10), *BG02790* (32.323 Mbp; P11), *BG02734* (36.721 Mbp; P12), *BG01881* (39.912 Mbp; P13), *BG02475* (42.131 Mbp; P14) and *BG02628* (48.593 Mbp; P15). Based on the regression curve, the second site recessive lethal mutation is located near the centromere of the third chromosome.

(B) The calculation of the projected molecular distances (Zhai et al, 2003) placed the recessive lethal mutation between P element insertions P7 and P8 (see A). The *solid line* represents the chromosomal region between the P element insertions P5 and P9 (see A) which are indicated by *triangles*. Cytolocations of these P element insertions are indicated by *green numbers*. The centromere is represented by the *red box*. A *red cross* on a *double-headed arrow* indicates the calculated projected molecular distance of the recessive lethal *Spc105^l* mutation between two flanking P elements.

(C) Complementation tests with deficiencies deleting parts of the chromosomal region between 76D – 83A placed the recessive lethal mutation between 77E1 – 78A2. The *thick solid line* represents the chromosomal region between 76D and 83A and the *vertical lines* divide this region into cytological bands. The centromere is depicted by the *red CEN box* and the division of pericentromeric heterochromatin into different segments (h47 – h58) is shown by red and black boxes. Regions deleted in deficiencies are indicated by *solid* and *dashed lines*. Furthermore, the cytolocation of their breakpoints is indicated in *green lettering*. Only *Df(3L)ri-XT1* did not complement the recessive lethal mutation.

(D) PCR experiments revealed a 4.2 kb insertion within the 3rd exon of *CG11451* amplified from *Spc105^l* homozygous mutant embryos. Genomic fragments of the *CG11451* region were amplified from DNA isolated from either *Spc105^l* embryos (*lanes 1, 3, 5, 7, 9, 11* and *13*) or sibling embryos homozygous for the balancer chromosome (*lanes 2, 4, 6, 8, 10, 12* and *14*) using the primer pairs RaS146/RC15 (*lanes 1* and *2*), RC/RC2 (*lanes 3* and *4*), RaS175/RaS176 (*lanes 5* and *6*), RC20/RaS177 (*lanes 7* and *8*), RC26/RaS178 (*lanes 9* and *10*), RC21/RaS179 (*lanes 11* and *12*) and RC24/RaS179 (*lanes 13* and *14*). The absence of a band in *line 9* suggested the presence of an insertion in *Spc105^l* within the region flanked by RC26 and RaS178. By increasing the elongation time during the PCR, a fragment could be successfully amplified with this primer pair from *Spc105^l* DNA (*lane A*). This fragment was 4.2 kb longer than the fragment amplified with the same primer pair from balancer DNA (*lane B*). DNA molecular weight marker fragments (*lanes M*) were loaded for size estimation. The *numbers* are given in kilobases (kb).

Supplementary Figure 11



Supplementary Figure 11. Cloning strategy for the generation of *DmSpc105* transgene constructs with varying numbers of *Drosophila willistoni* repeats in place of the *Drosophila melanogaster* repeats.

Step 1: Addition of an *NcoI* and an *NheI* restriction site into the multiple cloning site of the *pBluescript II KS+* (*pBS*) vector by introducing the primer hybrid RaS195/RaS196 into the *SpeI* and *SalI* sites. **Step 2:** Introduction of the PCR fragment *Spc105-1* (amplified from the cDNA clone *LP22061^{FL}* with RC1 and RaS199) into the *NotI* and *SpeI* sites of the cloning intermediate after step 1. **Step 3:** Introduction of the PCR fragment *Spc105-3* (amplified from the cDNA clone *LP22061^{FL}* with RaS202 and RaS203) into the *NcoI* and *NheI* sites of the cloning intermediate after step 2. **Step 4:** Introduction of the PCR fragment *Spc105-2* (amplified from the cDNA clone *LP22061^{FL}* with RaS200 and RaS201) into the *SpeI* and *NcoI* sites of the cloning intermediate after step 3. **Step 5:** Introduction of the PCR fragment *Spc105-4* (amplified from the cDNA clone *LP22061^{FL}* with RaS204 and RaS205) into the *NheI* and *SalI* sites of the cloning intermediate after step 4 resulting in *pBS-Spc105^{wr1}*. **Step 6:** Removal of the *EcoRI* restriction site of the vector *pSLfa1101fa* (*pSL*). **Step 7:** Introduction of a PCR fragment (amplified with RaS207 and RaS208 from genomic *D. willistoni* DNA) containing the repeat region of *DwSpc105* into the *NcoI* and *HindIII* restriction sites of the cloning intermediate after step 7. **Step 8:** Removal of the *NcoI* restriction site of the cloning intermediate after step 8. **Step 9:** Introduction of an *NcoI* restriction site between *NdeI* and *MunI* (see text). **Step 10:** Introduction of an *NcoI* restriction site between *EcoRI* and *HindIII* (see text) resulting in *pSL-Dw_wr30*. **Step 11:** Partial digestion of *pSL-Dw_wr30* with *BglIII* and identification of the resulting deletions by DNA sequencing. *pSL-Dw_wr18* was selected for the subsequent construction. **Step 12:** Introduction of the *NcoI* fragments of *pSL-DwSpc105^{wr30}* as well as of *pSL-DwSpc105^{wr18}* into *pBS-Spc105^{wr1}* resulting in *pBS-Spc105^{wr30}* and *pBS-Spc105^{wr18}*. Based on these three constructs, we generated *pP{CaSpeR-4}-gSpc105^{wr1}*, *pP{CaSpeR-4}-gSpc105^{wr18}* and *pP{CaSpeR-4}-gSpc105^{wr30}* (see text).

Supplementary Table I. Results of the Exelixis Deficiency Screen

Males carrying an Exelixis deficiency over a balancer chromosome were crossed to females carrying transgenes driving *GMR*-controlled overexpression of various proteins (*GMR-thrΔC-myc*, *GMR-GAL4 > UAS-pim-myc*, *GMR-GAL4 > UAS-EGFP-Cenp-C(C)*, *GMR-OTD M.1* and *GMR-GAL4 > UAS-OTD*). The rough eye phenotype of adult progeny flies carrying either the deficiency or the balancer chromosome in addition to the transgenes directing *GMR*-controlled overexpression was compared and used for the classification of the interaction character of individual deficiencies: E+++ > E++ > E+ > E > e > n/e > n > n/s > s / S > S > S+ > S++ > S+++ (E/S: strong enhancer/suppressor; e/s: weak enhancer/suppressor; n: no interaction). In addition, some crosses were not set up (“-”). From a few crosses the desired flies did not hatch, indicating a synthetic lethality between the deficiency and the *GMR*-chromosome (“synthetic lethal”). Moreover, some crosses did not produce progeny at all (“sterile”) and in a few cases, the deficiency carrying line was lost prematurely (“line dead”). Finally, in a few cases, offspring males showed a suppressed phenotype while offspring females displayed an enhanced phenotype (“♂S / ♀E”).

Bloomington Stock#	Symbol	<i>GMR-thrΔC</i>	<i>GMR-GAL4, UAS-pim-myc</i>	<i>GMR-GAL4, UAS-EGFP-CenpC(C)</i>	<i>GMR-OTD M.1</i>	<i>GMR-GAL4, UAS-OTD</i>
7488	Df(2L)Exel6001	n	n	n	-	-
7489	Df(2L)Exel6002	n	n	n	-	-
7490	Df(2L)Exel6003	e	E+	E	n	n
7491	Df(2L)Exel6004	e	E+	e	n	n
7492	Df(2L)Exel6005	n	n	n	-	-
7493	Df(2L)Exel6007	n	s	n	-	-
7494	Df(2L)Exel6008	n	n	n	-	-
7495	Df(2L)Exel6009	n	n	n	-	-
7496	Df(2L)Exel6010	n	n	n	-	-
7497	Df(2L)Exel6011	n	n	synthetic lethal	n	n
7498	Df(2L)Exel6012	n	n	n	n	n
7499	Df(2L)Exel6013	s	n	n	-	-
7500	Df(2L)Exel6014	n	n	n	-	-
7501	Df(2L)Exel6015	n	s	sterile	-	-
7502	Df(2L)Exel6016	n	n	n	-	-
7503	Df(2L)Exel6017	n	e	e	-	-
7504	Df(2L)Exel6018	n	n	n	-	-
7505	Df(2L)Exel6021	n	n	e	-	-
7506	Df(2L)Exel6022	n	s	e	-	-
7507	Df(2L)Exel6024	n	n	n	-	-
7508	Df(2L)Exel6025	n	n	e	-	-
7510	Df(2L)Exel6027	n	n	E+(+)	n	n
7511	Df(2L)Exel6028	n	n	sterile	n	n
7512	Df(2L)Exel6029	n	s	n	-	-
7513	Df(2L)Exel6030	n	n	e	-	-
7514	Df(2L)Exel6031	n	s	n	-	-
7515	Df(2L)Exel6032	n	n	n	-	-
7516	Df(2L)Exel6033	n	n	n	n	n
7517	Df(2L)Exel6034	n	s	n	♂S / ♀E	♂S / ♀E
7518	Df(2L)Exel6035	n	n	e	n	n
7519	Df(2L)Exel6036	n	n	n	n	n
7521	Df(2L)Exel6038	n	s	e	e	e
7522	Df(2L)Exel6039	n	n	e	e	e
7523	Df(2L)Exel6041	n	S++	n	n	n
7524	Df(2L)Exel6042	n	S++	n	n	n
7525	Df(2L)Exel6043	n	n	e	n	n
7526	Df(2L)Exel6044	e	n	n	-	-
7527	Df(2L)Exel6045	n	s	E	n	n
7528	Df(2L)Exel6046	n	s	n	n	n
7529	Df(2L)Exel6047	n	E+	n	n	n
7530	Df(2L)Exel6048	s	s	n	sterile	sterile
7531	Df(2L)Exel6049	n/e	n	n	n	n
7532	Df(2R)Exel6050	n	n	n	n	n
7533	Df(2R)Exel6051	n	s	e	n	n
7534	Df(2R)Exel6052	n	s	n	n	n
7535	Df(2R)Exel6053	s	n	n	-	-
7536	Df(2R)Exel6054	n	s	E	n	n
7537	Df(2R)Exel6055	n	n	n	-	-
7538	Df(2R)Exel6056	E++	E++	e	n	n
7539	Df(2R)Exel6057	n	s	n	-	-
7540	Df(2R)Exel6058	n	n	e	-	-
7541	Df(2R)Exel6059	n	n	E	n	n
7542	Df(2R)Exel6060	n	n	n	-	-
7543	Df(2R)Exel6061	n	n	n	-	-
7544	Df(2R)Exel6062	n	n	n	-	-
7545	Df(2R)Exel6063	n	n	n	-	-
7546	Df(2R)Exel6064	n	n	E++	n	n
7547	Df(2R)Exel6065	n	n	e	-	-
7548	Df(2R)Exel6066	n	n	e	-	-
7549	Df(2R)Exel6067	n	n	E	s	s
7550	Df(2R)Exel6068	E+	E+	e	n	n
7551	Df(2R)Exel6069	n	n	e	-	-
7552	Df(2R)Exel6070	n	n	n	-	-
7553	Df(2R)Exel6071	n	e	E(+)	n	n
7554	Df(2R)Exel6072	e	s	e	n	n
7556	Df(2R)Exel6076	n	n	n	-	-
7557	Df(2R)Exel6077	n	n	n	-	-
7558	Df(2R)Exel6078	n	n	n	-	-

Bloomington Stock#	Symbol	<i>GMR-thrΔC</i>	<i>GMR-GAL4, UAS-pim-myc</i>	<i>GMR-GAL4, UAS-EGFP-CenpC(C)</i>	<i>GMR-OTD M.1</i>	<i>GMR-GAL4, UAS-OTD</i>
7559	Df(2R)Exel6079	n	n	n	-	-
7561	Df(2R)Exel6082	n	n	n	-	-
7562	Df(3L)Exel6083	n	n	n	-	-
7563	Df(3L)Exel6084	n	s	s	-	-
7564	Df(3L)Exel6085	n	n	n	-	-
7565	Df(3L)Exel6086	n	n	n	-	-
7566	Df(3L)Exel6087	n	n	n	-	-
7567	Df(3L)Exel6088	s	e	n	-	-
7568	Df(3L)Exel6089	s	n	n	-	-
7569	Df(3L)Exel6090	n	n	e	-	-
7570	Df(3L)Exel6091	n	n	n	-	-
7571	Df(3L)Exel6092	n	n	n	-	-
7572	Df(3L)Exel6093	n	n	e	-	-
7573	Df(3L)Exel6094	s	n	n	-	-
7574	Df(3L)Exel6095	s	n	e	-	-
7575	Df(3L)Exel6096	n	n	n	-	-
7576	Df(3L)Exel6097	n	n	n	-	-
7577	Df(3L)Exel6098	e	e	n	-	-
7578	Df(3L)Exel6099	n	n	n	-	-
7580	Df(3L)Exel6101	n	n	n	-	-
7581	Df(3L)Exel6102	n	e	e	-	-
7582	Df(3L)Exel6103	n	n	n	-	-
7583	Df(3L)Exel6104	n	s	s	-	-
7584	Df(3L)Exel6105	n	n	e	-	-
7585	Df(3L)Exel6106	n	n	n	-	-
7586	Df(3L)Exel6107	n	e	n	-	-
7587	Df(3L)Exel6108	s	n	s	n	n
7588	Df(3L)Exel6109	n	n	e	-	-
7589	Df(3L)Exel6110	s	n	n	n	n
7591	Df(3L)Exel6112	n	n	s	-	-
7593	Df(3L)Exel6114	n	s	n	-	-
7594	Df(3L)Exel6115	s	s	s	n	n
7595	Df(3L)Exel6116	s	e	n	-	-
7596	Df(3L)Exel6117	n	n	e	-	-
7597	Df(3L)Exel6118	s	n	n	-	-
7598	Df(3L)Exel6119	s	n	e	-	-
7599	Df(3L)Exel6120	n	n	n	-	-
7600	Df(3L)Exel6121	s	n	n	-	-
7601	Df(3L)Exel6122	n	n	n	-	-
7602	Df(3L)Exel6123	n	e	synthetic lethal	s	s
7604	Df(3L)Exel6125	n	n	e	n	n
7605	Df(3L)Exel6126	s	e	n	-	-
7606	Df(3L)Exel6127	n	n	s	n	n
7607	Df(3L)Exel6128	s	n	e	-	-
7608	Df(3L)Exel6129	s	n	S	n	n
7609	Df(3L)Exel6130	E+	E+	n	s	s
7610	Df(3L)Exel6131	S++	S+	n	n	n
7611	Df(3L)Exel6132	n	n	E++	sterile	sterile
7612	Df(3L)Exel6133	s	n	n	-	-
7613	Df(3L)Exel6134	s	s	S+	n	n
7614	Df(3L)Exel6135	s	s	E+++	s	s
7615	Df(3L)Exel6136	s	S++	n	s	s
7616	Df(3L)Exel6137	s	s	S+++	n	n
7617	Df(3L)Exel6138	s	s	n	-	-
7619	Df(3R)Exel6140	s	s	e	n	n
7620	Df(3R)Exel6141	n	n	n	-	-
7621	Df(3R)Exel6142	e	n	e	n	n
7622	Df(3R)Exel6143	n	e	n	-	-
7623	Df(3R)Exel6144	s	s	n	sterile	sterile
7624	Df(3R)Exel6145	n	n	S+	n	n
7625	Df(3R)Exel6146	n	n	n	-	-
7626	Df(3R)Exel6147	n	e	e	-	-
7627	Df(3R)Exel6148	n	n	E+++	n	n
7628	Df(3R)Exel6149	E+++	E++(+)	e	n	n
7629	Df(3R)Exel6150	S++	n	n	n	n
7630	Df(3R)Exel6151	s	s	e	n	n
7631	Df(3R)Exel6152	S++	S+	n	n	n
7632	Df(3R)Exel6153	n	n	e	-	-

Bloomington Stock#	Symbol	<i>GMR-thrΔC</i>	<i>GMR-GAL4, UAS-pim-myc</i>	<i>GMR-GAL4, UAS-EGFP-CenpC(C)</i>	<i>GMR-OTD M.1</i>	<i>GMR-GAL4, UAS-OTD</i>
7633	Df(3R)Exel6154	n	n	n	-	-
7634	Df(3R)Exel6155	n	n	n	-	-
7635	Df(3R)Exel6156	n	n	n	n	n
7636	Df(3R)Exel6157	E++	E++	E	n	n
7637	Df(3R)Exel6158	n	n	n	-	-
7638	Df(3R)Exel6159	s	n	e	-	-
7639	Df(3R)Exel6160	s	s	n	-	-
7640	Df(3R)Exel6161	n/s	s	S	n	n
7641	Df(3R)Exel6162	n	n	E++(+)	n	n
7642	Df(3R)Exel6163	n	S+	n	n	n
7643	Df(3R)Exel6164	E++	E++	e	n	n
7644	Df(3R)Exel6165	n	n	e	-	-
7645	Df(3R)Exel6166	s	n	n	-	-
7646	Df(3R)Exel6167	n	s	n	-	-
7647	Df(3R)Exel6168	e	n	S	n	n
7648	Df(3R)Exel6169	n	n	n	-	-
7649	Df(3R)Exel6170	s	n	n	-	-
7650	Df(3R)Exel6171	e	n	s	-	-
7651	Df(3R)Exel6172	s	n	n	-	-
7652	Df(3R)Exel6173	n	e	n	-	-
7653	Df(3R)Exel6174	n	n	e	-	-
7654	Df(3R)Exel6175	s	s	n	-	-
7655	Df(3R)Exel6176	n	n	n	n	n
7657	Df(3R)Exel6178	n	n	S	sterile	sterile
7658	Df(3R)Exel6179	s	n	s	-	-
7659	Df(3R)Exel6180	e	e	n	-	-
7660	Df(3R)Exel6181	n	n	e	-	-
7661	Df(3R)Exel6182	s	n	n	-	-
7662	Df(3R)Exel6183	n	e	n	-	-
7663	Df(3R)Exel6184	n	n	n	-	-
7664	Df(3R)Exel6185	n	n	n	-	-
7665	Df(3R)Exel6186	n	n	n	-	-
7666	Df(3R)Exel6187	n	n	n	-	-
7667	Df(3R)Exel6188	n	n	S++	n	n
7668	Df(3R)Exel6189	e	e	S+	n	n
7669	Df(3R)Exel6190	S+	s	s	n	n
7670	Df(3R)Exel6191	S++	S++	s	n	n
7671	Df(3R)Exel6192	n	n	n	-	-
7672	Df(3R)Exel6193	E++(+)	E+	E++	n	n
7673	Df(3R)Exel6194	n	e	n	-	-
7674	Df(3R)Exel6195	n	n	S	n	n
7675	Df(3R)Exel6196	n	n	n	-	-
7676	Df(3R)Exel6197	s	s	n	n	n
7677	Df(3R)Exel6198	n	e	n	n	n
7678	Df(3R)Exel6199	S++(+)	S++	e	n	n
7679	Df(3R)Exel6200	s	s	n	-	-
7680	Df(3R)Exel6201	n	n	S++	n	n
7681	Df(3R)Exel6202	S++	S++	e	n	n
7682	Df(3R)Exel6203	s	n	n	-	-
7683	Df(3R)Exel6204	n	n	n	-	-
7684	Df(3R)Exel6205	n	n	n	-	-
7685	Df(3R)Exel6206	n	n	n	-	-
7686	Df(3R)Exel6208	n	n	S(+)	n	n
7687	Df(3R)Exel6209	n	n	n	-	-
7688	Df(3R)Exel6210	synthetic lethal	synthetic lethal	synthetic lethal	-	-
7689	Df(3R)Exel6211	n	n	n	-	-
7690	Df(3R)Exel6212	n	e	n	-	-
7691	Df(3R)Exel6213	n	n	n	-	-
7692	Df(3R)Exel6214	s	n	n	-	-
7693	Df(3R)Exel6215	n	n	s	-	-
7694	Df(3R)Exel6216	S++	S+	n	n	n
7695	Df(3R)Exel6217	n	s	s	-	-
7696	Df(3R)Exel6218	n	n	S	n	n
7697	Df(3R)Exel6219	e	e	S++(+)	n	n
7699	Df(1)Exel6221	n	n	n	-	-
7700	Df(1)Exel6223	n	n	n	-	-
7702	Df(1)Exel6225	n	e	n	-	-
7703	Df(1)Exel6226	n	n	n	-	-

Bloomington Stock#	Symbol	GMR-thrΔC	GMR-GAL4, UAS-pim-myc	GMR-GAL4, UAS-EGFP-CenpC(C)	GMR-OTD M.1	GMR-GAL4, UAS-OTD
7704	Df(1)Exel6227	n	n	n	-	-
7705	Df(1)Exel6230	n	n	n	-	-
7706	Df(1)Exel6231	e	e	n	-	-
7707	Df(1)Exel6233	n	n	n	-	-
7708	Df(1)Exel6234	e	e	n	-	-
7709	Df(1)Exel6235	n	n	n	-	-
7710	Df(1)Exel6236	n	n	n	-	-
7711	Df(1)Exel6237	n	n	n	-	-
7712	Df(1)Exel6238	line dead	line dead	line dead	-	-
7713	Df(1)Exel6239	n	e	n	-	-
7714	Df(1)Exel6240	n	n	n	-	-
7715	Df(1)Exel6241	n	e	n	-	-
7716	Df(1)Exel6242	n	n	n	-	-
7717	Df(1)Exel6244	n	e	n	-	-
7718	Df(1)Exel6245	n	n	n	-	-
7719	Df(1)Exel6248	n	n	n	-	-
7720	Df(1)Exel6251	e	e	n	-	-
7721	Df(1)Exel6253	e	e	n	-	-
7722	Df(1)Exel6254	n	n	n	-	-
7723	Df(1)Exel6255	n	n	n	-	-
7724	Df(2L)Exel6256	n	n	s	-	-
7726	Df(3R)Exel6259	n	n	S++	n	n
7729	Df(3L)Exel6262	n	n	n	-	-
7730	Df(3R)Exel6263	e	e	e	n	n
7731	Df(3R)Exel6264	n	n	e	n	n
7732	Df(3R)Exel6265	s	n	n	n	n
7734	Df(3R)Exel6267	n	n	n	-	-
7736	Df(3R)Exel6269	S+	n	S+++	sterile	sterile
7737	Df(3R)Exel6270	n	n	S+(+)	n	n
7739	Df(3R)Exel6272	n	n	e	-	-
7740	Df(3R)Exel6273	S+(+)	S+	n	n	n
7741	Df(3R)Exel6274	n	n	n	-	-
7742	Df(3R)Exel6275	n	n	e	n	n
7743	Df(3R)Exel6276	n	n	s	-	-
7744	Df(2L)Exel6277	e	n	n	-	-
7745	Df(3L)Exel6279	n	n	n	-	-
7746	Df(3R)Exel6280	n	n	n	-	-
7748	Df(2R)Exel6283	n	n	s	-	-
7749	Df(2R)Exel6284	n	S+	s	n	n
7750	Df(2R)Exel6285	s	s	n	-	-
7752	Df(3R)Exel6288	e	n	n	n	n
7753	Df(1)Exel6290	n	n	n	-	-
7754	Df(1)Exel6291	n	n	n	-	-
7759	Df(1)Exel9050	n	n	n	-	-
7760	Df(1)Exel9053	n	e	n	-	-
7761	Df(1)Exel7463	n	n	n	-	-
7762	Df(1)Exel9051	s	e	n	-	-
7763	Df(1)Exel9054	s	s?	n	-	-
7764	Df(1)Exel7464	n	n	n	-	-
7765	Df(1)Exel9067	n	n	n	-	-
7766	Df(1)Exel7465	n	n	e	-	-
7767	Df(1)Exel9068	n/s	s	n	-	-
7768	Df(1)Exel7468	n	n	n	-	-
7769	Df(1)Exel8196	E+++	sterile	sterile	n	n
7770	Df(1)Exel9049	E+	e	n	n	n
7772	Df(2L)Exel7002	n	e	s	-	-
7774	Df(2L)Exel8003	e	E++	s	n	n
7775	Df(2L)Exel7005	n	n	n	-	-
7776	Df(2L)Exel7006	n	n	s	-	-
7777	Df(2L)Exel8004	s	n	n	-	-
7778	Df(2L)Exel7007	n	n	n	-	-
7779	Df(2L)Exel8005	n	n	n	-	-
7780	Df(2L)Exel7008	n	n	n	-	-
7782	Df(2L)Exel7010	n	E++	n	n	n
7783	Df(2L)Exel7011	synthetic lethal	synthetic lethal	synthetic lethal	synthetic lethal	synthetic lethal
7784	Df(2L)Exel7014	n	s	n	n	n
7785	Df(2L)Exel7015	n	n	n	-	-
7786	Df(2L)Exel8008	n	n	n	-	-

Bloomington Stock#	Symbol	GMR-thrΔC	GMR-GAL4, UAS-pim-myc	GMR-GAL4, UAS-EGFP-CenpC(C)	GMR-OTD M.1	GMR-GAL4, UAS-OTD
7787	Df(2L)Exel7016	n	n	n	-	-
7789	Df(2L)Exel7018	n	s	n	-	-
7790	Df(2L)Exel8010	n	s	n	-	-
7792	Df(2L)Exel9062	s	n	n	-	-
7793	Df(2L)Exel8012	n	n	s	-	-
7794	Df(2L)Exel7022	n	n	e	-	-
7795	Df(2L)Exel7021	n	n	n	-	-
7796	Df(2L)Exel8013	n	n	n	-	-
7797	Df(2L)Exel7023	n	e	n	-	-
7798	Df(2L)Exel8016	n	e	n	-	-
7799	Df(2L)Exel7024	n	e	n	-	-
7800	Df(2L)Exel9038	n	n	n	-	-
7801	Df(2L)Exel7027	S++	s	n	s/n	s/n
7802	Df(2L)Exel7029	S+++	S	n	n	n
7803	Df(2L)Exel8019	n	n	n	-	-
7804	Df(2L)Exel7031	n	s	e	-	-
7805	Df(2L)Exel9031	n	n	s	-	-
7807	Df(2L)Exel7034	n	n	e	-	-
7808	Df(2L)Exel8021	s	n	n	-	-
7809	Df(2L)Exel7038	s	s	n	-	-
7810	Df(2L)Exel7039	n	n	n	-	-
7811	Df(2L)Exel7040	n	n	e	-	-
7812	Df(2L)Exel7042	n	n	n	-	-
7813	Df(2L)Exel8022	n	n	e	-	-
7814	Df(2L)Exel9064	n	n	n	-	-
7815	Df(2L)Exel9040	n	n	s	-	-
7816	Df(2L)Exel7043	n	s	n	-	-
7817	Df(2L)Exel8024	n	n	n	-	-
7818	Df(2L)Exel9032	n	n	n	-	-
7819	Df(2L)Exel7046	n	n	e	n	n
7820	Df(2L)Exel8026	e	n	n	-	-
7821	Df(2L)Exel7049	n	e	n	-	-
7822	Df(2L)Exel8028	e	e	e	n	n
7823	Df(2L)Exel7055	n	n	n	-	-
7826	Df(2L)Exel7059	n	n	s	-	-
7828	Df(2L)Exel8033	n	n	s	-	-
7830	Df(2L)Exel8034	n	n	s	-	-
7831	Df(2L)Exel7063	s	n	s	n	n
7833	Df(2L)Exel7066	line dead	line dead	line dead	-	-
7834	Df(2L)Exel7067	n	n	n	-	-
7835	Df(2L)Exel8036	e	n	s	-	-
7836	Df(2L)Exel9044	n	n	n	-	-
7837	Df(2L)Exel7069	n	n	n	-	-
7838	Df(2L)Exel7068	n	n	n	-	-
7839	Df(2L)Exel7070	n	n	s	-	-
7840	Df(2L)Exel8038	n	s	sterile	-	-
7841	Df(2L)Exel9033	n	n	n	-	-
7843	Df(2L)Exel7071	s	S++	n	n	n
7844	Df(2L)Exel7072	n	e	n	n	n
7845	Df(2L)Exel7073	n	n	n	-	-
7846	Df(2L)Exel8039	n	s	n	-	-
7847	Df(2L)Exel8040	n	n	E	sterile	sterile
7848	Df(2L)Exel7075	n	s	e	-	-
7849	Df(2L)Exel8041	E+(+)	E++	e	n	n
7850	Df(2L)Exel7077	n	s	S++(+)	n	n
7851	Df(2L)Exel7078	n	n	n	-	-
7852	Df(2L)Exel7079	n	s	n	-	-
7853	Df(2L)Exel7080	n	n	s	-	-
7855	Df(2L)Exel7081	n	n	n	-	-
7858	Df(2R)Exel7092	n	n	n	-	-
7859	Df(2R)Exel7094	E++	E+	n	n	n
7860	Df(2R)Exel7095	n	n	n	-	-
7862	Df(2R)Exel7096	n	n	n	-	-
7863	Df(2R)Exel8047	n	n	s	n	n
7864	Df(2R)Exel7098	S+	S+	s	n	n
7866	Df(2R)Exel8049	n	S+	s	n	n
7867	Df(2R)Exel9016	n	s	n	-	-
7869	Df(2R)Exel7121	n	n	n	-	-

Bloomington Stock#	Symbol	GMR-thrΔC	GMR-GAL4, UAS-pim-myc	GMR-GAL4, UAS-EGFP-CenpC(C)	GMR-OTD M.1	GMR-GAL4, UAS-OTD
7870	Df(2R)Exel7123	E++	e	e	n	n
7871	Df(2R)Exel8057	E+(+)	E+	n	n	n
7872	Df(2R)Exel7124	E++	E+	n	n	n
7873	Df(2R)Exel7128	n	n	n	-	-
7875	Df(2R)Exel7130	e	E++	S+	n	n
7876	Df(2R)Exel7131	n	n	n	-	-
7877	Df(2R)Exel8059	n	n	n	-	-
7879	Df(2R)Exel7135	n	n	n	-	-
7880	Df(2R)Exel9015	s	n	n	-	-
7881	Df(2R)Exel9026	n	n	s	-	-
7882	Df(2R)Exel7137	n	n	s	-	-
7883	Df(2R)Exel7138	n	n	n	-	-
7884	Df(2R)Exel7139	n	n	n	-	-
7885	Df(2R)Exel9060	n	n	s	-	-
7886	Df(2R)Exel7142	n	n	S	n	n
7887	Df(2R)Exel7145	n	n	s	-	-
7888	Df(2R)Exel7144	n	n	n	-	-
7890	Df(2R)Exel7149	n	n	n	-	-
7891	Df(2R)Exel7150	n	e	n	-	-
7893	Df(2R)Exel7153	n	n	n	-	-
7894	Df(2R)Exel7157	n	n	n	-	-
7895	Df(2R)Exel7158	n	e	n	-	-
7896	Df(2R)Exel7162	n	n	E++(+)	n	n
7897	Df(2R)Exel7163	e	n	n	-	-
7898	Df(2R)Exel7164	n	n	n	-	-
7900	Df(2R)Exel7169	n	n	e	-	-
7901	Df(2R)Exel7170	E+	E+(+)	n	n	n
7902	Df(2R)Exel7171	E+	E+	E++	n	n
7903	Df(2R)Exel7173	n	n	e	-	-
7904	Df(2R)Exel7174	s	s	n	-	-
7905	Df(2R)Exel7176	n	n	n	-	-
7906	Df(2R)Exel7177	n	n	n	-	-
7908	Df(2R)Exel7178	n	s	s	-	-
7909	Df(2R)Exel7180	s	n	sterile	-	-
7910	Df(2R)Exel7182	n	n	n	-	-
7912	Df(2R)Exel7184	n	n	s	-	-
7913	Df(2L)Exel9043	n	n	n	-	-
7914	Df(2R)Exel7185	n	n	s	-	-
7916	Df(2R)Exel8056	E++(+)	E++	n	n	n
7917	Df(3R)Exel9020	s	n	e	-	-
7918	Df(3R)Exel8194	n	n	s	-	-
7919	Df(3R)Exel7379	n	n	s	-	-
7920	Df(3L)Exel9057	n	e	s	-	-
7921	Df(3L)Exel9000	S+	S+	s	n	n
7922	Df(3L)Exel8098	n	n	n	-	-
7923	Df(3L)Exel9058	n	n	n	-	-
7924	Df(3L)Exel9001	s	S++	n	n	n
7925	Df(3L)Exel9028	n	n	n	-	-
7926	Df(3L)Exel7208	n	e	n	-	-
7927	Df(3L)Exel7210	s	n	n	-	-
7928	Df(3L)Exel8101	n	n	n	-	-
7929	Df(3L)Exel8104	n	n	n	-	-
7930	Df(3L)Exel9034	S++	s	e	n	n
7931	Df(3R)Exel7315	n	n	n	-	-
7932	Df(3R)Exel7317	n	n	n	-	-
7933	Df(3L)Exel9048	n	n	n	-	-
7934	Df(3L)Exel9017	s	s	n	-	-
7935	Df(3L)Exel9002	n	n	n	-	-
7936	Df(3L)Exel9003	n	s	n	-	-
7937	Df(3L)Exel9004	n	n	n	-	-
7938	Df(3L)Exel7253	S+	s	n	n	n
7940	Df(3L)Exel9006	n	s	s	-	-
7941	Df(3L)Exel9046	n	s	n	-	-
7942	Df(3L)Exel9007	s	n	e	-	-
7943	Df(3L)Exel9008	n	n	n	-	-
7944	Df(3L)Exel9009	s	s	S	s/n	s/n
7945	Df(3L)Exel9011	n	n	s	-	-
7946	Df(3L)Exel9061	s	S++	s	s/n	s/n

Bloomington Stock#	Symbol	<i>GMR-thrΔC</i>	<i>GMR-GAL4, UAS-pim-myc</i>	<i>GMR-GAL4, UAS-EGFP-CenpC(C)</i>	<i>GMR-OTD M.1</i>	<i>GMR-GAL4, UAS-OTD</i>
7947	Df(3L)Exel9045	n	n	n	-	-
7948	Df(3R)Exel7357	n	n	e	-	-
7949	Df(3L)Exel9065	n	n	n	-	-
7950	Df(3L)Exel9066	n	n	n	-	-
7951	Df(3R)Exel9029	n	s	s	-	-
7952	Df(3R)Exel7283	E++	E++	n	n	n
7953	Df(3R)Exel7284	n/e	n	e	-	-
7954	Df(3R)Exel8143	S+	n	n	n	n
7955	Df(3R)Exel9036	n	s	S++	s/n	s/n
7956	Df(3R)Exel7305	s	s	n	-	-
7957	Df(3R)Exel7306	n	n	n	-	-
7958	Df(3R)Exel8152	s	s	n	-	-
7959	Df(3R)Exel7308	n	n	n	-	-
7960	Df(3R)Exel7309	n	n	n	n	n
7961	Df(3R)Exel8154	S+	s	s	n	n
7962	Df(3R)Exel9018	s	s	n	-	-
7963	Df(3R)Exel8153	n	s	n	-	-
7964	Df(3R)Exel9019	s	n	n	-	-
7965	Df(3R)Exel7310	s	n	s	s	s
7966	Df(3R)Exel7312	n	s	n	-	-
7967	Df(3R)Exel8155	S++	s	n	s/n	s/n
7968	Df(3R)Exel7313	n	n	n	-	-
7969	Df(3R)Exel7314	n	n	n	-	-
7970	Df(3R)Exel7316	n	n	E	n	n
7972	Df(3R)Exel7318	n	n	n	-	-
7973	Df(3R)Exel8157	S++	s	S	n	n
7974	Df(3R)Exel8158	S++	S+	n	n	n
7975	Df(3R)Exel7320	S++	S+	s	n	n
7976	Df(3R)Exel8159	n	s	n	-	-
7977	Df(3R)Exel7321	e	n	n	-	-
7978	Df(3R)Exel8160	n	n	n	-	-
7980	Df(3R)Exel7326	n	n	n	-	-
7981	Df(3R)Exel8162	s	s	e	s/n	s/n
7982	Df(3R)Exel7327	n	n	S+++	n	n
7983	Df(3R)Exel7328	n	sterile	sterile	-	-
7984	Df(3R)Exel7329	n	n	n	-	-
7985	Df(3R)Exel7330	S++(+)	s	n	n	n
7986	Df(3R)Exel9055	n	n	n	-	-
7987	Df(3R)Exel8163	n	n	n	-	-
7988	Df(3R)Exel8165	n	n	n	-	-
7989	Df(3R)Exel9030	n	n	e	♂S / ♀E	♂S / ♀E
7990	Df(3R)Exel9012	n	n	n	-	-
7991	Df(3R)Exel9013	n	n	n	-	-
7992	Df(3R)Exel9014	E+++	E+++!	n	n	n
7993	Df(3R)Exel8178	n	n	n	-	-
7994	Df(3R)Exel9056	n	n	n	-	-
7995	Df(3R)Exel9025	n	n	n	-	-
7997	Df(3R)Exel7378	S++(+)	S++	n	n	n
7998	Df(2R)Exel7166	n	n	steril/line dead	-	-
7999	Df(2L)Exel7048	n	n	n	-	-
8000	Df(2L)Exel6006	n	n	S+++	♂S / ♀E	♂S / ♀E

Supplementary Table II: Primer sequences

Primer	Sequence (5'>3')	Primer	Sequence (5'>3')
ANW39	AGAATTCTATTTGGAAATTTGGATAATCTTA	RaS202	TGATGTTCCGTCATCCAGAA
ANW40	GGCTGCGCCGCCGCGTTCGCTTCGTTTGT	RaS203	TCGTGCTAGCATTTCATCGGC
ANW41	GCACTAGTATGGAGCCAGCCGAAAGTC	RaS204	TGAATGCTAGCGACGAGATCGAG
ANW42	ATCTAGACGATTTGTTCAATGAATTTCCG	RaS205	ACATGTGCACTTATTTCTAAGGTAAGTCTGCTG
ANW43	ACGCGCGCCGCTATGGTGAGCAAGGGCGAGG	RaS207	ACGGCGTACTAGCAGAATC
CS4	ATTGGCGTACGTGGTGAGCAAGGGCGAGG	RaS208	CACCTGTATTCCGGGTTCAA
CS5	AGCCGCGTACGACTTGTACAGCTCGTCCATG	RaS249	ATGTCCAGGCCTATGGACTTTCAAAGCCCGC
HS6	GGACTAGTCTTGTACAGCTCGTCCATGC	RaS250	CTGCAAAGGCCTGTCTACCATGAGCGCTTCTC
RaS80	GGTCTAGATTACTTGTACAGCTCGTCCATG	RC1	ATTGAGCGCGCGCTATGGTAGACCTACTCTTCTTG
RaS92	AATCTAGATTAGCGCCGGTGGAGTG	RC2	CAGTTCGGTACCTTCGCAAGTTGTCTCCCTTC
RaS135	GAATTGGTTAACCATGGTGAGCAAGGGCGAG	RC3	GACTAGCGCGCCGCGACGCAGTCGAGAAATACGTC
RaS136	CGAGCCGTTAACGCCTTGTACAGCTCGTC	RC4	ATCTCGAGTTAGATTGCATTAAGTCCGGAC
RaS140	AGAAGTCAAGCAAAAGTTACAC	RC5	CTATGGCGCGCCGCGATGGACTTTCAAAGCCCGC
RaS141	CATACGCATGCTAGCTTTTCTAAGGTAAGTCTCGGG	RC6	TAACATGGTACCTTATTTCTAAGGTAAGTCTCG
RaS142	AGAAAAGCTAGCATGCGTATGTTAGACTACCTTT	RC7	CTAGGCCATATGACGCAGTCGAGAAATACGTC
RaS143	GAAAGCAAATGCAAGCAAAACAC	RC8	ATGGATCCTTAGATTGCATTAAGTCCGGAC
RaS144	GCTCTAGAATGGTGAGCAAGGGCGAG	RC9	ATGTCCCATATGATGGACTTTCAAAGCCCGC
RaS145	AGTCTAGAATGGCCTCTCCGAGGAC	RC10	ATGGATCCTTATTTCTAAGGTAAGTCTCG
RaS146	GACACCCTCTCCAGGGC	RC11	TTAACTCATATGATGGACTTCAATAGCCTAGC
RaS175	CGGATGAGATGATGCTTGAC	RC12	AGGGATCCTTAATCAGTCTCCTTCTTTATC
RaS176	ATTGCCCTCTCTCTATCG	RC15	TGGAATCCCTCACGGACTTCTTGCC
RaS177	GTCTATCGGCACTGGTTGGT	RC17	TGAGAACATATGATGGTAGACCTACTCTTCTTG
RaS178	AGTGGGCACGTCAATTGTCTA	RC18	AGGGATCCTTATTCGCAAGTTGTCTCCCTTC
RaS179	TTCCAGCTTCCAAGTGATCC	RC20	GAAGATAAAGTACGAATGCC
RaS189	CAGAACCCATGGAAGAAGACTTGG	RC21	AAATTCATCAATCTGACCGGG
RaS190	CCAAGTCTTCTCCATGGTTCTG	RC24	CGAATCGTGGTGAAGTACC
RaS191	GTCAGAACCCATGGAAGAGGACAG	RC26	AGAGATGTGCAAGACCCCG
RaS192	CTGTCTCTTCCATGGGTTCTGAC	RC50	GCGGCCCATATGGAGCCAGCCGAAAGTC
RaS194	TACGGTCGACTTTTCTAAGGTAAGTCTGCTCG	RC51	TCTAGACCCGGGTACCCTTGGTTGGCCATATTC
RaS195	CTAGTACACCATGGTGTGGCTAGCACACG	RC52	GCGGCCCATATGGAGGATTGCGGAAGCCG
RaS196	TCGACGTGTGCTAGCCACACCATGGTGTGTA	RC53	GGTACCCCGGGTCAAGTCTGTTCAATGC
RaS199	GGACTAGTTTTTCGTCGGCGTC	RC55	GCATCCCGGGTTAAGAGACCTGGCATAGGCG
RaS200	AAACTAGTCCAGTTGGAAGAAGAAC	RC56	CCGGCCACGTGGCCATGGCCATGCCTCGTAC
RaS201	TCCTCCATGGTTTCTGCATC		